EURADOS
European Radiation Dosimetry Group e. V.

EURADOS Report 2021-03

Neuherberg, April 2021

Comparison of Codes Assessing Radiation Exposure at Aviation Altitudes in Case of Solar Particle Events

P. Beck, J.F. Bottollier-Depois, R. Bütikofer, E. Flückiger, N. Fuller, K.-L. Klein, M. Latocha, V. Mares, D. Matthiä, W. Rühm

ISSN 2226-8057

ISBN 978-3-943701-27-2

DOI: 10.12768/zmq7-bv59

European Radiation Dosimetry Group e. V.

EURADOS Report 2021-03

Neuherberg, April 2021

Comparison of Codes Assessing Radiation Exposure at Aviation Altitudes in Case of Solar Particle Events

P. Beck[1], J.F. Bottollier-Depois[2], R. Bütikofer[3], E. Flückiger[3], N. Fuller[4], K.-L. Klein[4], M. Latocha[1], V. Mares[5], D. Matthiä[6], W. Rühm[5]

[1] Seibersdorf Laboratories, Forschungszentrum Seibersdorf, 2444 Seibersdorf, Austria

[2] IRSN Institute for Radiological Protection and Nuclear Safety, 92262 Fontenay-aux-Roses, France

[3] University of Bern & International Foundation HFSJG, Sidlerstrasse 5, 3012 Bern, Switzerland

[4] LESIA, Observatoire de Paris, 92195 Meudon cedex, France

[5] HMGU Helmholtz Zentrum München, Institute of Radiation Medicine 85764 Neuherberg, Germany

[6] German Aerospace Center, (DLR), Institute of Aerospace Medicine, Linder Höhe, 51147 Köln, Germany

ISSN 2226-8057

ISBN 978-3-943701-27-2

DOI: 10.12768/zmq7-bv59

Imprint

Issued by:
European Radiation Dosimetry e.V.
Postfach 1129
D-85758 Neuherberg
Germany
office@eurados.org
www.eurados.org

The European Radiation Dosimetry e.V. is a non-profit organization promoting research and development and European cooperation in the field of the dosimetry of ionizing radiation. It is registered in the Register of Associations (Amtsgericht München, registry number VR 207982) and certified to be of non-profit character (Finanzamt München, notification from 2021-04-23).

Liability Disclaimer

No liability will be undertaken for completeness, editorial, or technical mistakes, omissions as well as for correctness of the contents.

Members of the editorial group

This comparison exercise was organised and the report was prepared by the following members of EURADOS Working Group 11 on "High Energy Radiation Fields":

Beck, Peter	Seibersdorf Laboratories, Radiation Protection Dosimetry, Forschungszentrum Seibersdorf, 2444 Seibersdorf, Austria
Bottollier-Depois, Jean-François	IRSN Institute for Radiological Protection and Nuclear Safety F-92262 Fontenay-aux-Roses, France
Bütikofer, Rolf	University of Bern & International Foundation HFSJG, Sidlerstrasse 5, 3012 Bern, Switzerland
Flückiger, Erwin	University of Bern & International Foundation HFSJG, Sidlerstrasse 5, 3012 Bern, Switzerland
Fuller, Nicolas	LESIA, Observatoire de Paris, 92195 Meudon cedex, France
Klein, Karl Ludwig	LESIA, Observatoire de Paris, 92195 Meudon cedex, France
Latocha, Marcin	Seibersdorf Laboratories, Radiation Protection Dosimetry, Forschungszentrum Seibersdorf, 2444 Seibersdorf, Austria
Mares, Vladimir	HMGU Helmholtz Zentrum München, Institute of Radiation Medicine 85764 Neuherberg, Germany
Matthiä, Daniel	German Aerospace Center (DLR) Institute of Aerospace Medicine Linder Höhe, 51147 Köln, Germany
Rühm, Werner	HMGU Helmholtz Zentrum München Institute of Radiation Medicine 85764 Neuherberg, Germany

List of contributors providing data to the report

Al Anid, Hani	PCAIRE data PCaire Inc. 38 Colonnade Rd, Ottawa, Canada
Bütikofer, Rolf Flückiger, Erwin	PLANETOCOSMICS (Bern Model) University of Bern, Sidlerstrasse 5, 3012 Bern, Switzerland
Clairand, Isabelle	SIEVERT IRSN Institute for Radiological Protection and Nuclear Safety F-92262 Fontenay-aux-Roses, France
Fuller, Nicolas Klein, Ludwig	SiGLE LESIA, Observatoire de Paris, 92195 Meudon cedex, France
Hands, Alexander	QARM data Surrey Space Centre Faculty of Engineering and Physical Sciences University of Surrey Guildford, GU2 7XH, UK
Latocha, Marcin Beck, Peter	AVIDOS, SOLARDOS Data Seibersdorf Laboratories, Radiation Protection Dosimetry, Forschungszentrum Seibersdorf, 2444 Seibersdorf, Austria
Mares, Vladimir Pioch, Christian	EPCARD.Net and GEANT4 HMGU Helmholtz Zentrum München, Institute of Radiation Medicine 85764 Neuherberg, Germany
Matthiä, Daniel	PANDOCA data German Aerospace Center (DLR) Institute of Aerospace Medicine Linder Höhe, 51147 Köln, Germany
Wissmann, Frank	FDOScalc data Physikalisch-Technische Bundesanstalt, Bundesallee 100, 38116 Braunschweig, Germany
Yasuda, Hiroshi	WASAVIES | JISCARD EX data Hiroshima University Department of Radiation Biophysics, Research Institute for Radiation Biology and Medicine 1-2-3 Kasumi, Minami-Ku, Hiroshima, 734-8553 Japan

Acknowledgements

We gratefully acknowledge the Neutron Monitor Database (NMDB), funded under the European Union's FP7 programme (contract no. 213007), as the neutron monitor data provider. In particular, we thank the PIs and teams of the neutron monitor stations Inuvik, Kiel, McMurdo, Newark, Oulu, Rome, Terre Adélie, and Thule from which data are used.

Flight routes and altitude profiles are taken from EURADOS Report 2012-03 (EURADOS, 2012).

Finally, we thank all contributors to the report for their input, which was essential for the comparison of the assessed flight doses by the different models during the two investigated solar cosmic ray events.

Content:

Figures

Tables

List of Abbreviations

AER	Aerodrome
ALARA	As Low As Reasonably Achievable
AVIDOS	Aviation Dosimetry - Software Package for European Accredited Aviation Dosimetry (Seibersdorf Laboratories)
BSS	Basic Safety Standards
DGAC	Direction Générale de l'Aviation Civile (French Civil Aviation Authority)
DLR	Deutsches Zentrum für Luft- und Raumfahrt (German Aerospace Center)
EAN	European ALARA Network
EPCARD	European Program Package for the Calculation of Aviation Route Doses
ESA	European Space Agency
EC	European Commission
EU	European Union
EURADOS	European Radiation Dosimetry e.V. (non-profit organization)
FAA	Federal Aviation Administration
FDOScalc	Code for Dose Rate Calculations (Physikalisch-Technische Bundesanstalt, Braunschweig, PTB)
FL	Flight Level
FLUKA	Particle Physics Monte-Carlo Simulation Package
GCR	Galactic Cosmic Rays
GEANT4	Toolkit for the Simulation of the Passage of Particles Through Matter
GEO coordinates	Geographic Coordinates
GLE	Ground Level Enhancement / Event
GOES	Geostationary Operational Environmental Satellite
HFSJG	International Foundation High Altitude Research Stations Jungfraujoch and Gornergrat
HMGU	Helmholtz Zentrum München - Deutsches Forschungszentrum für Gesundheit und Umwelt
H*(10)	Ambient Dose Equivalent
ICAO	International Civil Aviation Organization
ICRP	International Commission on Radiological Protection
ICRU	International Commission on Radiation Units & Measurements
IGRF	International Geomagnetic Reference Field
ILAC	International Laboratory Accreditation Cooperation
INT	Intermediate Waypoint
INVK	Inuvik
IPEV	Institut Polaire Français Paul-Emile Victor
IRSN	Institute for Radiological Protection and Nuclear Safety
ISO	International Organization for Standardization
JAM / JQMD	Hadronic Cascade Model / Jaeri Quantum Molecular Dynamics Model
JISCARD	Program Package for the Evaluation of Radiation Exposure for Aircraft Crew (Japan National Institute of Radiological Sciences)
LESIA	Laboratoire d'Etudes Spatiales et d'Instrumentation en Astrophysique, Observatoire de Paris
MAIRE	Model of Atmospheric Ionising Radiation Effects

NASA	National Aeronautics and Space Administration
NEST	NMDB Event Search Tool
NM	Neutron Monitor
NMDB	Neutron Monitor Data Base
PANDOCA	Professional Aviation Dose Calculator
PCAIRE	Predictive Code for Aircrew Radiation Exposure
PLANETOCOSMICS	Simulation Framework based on Geant4 that allows Computing the Hadronic and Electromagnetic Interactions of Cosmic Rays with the Earth, Mars and Mercury (L. Desorgher, University of Bern)
SCR	Solar Cosmic Rays
SIEVERT	A System for Evaluating Exposure to Cosmic Radiation in Air Transport (IRSN)
SiGLE	Computing Radiation Doses due to GLEs Onboard Aircrafts within the SIEVERT System
SILSO	Sunspot Index and Long-term Solar Observations
SOLARDOS	Assessment of the Radiation Exposure due to Solar Particle Events at Aircraft Altitude (Seibersdorf Laboratories)
SEP	Solar Energetic Particle
SPE	Solar Particle Event
TEPC	Tissue-Equivalent Proportional Counter
TERA	Terre Adélie
THUL	Thule
TOC	Top of Climb
TOD	Top of Descent
QARM	QinetiQ Atmospheric Radiation Model
UT	Universal Time
UTC	Coordinated Universal Time
WASAVIES	Warning System for Aviation Exposure to Solar Energetic Particles (Japan National Institute of Information and Communications Technology, NICT)
WDC	World Data Center

Abstract

The European Radiation Dosimetry Group, EURADOS focuses, among other issues, on the harmonization of dose assessment within Europe and conformance with international practices. Along these lines, this EURADOS report compares route doses and dose rates at flight altitudes due to solar cosmic radiation (SCR) associated with ground level enhancements (GLEs) as calculated by means of nine available computer codes. Some of these codes are routinely used for the assessment of radiation exposure of aircraft crew due to galactic cosmic radiation (GCR), while others were specifically developed to address scientific issues associated with the assessment of exposures due to SCR. For all investigations, three representative flight routes were selected which are comparable to those that had been used in a previous EURADOS report on "Comparison of Codes Assessing Radiation Exposure of Aircraft Crew due to Galactic Cosmic Radiation": San Francisco – Paris, Chicago – Beijing, and Sydney – Johannesburg. Two ground level enhancements were chosen, i.e., GLE42 and GLE69, that occurred in September 1989 and January 2005, respectively. For GLE42 pre-defined solar particle characteristics were provided to all participants to ensure the same input data. In contrast, for GLE69 the participants were asked to define their individual solar proton characteristics on the basis of published data made available to them.

It was found that GCR route doses showed a standard deviation from the median consistent with the results published in the earlier EURADOS report on GCR exposure. For GLE42, a standard deviation from the median of about 30% is obtained for the SCR route doses. However, for GLE69 the corresponding standard deviation from the respective median is up to 50%. In some cases, for these investigations, the lowest and the highest SCR route doses obtained by the different codes for a certain flight differ by up to a factor of 10.

It is concluded that one of the main reasons for the differences in the standard deviations from the respective medians of the results for GLE42 and GLE69 is the unequal identification and handling of the SCR characteristics by the different codes. Therefore, we strongly suggest developing a traceable method to identify and handle the solar proton characteristics related to GLEs. Furthermore, we see an urgent need to validate codes used for dose assessment of radiation exposure due to solar particle events at aviation altitudes by experimental data.

1. Introduction

Aircrew and passengers are exposed to cosmic radiation of galactic and solar origin and secondary radiation produced in the atmosphere, the aircraft structure, and its contents (Reitz, 1991; Friedberg, 1993; Kelly, 1999; Beck, 1999; O'Sullivan, 1999). Since the primary and secondary fields of cosmic radiation in the atmosphere are very complex in terms of particle composition and particle energies, dose assessment for aviation is a very difficult task (EURADOS, 2004; EU, 2004; Lindborg, 2004; Beck, 2009a; EURADOS, 2012).

The primary galactic cosmic radiation and energetic solar particles interact with the atomic nuclei of atmospheric constituents producing a cascade of interactions and secondary reaction products that contribute to cosmic radiation exposures and that decreases in intensity with depth in the atmosphere from aviation altitudes to sea level (Grieder, 2001). Galactic cosmic radiation (GCR) originates from outside the heliosphere. It consists mainly of protons, but also of heavier ions, with energies up to 10^{20} eV. The number of particles decreases with increasing energy (see Figure 1). After the GCR penetrates the magnetic field of the solar system, the peak of its energy distribution near Earth is at a few hundred MeV to 1 GeV per nucleon, depending on solar magnetic activity. The fluence rate of GCR entering the solar system is almost constant with time, and these energetic ions approach the Earth isotropically. The variable magnetic field embedded in the solar wind as well as the magnetic field of the Earth alter the flux of GCR protons and heavier ions reaching the Earth's atmosphere.

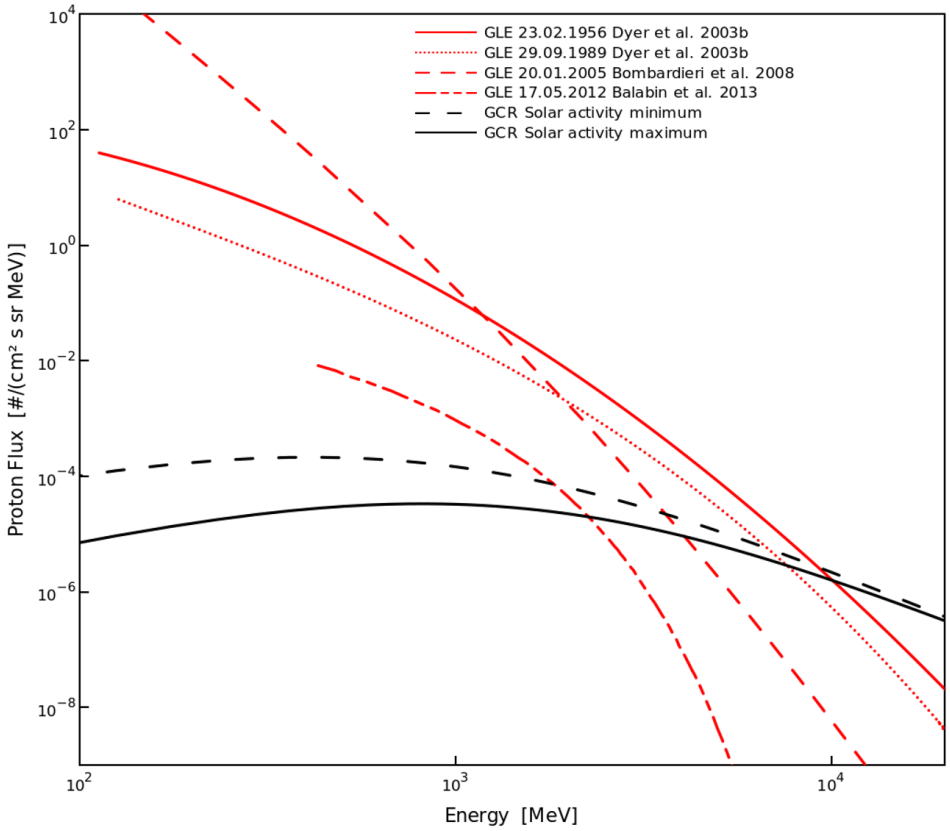

Figure 1: The solar cosmic ray proton peak flux during selected GLEs as derived from the data of the worldwide network of neutron monitors and the GCR proton spectrum during minimum and maximum solar activity. (Dyer, 2003b; Bombardieri, 2008; Balabin, 2013)

Solar cosmic radiation (SCR) occurs sporadically in association with high-energy phenomena on the Sun, e.g. solar flares and Coronal Mass Ejections (CMEs). These solar particle events (SPE), which are also called solar proton events, are observed typically below 100 MeV and only rarely above 10 GeV. SPEs are of short duration, a few hours to a few days, and highly variable in intensity. On average, one SPE per year is intense enough to cause significant dose rates at flight altitudes, in particular at high latitudes (see chapter 3.2). Most of these intense events can be observed e.g. by neutron monitors (NM) on the ground and are therefore called ground level enhancements (GLEs) (ISO 20785-1, Poluianov, 2017). The proton spectra of a few selected GLEs during the peak phase are illustrated in Figure 1 compared with the GCR proton spectra during minimum and maximum solar activity. At aircraft altitudes, the radiation exposure is mainly due to GCR, and only during large SPEs the contribution of SCR can become significant with respect to radiation protection.

Following recommendations of the International Commission on Radiological Protection (ICRP) in Publication 60 (ICRP, 1991), the Council of the European Union (EU) laid down in its Council Directive 96/29/EURATOM of 13 May 1996 (EU, 1996) Basic Safety Standards (BSS) categorizing exposure to natural sources of ionizing radiation, including cosmic radiation, as occupational exposure for aircrew. A year later, the European Commission published recommendations on the implementation of the BSS i.e. recommending control dose limits for aircraft crew, permitting computer programs to be used for dose estimation and noting that frequent flyers may also require arrangements for determining doses (EU, 1997). The implementation of BSS (EU, 1996) found also place in other European technical requirements and administrative procedures applicable to commercial transportation by aeroplane (EU, 2000). The European Directive from 1996 (EU, 1996) has been incorporated into laws and regulations of many EU Member States and their implementation in Europe has been monitored (Thierfeldt, 2009; Drouet, 2012). Other countries such as Canada, Japan and United States have issued advisories to their airline industries to manage aircraft crew exposure e.g. FAA advisory circular in the United States (FAA, 2014). Based on recent scientific information of the biology and physics of radiation exposure, the recommendations by ICRP 60 (ICRP, 1991), ICRP 74 (ICRP, 1996) and ICRP 75 (ICRP, 1997) and were revised and ICRP Publications 103 (ICRP, 2007) and ICRP 132 (ICRP, 2016) have been issued. Furthermore, by 2018, the EU Member States had to adapt their laws to comply with the Council Directive 2013/59/EURATOM of 5 December 2013 (EU, 2014). This EU Council Directive sustains the earlier BSS stating that appropriate measures have to be undertaken when the effective dose to aircraft crew is liable to be above 1 mSv per year. It then identifies the following four protection measures:

- to assess the exposure of the crew concerned
- to take into account the assessed exposure when organising working schedules with a view to reducing the doses of highly exposed crew
- to inform the workers concerned of the health risks their work involves
- to apply the same special protection during pregnancy to female crew in respect of the 'child to be born' as to other female workers

In practice, various models are currently used to assess the dose due to GCR on-board aircrafts (EURADOS, 2012). Most of them are used on a routine basis for occupational dosimetry as they have been validated by GCR measurements (EURADOS, 2004; EU, 2004; Lillhök, 2007). Regarding solar particle events, calculation models exist but most are not used on a routine basis in particular because they are not completely validated by experimental data, which is still needed (Beck, 2008). The objective of this report is to compare the existing models used for evaluation of doses due to SPE at aircraft altitudes.

2. Objective of the Report

The aim of this report is to compare radiation dose rates and flight route doses calculated by various codes for which the providers have agreed to perform the calculations. This objective has been set in the view of the fact that dose measurements on-board aircraft during solar energetic particle events are very rare (e.g. Beck, 2009b) and therefore measurement-code comparisons are difficult to carry out (e.g. Beck, 2008). This comparison is of major importance to support the harmonization of aircrew dosimetry practices in European countries.

The study was conducted for a set of representative flight routes around the globe. The results are presented in an anonymous way. In particular, the spread in both the ambient dose equivalent and the effective dose is discussed. The report may provide some idea of whether the calculated doses agree with each other within a range that can be accepted for purposes of radiation protection to estimate the radiation exposure during energetic solar particle events.

Because using codes and models for the assessment of aircrew doses due to GCR is a common practice and measurements on-board aircraft during solar energetic particle events are very rare, further research to improve the calculation of doses due to SEP is expected and it is supported by this report.

3. Radiation Exposure at Aviation Altitudes

3.1 Quantities used for dosimetry

Effective Dose

The effective dose, E, is the radiation protection quantity defined as the tissue-weighted sum of the equivalent doses in all specified tissues and organs of the body, given by the expression:

$$E = \sum_{T} w_T H_T = \sum_{T} w_T \sum_{R} w_R D_{T,R} \qquad \text{Equation 1}$$

where H_T is the equivalent dose in a tissue or organ T given by $\sum_{R} w_R D_{T,R}$; $D_{T,R}$ is the mean absorbed dose from radiation type R in a tissue or organ T, and w_R and w_T are the radiation and tissue weighting factors, respectively, defined by the ICRP (ICRP, 1991; ICRP, 2007). The SI unit for the effective dose is joule per kilogram (J/kg) and its special name is sievert (Sv) as defined in ICRU 51 (ICRU, 1993).

According to ICRP 103 (ICRP, 2007) use of the effective dose is recommended for *"the prospective dose assessment for planning and optimisation in radiological protection, and demonstration of compliance with dose limits for regulatory purposes"*. It is also recommended that the effective dose should not be used *"for epidemiological evaluations, nor should it be used for detailed specific retrospective investigations of individual exposure and risk"*.

The body-related protection quantities (equivalent dose and effective dose) are not measurable in practice. However, codes used routinely for aviation dosimetry should be able to assess the effective dose.

Ambient dose equivalent

The ambient dose equivalent, $H^*(10)$, is one of the operational quantities used as an estimator of the effective dose and is defined by ICRP 103 as follows: "*The ambient dose equivalent, H*(d), at a point in a radiation field is the dose equivalent that would be produced by the corresponding expanded and aligned field in the ICRU sphere at a depth, d (in mm), on the radius opposing the direction of the aligned field. The unit of ambient dose equivalent is joule per kilogram (J/kg) and its special name is sievert (Sv)"*.

Codes calculating the doses at aviation altitudes can be validated by comparing the measured route ambient dose equivalent $H^*(10)$ or ambient dose equivalent rates to the calculated values. For validation purposes, all codes should be able to calculate $H^*(10)$.

The codes involved in this comparison provided ambient dose equivalents or effective doses or both. It should be mentioned here that in the ICRP 103 recommendations (ICRP, 2007) the tissue- and radiation weighting factors – among others – have changed compared to the earlier ICRP 60 recommendations (ICRP, 1990). The new European Union Council Directive 2013/59/EURATOM of 5 December (EU, 2014) directly calls for the implementation of the ICRP 103 recommendations and in 2018, the EU Member States should have adapted their laws to comply with it. The consolidation of this report was earlier and effective dose values presented here base on the previous ICRP 60 recommendations (ICRP, 1991). Nevertheless, initial investigations (Sato, 2009; Mares, 2009; Meier, 2019) show that implementation of the new ICRP 103 recommendations result in a decrease of estimated effective dose values. The decrease has been predominantly attributed to the changed radiation weighting factors for protons (radiation weighting factor of 2 instead of 5) and neutrons (a continuous function instead of a step function).

3.2 Cosmic radiation field

Primary cosmic radiation at the top of the Earth's atmosphere includes a continuous galactic component and a sporadic solar component. Both components consist mainly of protons and to a lesser extent of helium and heavier ions. The intensity of galactic cosmic rays near Earth is modulated by the characteristics of the interplanetary magnetic field varying with solar activity. The intensity of the sporadic solar cosmic radiation at the top of the Earth's atmosphere depends on the magnitude of the energetic particle event at the Sun, the location where the solar particles are accelerated, and the configuration of the interplanetary magnetic field linking this source location with the Earth. Both components, i.e. the galactic and the solar cosmic radiation, are affected by the geomagnetic field. For this reason, the cosmic radiation field at the top of the atmosphere depends on the geomagnetic location and the geomagnetic field strength. Shielding by the geomagnetic field is most effective at low geomagnetic latitudes, and less effective close to the geomagnetic poles.

For the characterization of charged particle-motion in magnetic fields, the parameter magnetic rigidity, P, is generally used (ISO 20785-1). For simplicity, we use "rigidity" for "magnetic rigidity" in the whole document. Rigidity is momentum per charge and is a canonical unit that is especially useful because all particles having the same rigidity, charge sign, initial location, and direction of movement will have identical trajectories in the magnetic field, independent of elemental or isotopic composition, particle mass or atomic charge (Smart, 2000). The parameter used to quantify the shielding effect of the Earth's magnetosphere is the geomagnetic cutoff rigidity, P_c. Geomagnetic cutoff rigidity depends on the location, the angle of particle incidence, and geomagnetic activity. Often, vertical incidence to the Earth's surface is assumed, in which case the effective vertical geomagnetic cutoff rigidity is interpreted as the minimum magnetic rigidity a vertically incident particle can have and still reach a given location above the Earth (ISO 20785-1). A detailed discussion of cosmic ray cutoff terminology and a description of the calculation procedure for the effective cutoff rigidity can be found elsewhere (Cooke, 1991). The standard procedure for the determination of cutoff rigidities is the trajectory computations of cosmic ray particles in a model magnetic field given for example in (Smart, 2000).

Particles of cosmic radiation that penetrate into the atmosphere produce a complex field of secondary particles including, for example, protons, neutrons, electrons, positrons, photons, muons, and pions. The energy range involved covers many orders of magnitude and depends on particle type. Due to the competing processes of secondary particle production and absorption, the relative contribution to the radiation exposure of different particles depends on the altitude (see Figure 2). At typical flight altitudes, the major contribution to the effective dose is caused by neutrons, protons, and electrons. More details on the various parameters that influence the doses due to cosmic radiation in aviation are given for example in (EURADOS, 2004; EU, 2004).

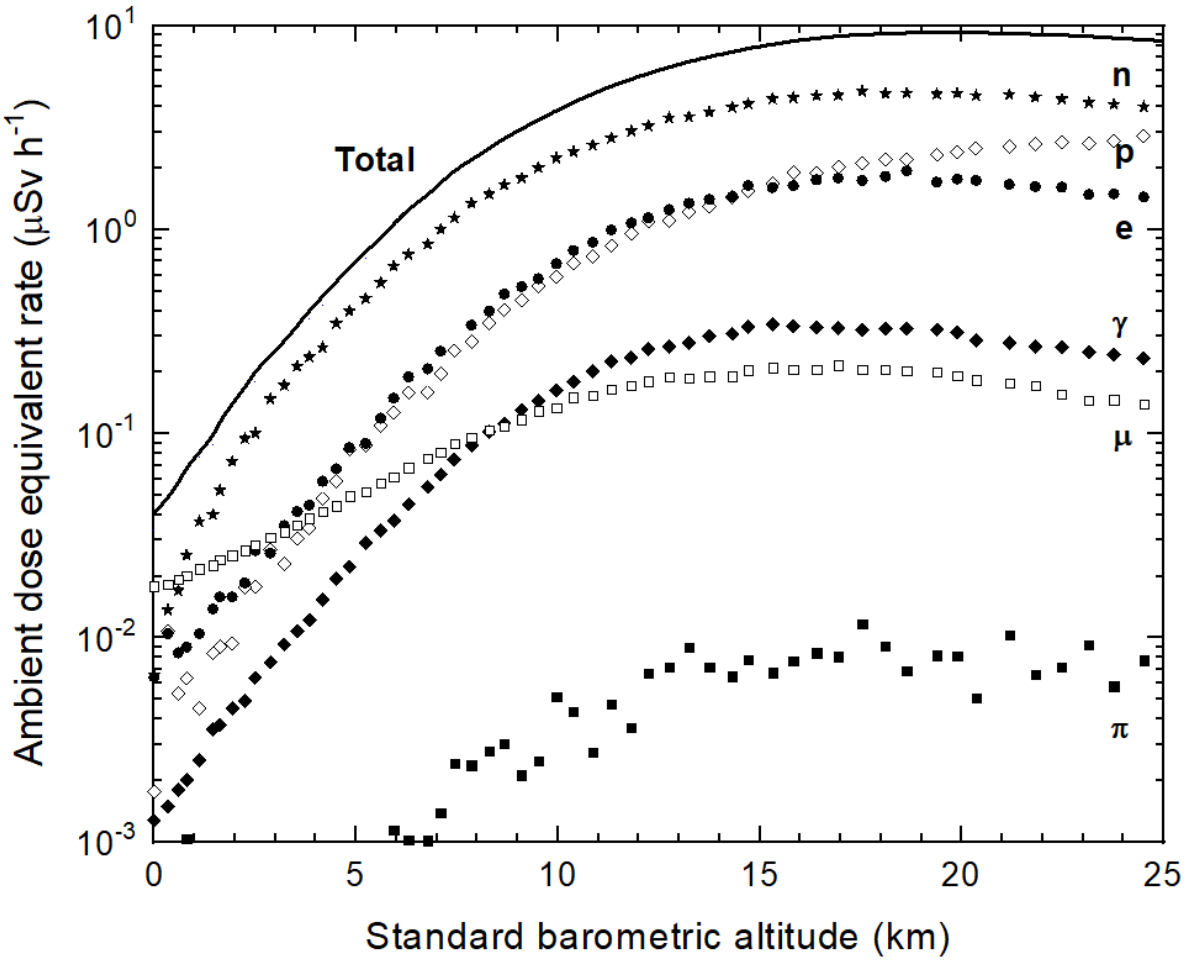

Figure 2: Ambient dose equivalent rate as a function of standard barometric altitude at 2 GV vertical geomagnetic cutoff rigidity and mid solar cycle, for various particles of the cosmic radiation field in the atmosphere calculated using the Monte Carlo radiation transport code FLUKA (ICRU, 2010).

3.3 Solar particle events and spectral data

A solar particle event is a large flux of energetic particles of solar origin accelerated and ejected into space in association with an eruptive high-energy solar process (Shea, 1990). Such events occur at random and are at present stage not predictable in time and intensity (Shea, 1999).

Major solar particle events consist primarily of energetic protons and electrons and are therefore often termed as "solar proton events", but may also contain a variable flux of ions of heavier elements as well as of neutrons as described for example in (Reames, 2004; Mewaldt, 2005).

The Earth's atmosphere provides a minimum shielding mass at flight altitude of about 180 g/cm at 12.5 km (41 000 ft) (NASA, 1976). The minimum energy a proton must have at the top of the atmosphere to penetrate this shielding and reach the corresponding altitude is approximately 600 MeV (NIST, 2019). Through indirect processes, however, especially the production of a secondary neutron field, also protons of lower energies can affect the radiation dose at aviation altitudes. The contribution of protons below this threshold depends on the primary spectrum on top of the atmosphere. For GCR, for which the spectrum at these energies is flat or even decreasing to lower energies, the contribution below the threshold is negligible (Figure 1).

The Earth's magnetic field also acts as a natural shield against the charged cosmic ray particles. The minimum rigidity that a charged cosmic ray particle must have to penetrate the geomagnetic field and to access the upper atmosphere from the vertical direction increases from 0 GV at the Polar Regions to a maximum value of 17 GV in the equatorial regions (see Figure 3).

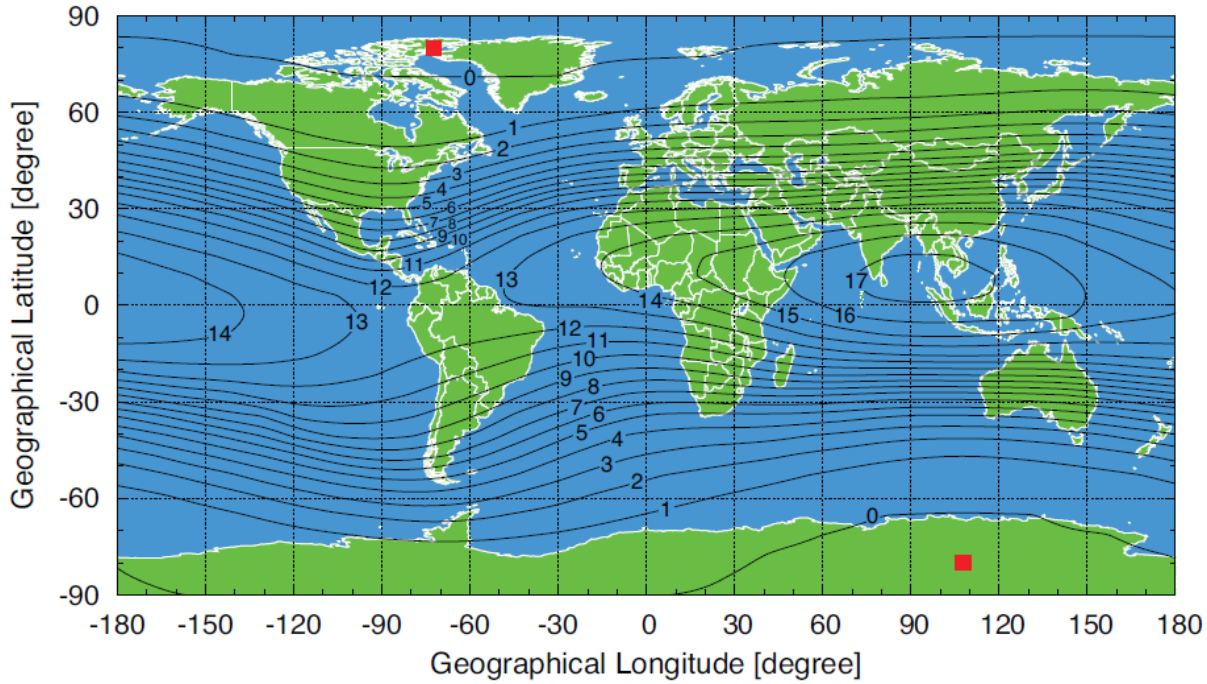

Figure 3: World map with computed geomagnetic vertical cutoff rigidity (in GV) contour lines for years 2010 to 2015, and quiescent geomagnetic conditions (Finlay, 2010a, b; Macmillan, 2011) and the model by Tsyganenko, 1989. Red squares indicate the positions of the magnetic poles in the year 2010 (Pioch, 2012).

Some of the SPEs are long enough in duration and produce particles with intensities and energies high enough to cause, when they hit the Earth, a significant increase of radiation exposure observed at flight altitudes and on the ground.

Figure 4 shows the number of GLEs per year from 1955 (beginning of solar cycle 19) until December 2017 (end phase of solar cycle 24) and the smoothed sunspot number (WDC-SILSO, Royal Observatory of Belgium, Brussels). The frequency of occurrence of GLEs is correlated with the ~11-year solar activity cycle. On a long-term average, about one GLE occurs per year. They are most prevalent during periods of intense solar activity. It is important however to note that significant solar particle events have also occurred during solar minimum, and there can be relatively long periods between individual events. Several events may also occur in clusters during a few successive days or weeks.

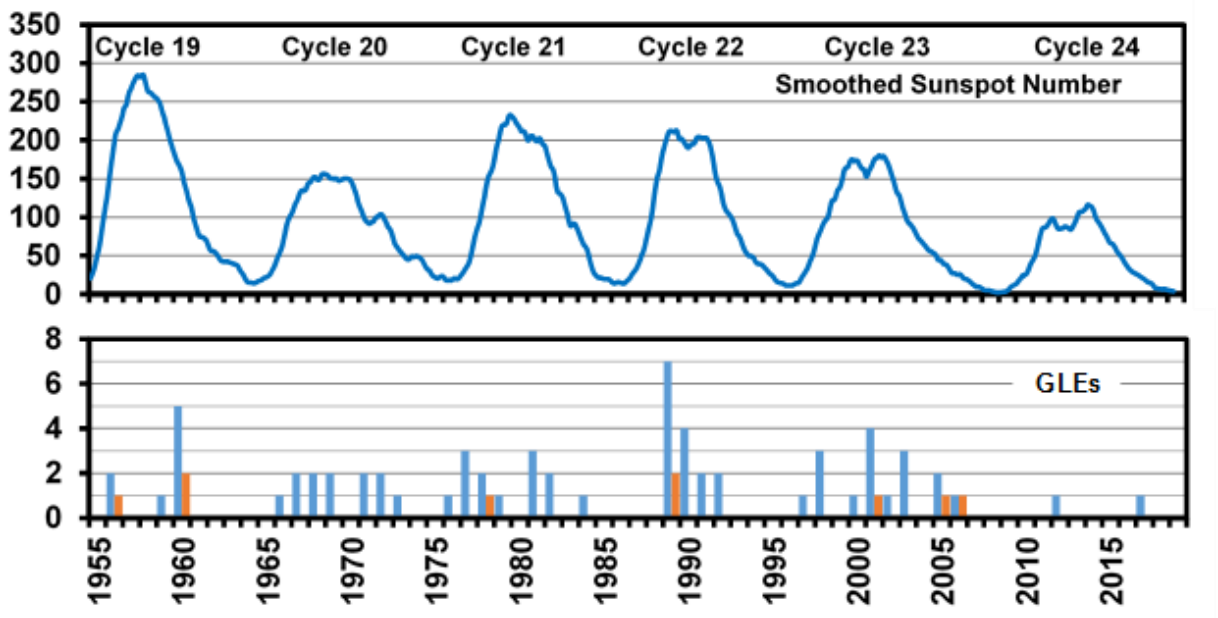

Figure 4: Smoothed sunspot number (top panel, source: WDC-SILSO, Royal Observatory of Belgium, Brussels) and the number of GLEs per year (bottom panel) during the solar cycles 19 - 24 (until December 2017). Blue bars: all GLES, red bars: GLEs with amplitude >70%. Figure after Shea and Smart, 1993 (Shea, 1993).

Significant dose rate increases at flight altitude are associated with GLEs. Minor particle events, which may be registered by detectors in space but not by sea-level neutron monitors, are expected to have a minor or no effect on the radiation exposure at aviation altitudes due to atmospheric and geomagnetic shielding. The standard ground-based detector for the continuous monitoring of cosmic rays since the International Geophysical Year 1957/58 is the neutron monitor (NM). Using the Earth's magnetic field as a giant spectrometer the worldwide NM network is still the state-of-the-art instrument for the quantitative investigation of the near-Earth spectral changes of the cosmic radiation in the energy range from about 450 MeV to 15 GeV. The NM database, Mares, 2004 (Mares, 2004) established between 2008 and 2009 (www.nmdb.eu) provides a unified web-based access to the data and a unique online tool for real-time applications such as e.g. GLE alerts. A comprehensive list of GLEs dates back to 1942. The GLE database with recorded neutron monitor count-rates during GLEs is currently maintained by the University Oulu (gle.oulu.fi).

GLEs are different from event to event. The duration of a GLE may last from a few minutes up to a few hours. Two examples illustrating the variety in the intensity-time records at different locations are shown in Figure 5: for GLE69 on 20 January 2005 and Figure 6 for GLE71 on 17 May 2012.

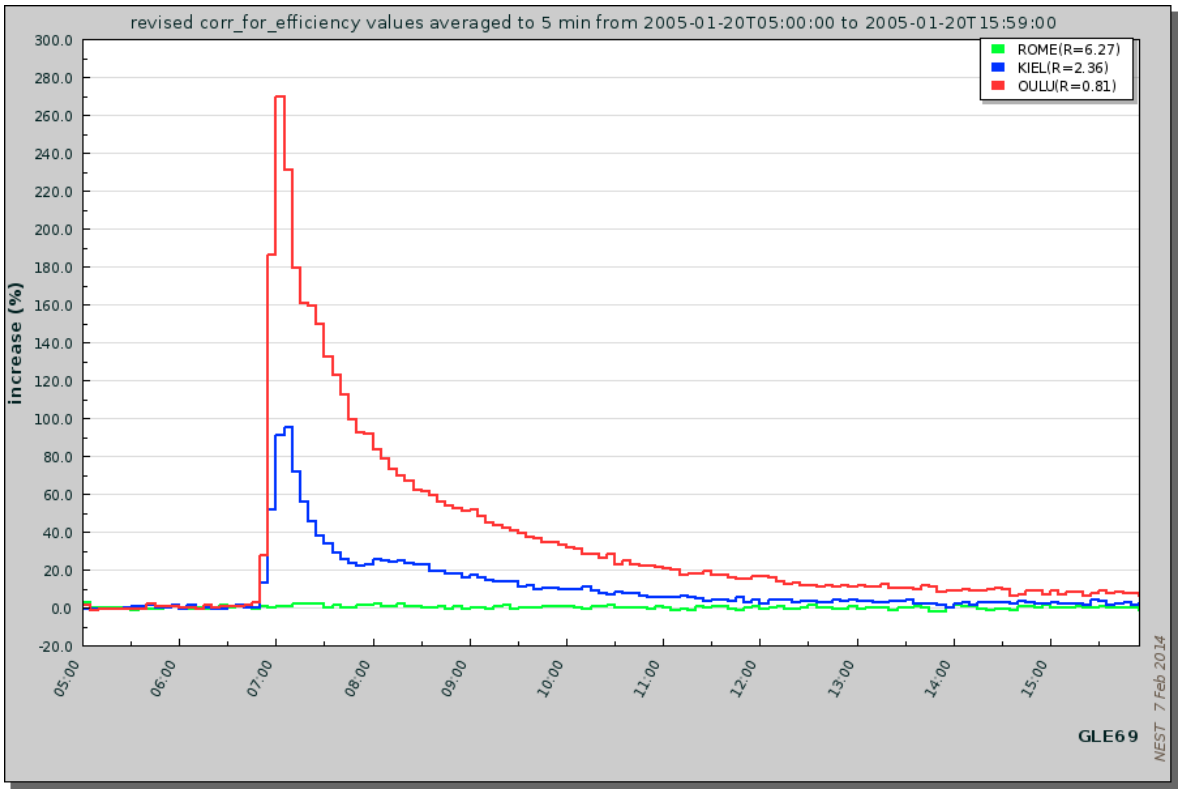

Figure 5: Relative 5 minutes count rate values for the neutron monitor stations Oulu (red), Kiel (blue), and Rome (green) plotted with NEST from www.nmdb.eu for the time interval 05:00-16:00 UT on 20 January 2005 (GLE69).

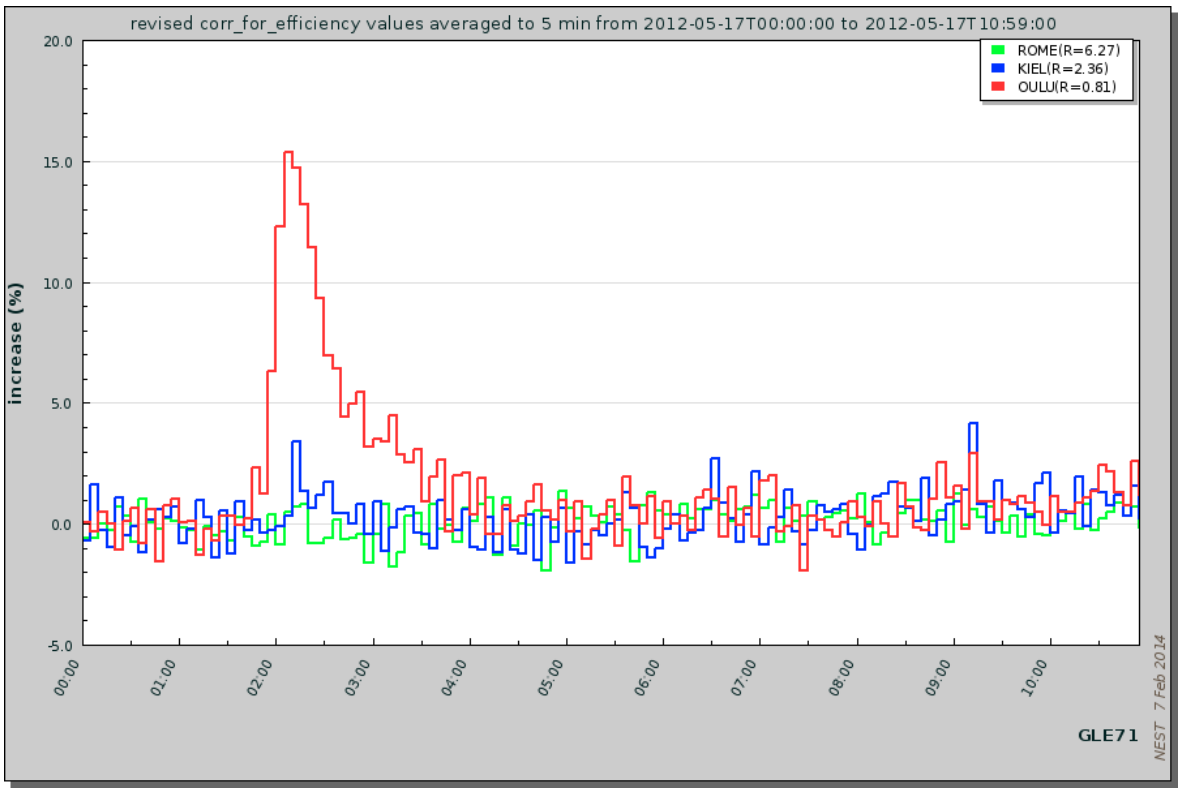

Figure 6: Relative 5 minutes count rate values for the neutron monitor stations Oulu (red), Kiel (blue), and Rome (green) plotted with NEST from www.nmdb.eu for the time interval 00:00-11:00 UT on 17 May 2012 (GLE71).

The near-Earth solar particle flux during a GLE is usually described by the following time dependent characteristics:

- composition
- anisotropy
- spectral form
- size

Composition:

The most pronounced component of the solar particle flux causing a GLE is protons. For specific applications however, and especially higher up in the atmosphere and in space, ions of heavier elements have to be considered as provided for example in (Tylka, 1997).

Anisotropy:

During solar cosmic ray events and especially in the initial phase of the events, the intensity of the primary particles is often anisotropically distributed. In these cases, additional information about the angular distribution of the particle flux is necessary to describe accurately the event and the related increase in particle intensity on top of the atmosphere and at aviation altitudes. Later in the event, the particle flux becomes more and more isotropic. As an example Figure 7 shows the relative count rate increases at the two polar neutron monitor stations Thule (76.5N, 68.7W) and Terre Adélie (66.65S, 140.0E) during GLE69 on 20 January 2005 (top) and the anisotropy, *a*, according to the formula:

$$\boldsymbol{a(t) = \frac{(\delta N(t)_{Terre\ Adélie} - \delta N(t)_{Thule})}{(\delta N(t)_{Terre\ Adélie} + \delta N(t)_{Thule})}} \qquad \textit{Equation 2}$$

where

$\delta N(t)_{Terre\ Adélie}$ is the value of the relative count rate increase at a given time t at the NM station Terre Adélie referring to the pre-increase baseline time interval 05:00-06:00 UTC and

$\delta N(t)_{Thule}$ is the corresponding value for the NM station Thule

In this event, the neutron monitor count rate increases at Terre Adélie and Thule are representative for the solar particle fluxes near Earth arriving from the Sun along the field lines of the interplanetary magnetic field (Terre Adélie) and of the opposite direction (Thule).

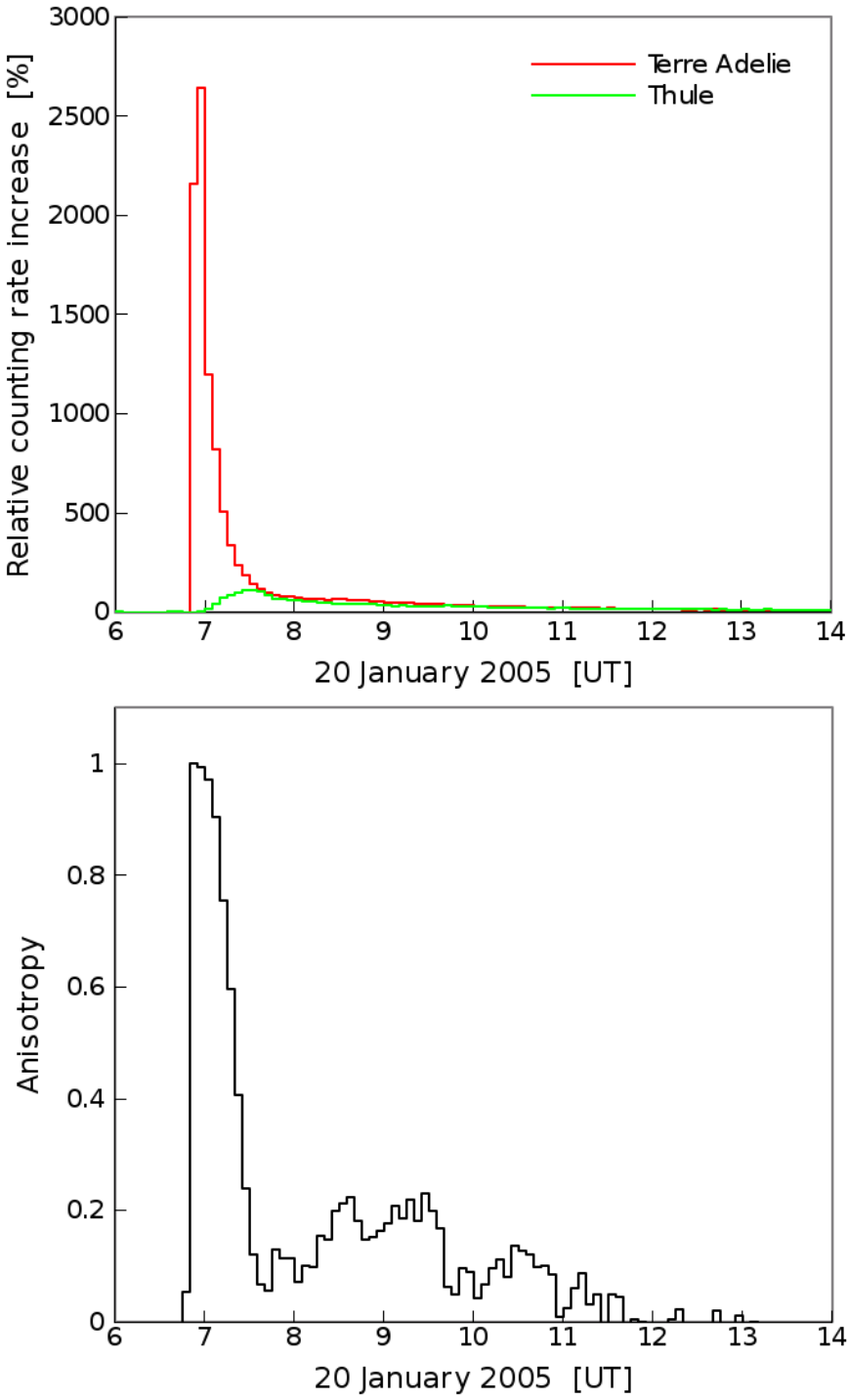

Figure 7: Relative count rate increases of the two polar neutron monitor stations Thule (76.5N, 68.7W; green) and Terre Adélie (66.65S, 140.0E; red) during GLE69 on 20 January 2005 (top) and the anisotropy according to Equation 2 (bottom).

Spectral form:

The fluence and peak flux spectra of solar energetic particles at $T > 30$ MeV are usually described by a simple power-law function of kinetic energy, T, or rigidity, P, (Mottl, 2001):

$$dI/dT \propto T^{\gamma} \quad \text{Equation 3}$$

$$dI/dP \propto P^{\gamma} \quad \text{Equation 4}$$

or a modified power law according to Ellison and Ramaty (Ellison, 1985).

The exponent γ varies from event to event, and it also changes during the course of an event. Typical values are in the range 4-6.

Size:

Several quantities are used to characterize the size of a solar particle event, e.g.

- maximum neutron monitor count rate increase
- peak particle intensity
- amplitude of event-integrated flux at 1 GeV
- event integrated fluence

For the determination of the GLE characteristics based on data of the worldwide NM network, the response of the NMs as well as the effect of the geomagnetic field on the particle trajectories must be known.

The response of a NM station i to relativistic solar protons can be expressed in the following simplified form:

$$\Delta N_i(t) = \int_{P=P_{Ci}}^{\infty} dP \cdot S_i(P) \cdot J_{||}(P,t) \cdot F(\delta_i(P),t) \quad \text{Equation 5}$$

where

$\Delta N_i(t)$ is the absolute count rate increase due to solar protons as function of time t,

P_{ci} is the effective vertical geomagnetic cutoff rigidity,

P is the particle rigidity,

$S_i(P)$ is the yield function for protons,

$J_{||}(P,t)$ is the directional solar proton flux in the presumed source direction,

$F(\delta_i(P),t)$ is the pitch angle distribution of solar particles with respect to the source direction,

$\delta_i(P)$ is the pitch angle, i.e. angular distance between the particle arrival direction (asymptotic directions) and the apparent source direction outside the geomagnetosphere for particles of vertical incidence at the specific neutron monitor location.

Yield functions for neutron monitors have been determined and published by different authors; for an overview see (Mishev, 2013). The cutoff rigidities and asymptotic directions are obtained by trajectory calculations in geomagnetic field models (Cooke, 1991; Smart, 2000). The GLE characteristics can then be determined by minimizing the squared differences between ΔN_{calc} and ΔN_{obs} for the selected set of NM data (Smart, 1971; Debrunner, 1980; Cramp, 1997). Typically, 5-10 parameters have to be determined with the data of ~20-30 NM stations. The determination of the GLE parameters is made either by a trial and error procedure or by a fitting algorithm. The least square fit must be repeated with widely varying initial parameter values to ensure finding the absolute minimum in the parameter space.

Figure 8 and Figure 9 summarize results obtained according to this procedure for the GLE60 on 15 April 2001 by different authors (Plainaki, 2010; Bombardieri, 2007; Matthiä, 2009; Vashenyuk, 2005).

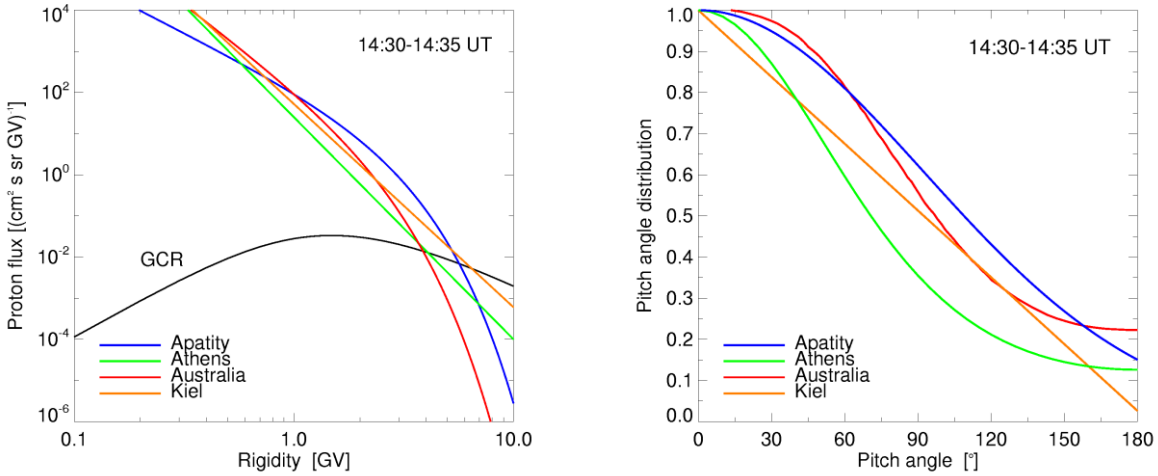

Figure 8: Solar cosmic ray spectra (left) and pitch angle distributions (right) during the main phase of GLE60 on 15 April 2001 as derived by the author groups: Vashenyuk et al., 2005 (Apatity), Plainaki et al., 2010 (Athens), Bombardieri et al., 2007 (Australia) and Matthiä, 2009 (Kiel). Figure from Bütikofer et al., 2013.

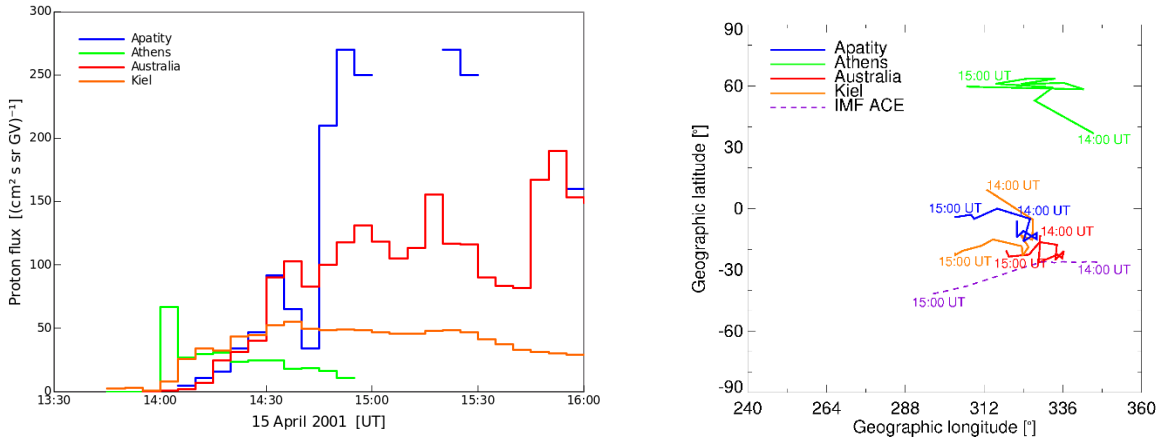

Figure 9: Solar cosmic ray flux at 1 GV in the direction of maximum intensity (left) and apparent arrival directions in GEO coordinates (right) during GLE60 on 15 April 2001 as derived by the author groups: Vashenyuk et al., 2005 (Apatity), Plainaki et al., 2010 (Athens), Bombardieri et al., 2007 (Australia) and Matthiä, 2009 (Kiel). Figure from Bütikofer et al., 2013.

4. Models Selected for this Study

Information on different codes used in this study is summarized in Table 1 and described more in detail in Appendix 1: Description of Models. Some of the codes are based on Monte Carlo simulations: AVIDOS, EPCARD, WASAVIES/JISCARD EX, PANDOCA, PLANETOCOSMICS (Bern code), and QARM. The SIEVERT/SiGLE code uses a worldwide grid of dose rates calculated with EPCARD for the GCR component and a semi-empirical model mainly based on measurements for SEP events. Other codes are based on measurements only (FDOScalc, PCAIRE) and some use the $E/H^*(10)$ conversion as calculated by some Monte Carlo codes.

Operational dose assessment with AVIDOS 2.0 code is accredited according to the testing laboratory standard EN ISO/IEC 17025, which is worldwide valid in ILAC member countries (International Laboratory Accreditation Cooperation)[1]. The SIEVERT and SiGLE codes are in operational use in France for the monitoring of radiation doses from galactic cosmic rays and solar energetic particles[1]. Versions of the PANDOCA, EPCARD, and PCAIRE codes are approved by the civil aviation authority in Germany for the assessment of occupational exposure of aircrew due to GCR[1]. For this comparison, however, the scientific version of PCAIRE, which is not approved in Germany, was used. All other codes are scientifically used by the responsible institutes.

A detailed discussion of the uncertainties of the calculation models is beyond the scope of this report. For some of the calculation models and for some aspects, in particular for accredited methods, uncertainties are provided within the descriptions of the calculation models. For basic considerations in this regard, we refer to further work (ICRU, 2010; Behrens 2010; EURADOS, 2012).

[1] At the time of the editorial meeting.

Table 1: Summary of the codes used in this study for the calculation of the radiation exposure at aircraft altitudes due to cosmic radiation.

Code / Model	SCR Input data	SCR Dose Assessment Approach	GCR Input Data	GCR Dose Assessment Approach	Reference
AVIDOS 2.0 / SOLARDOS	- neutron monitor data - primary time dependent SCR characteristics (isotropic spectrum)	GEANT4 (PLANETOCOSMICS), ICRP60 / 103 (ICRP, 1991; ICRP, 2007)	(Gaisser, 2001) (Beck, 2007)	FLUKA,GEANT4 (PLANETOCOSMICS), ICRP60 / 103 (ICRP, 1991; ICRP, 2007)	(Beck, 2007) (Latocha, 2009) (Latocha, 2016)
EPCARD.Net 5.4.3 / GEANT4-GLE Module	- primary time dependent SCR characteristics (isotropic spectrum) - neutron monitor database (NMDB)	GEANT4 (HMGU-Application), ICRP60	(Badhwar, 1996) (Burger, 2000)	FLUKA, GEANT4 (HMGU-Application), ICRP60	(Roesler, 2002), (Mares, 2009), (Pioch, 2012) www.helmholtz-muenchen.de/epcardnet
FDOScalc 2.0	Not applied	semi-empirical	n.a.	semi-empirical	(Schrewe, 2000) (Wissmann, 2006) (Wissmann, 2010)
JISCARD EX WASAVIS	n.a.	Determination of SEP flux Air-shower simulation by PHITS ICRP60 / 103	(Nymmik, 1992)	PHITS-based analytical code PARMA ICRP60 / 103	(Yasuda, 2011) (Sato, 2008; 2014) (Kataoka, 2014)
PANDOCA	- neutron monitor data - primary, time dependent SCR characteristics (anisotropic spectrum) - satellite data	GEANT4 (PLANETOCOSMICS), ICRP60	(Matthiä, 2013)	GEANT4 (PLANETOCOSMICS), ICRP60	(Matthiä, 2009) (Matthiä, 2009a) (Matthiä, 2014)
PCAIRE	not applied	semi-empirical	n.a.	n.a.	(Lewis, 2001) (Lewis, 2002) (Lewis, 2004) (Takada, 2007)
BERN GLE Model	- neutron monitor data - primary time dependent SCR characteristics (anisotropic spectrum)	GEANT4 (PLANETOCOSMICS), ICRP60	(Gleeson, 1968a) (Garcia, 1975) (Caballero, 2004) Heliocentric potential from https://www.faa.gov/data_research/research/med_humanfacs/aeromedical/media/MV-DATES.zip	GEANT4 (PLANETOCOSMICS), ICRP60	(Desorgher, 2005) (Desorgher 2006)
QARM 1.0	n.a.	n.a.	(Badhwar, 2001)	n.a.	(Lei, 2004) (Lei, 2006) (Dyer, 2007) (mcnpx.lanl.gov)
SIEVERT PN 1.0, SiGLE	- neutron monitor data - primary, time dependent SCR characteristics (including North/South anisotropy)	semi-empirical, ICRP60	(Badhwar, 2001)	EPCARD.NET 5.4.3, ICRP60	(Lantos, 2003a) (Lantos, 2003b) (Lantos, 2004) (Lantos, 2006) (sievert-system.org) (Bottollier-Depois, 2007)

5. Comparison of Doses in Case of Solar Particle Events as Assessed by Selected Models

Nine models for the calculation of radiation exposure at aviation altitudes during solar energetic particle events are compared in two different investigations.

In the first investigation, the primary solar particle spectrum was pre-defined and distributed to the contributors to avoid uncertainties arising from differences in the primary particle spectrum. The definition of the primary particle spectrum was based on the ground level enhancement GLE42 on 29 September 1989. It has to be emphasized that the defined input parameters are not identical to the real event. Rather, the real event was used as a guideline for the creation of a hypothetical event, in the following also called "simplified GLE42" event.

In the second investigation of the comparison, information about publications concerning the GLE69 on 20 January 2005 was provided to the contributors. It was left to the different groups how the input parameters for the primary spectrum were derived using the provided publications or other means.

The radiation dose rates during a GLE due to the GCR radiation field depends on the respective solar cycle modulation. For the two GLEs investigated, the corresponding GCR modulation is illustrated in Figure 10. The reference doses due to GCR had to be assessed by each contributor individually, using his own model.

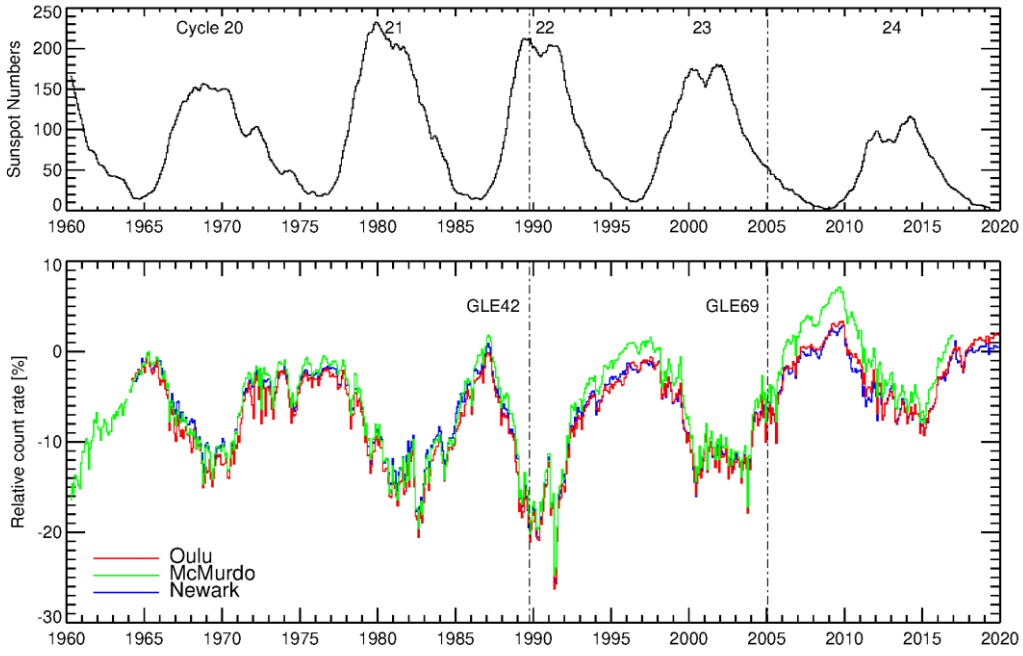

Figure 10: Smoothed sunspot numbers (top panel), pressure corrected monthly counting rates of the neutron monitor stations Oulu, McMurdo, and Newark (bottom panel) for the years 1960-2019. The neutron monitor count rates are expressed in relative units with respect to May 1965. The vertical dashed-dotted lines indicate the time of the GLEs on 29 September 1989 (GLE42) and on 20 January 2005 (GLE69). The neutron monitor at McMurdo stopped operation in January 2017 and was moved to Jang Bogo.

The codes used in this comparison handle input data in different formats. Therefore, it was necessary for each participant to prepare his own input file fitting the specific data format of his code. The participants were themselves responsible for data transfer.

5.1 Characteristics of selected ground level enhancements

5.1.1 Ground level enhancement GLE42

The differential solar cosmic flux during the simplified GLE42 is based on the paper by Smart et al. (1991). The analyses by Smart et al. (1991) and also by other authors have shown that a modified power law rigidity spectrum of the solar cosmic ray flux could best fit the measurements of the worldwide neutron monitor network.

For this investigation, we assumed an isotropic solar cosmic ray flux near Earth and a constant rigidity dependence of the spectrum throughout the whole SPE. Only the amplitude varies with time.

The differential rigidity solar cosmic ray flux, $J_{SCR}(P,t) \equiv \frac{dI}{dP}$, as function of rigidity, *P*, expressed in GV, and UTC time, *t*, is described for $P \leq 2$ GV by:

$$J_{SCR}(P,t) = A(t) \cdot \left(\frac{P}{P_0}\right)^{-\gamma} \qquad \text{Equation 6}$$

and for $P > 2$ GV by:

$$J_{SCR}(P,t) = A(t) \cdot \left(\frac{P}{P_0}\right)^{-(\gamma+\delta\gamma\cdot(P/P_0-2))} \qquad \text{Equation 7}$$

where $P_0 = 1$ GV. The amplitude values *A(t)* are listed in Table 2. The power law index is γ=3.0 and δγ=0.3.

As an example the values for $J_{SCR}(P,t)$ are listed in Table 3 for the time interval 13:30-14:30 UTC. Figure 11 shows the rigidity spectrum of the solar protons in the rigidity range 0.4 GV to 20 GV for selected time intervals.

Table 2: Amplitude *A* defined for the simplified GLE.

Time interval in UTC	Amplitude *A* in $(cm^2 \cdot s \cdot sr \cdot GV)^{-1}$
before 11:45	0
11:45 - 12:00	2
12:00 - 12:15	4.2
12:15 - 12:30	6.3
12:30 - 12:45	7.7
12:45 - 13:00	9
13:00 - 13:15	10
13:15 - 13:30	10.3
13:30 - 14:30	10.6
14:30 - 15:30	9.1
15:30 - 16:30	7.5
16:30 - 17:30	4.5
17:30 - 18:30	4
18:30 - 19:30	2.4
19:30 - 20:30	1.5
20:30 - 21:30	0.9
21:30 - 22:30	0.5
after 22:30	0

Table 3: Solar proton flux, $J_{SCR}(R)$, for the time interval 13:30-14:30 UTC

Rigidity in GV	J_{SCR} in $(cm^2 \cdot s \cdot sr \cdot GV)^{-1}$
0.5	84.8
1	10.6
1.5	3.14
2	1.33
3	0.282
5	0.0199
10	$4.22 \cdot 10^{-05}$
20	$1.25 \cdot 10^{-10}$

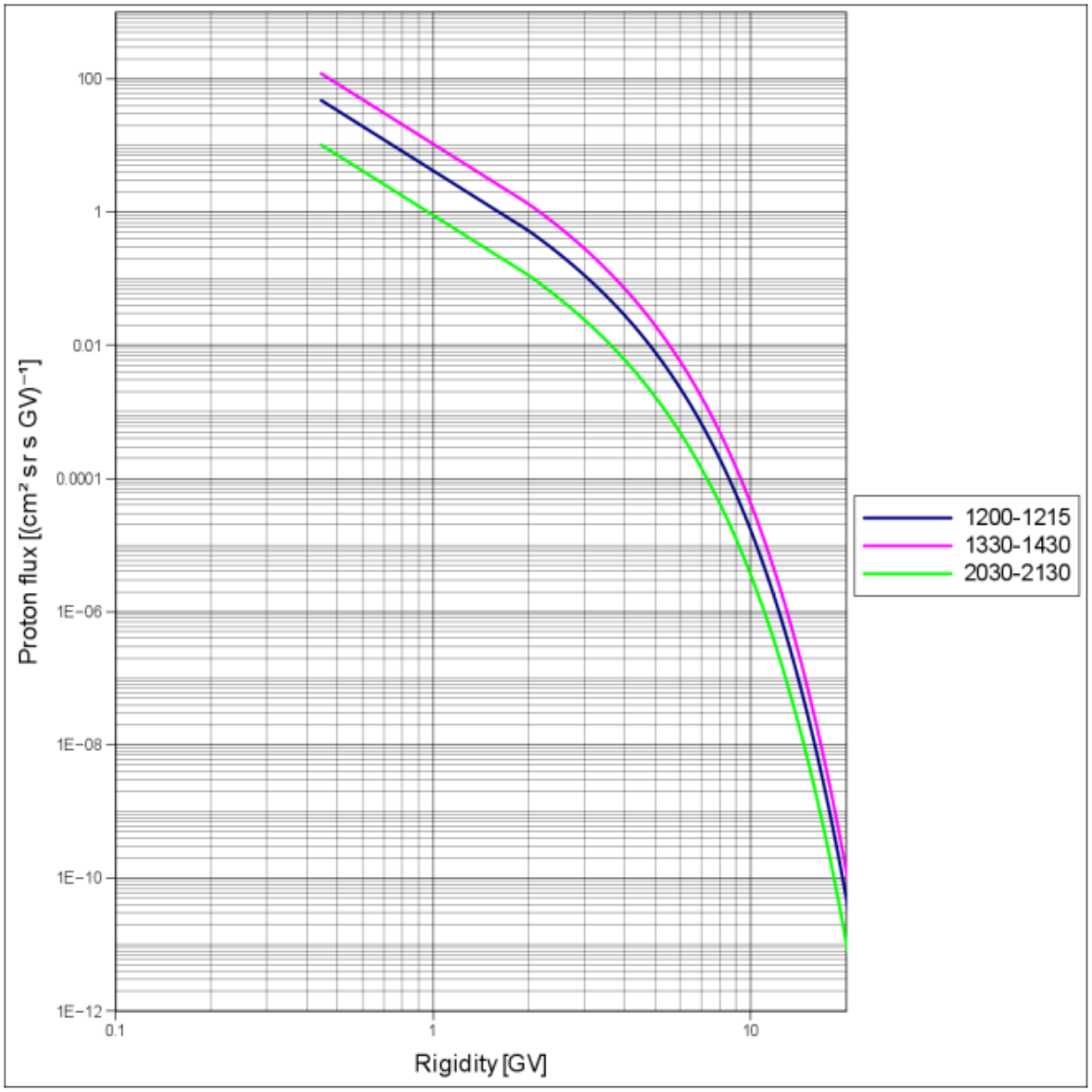

Figure 11: Differential rigidity spectrum for time intervals 12:00-12:15 UTC, 13:30-14:30 UTC, and 20:30-21:30 UTC.

5.1.2 Ground level enhancement GLE69

GLE 69 is the best-observed strong GLE in history, thanks to an extended network of neutron monitors, space-borne particle measurements at lower energies, observations of high-energy photons due to relativistic particles interacting at the Sun (e.g., Simnett 2006; Simnett 2007; Kuznetsov 2008; Grechnev 2008; McCracken 2008; Masson 2009; Klein 2014). This GLE occurred on 20 January 2005 during a very active period toward the end of solar cycle 23. This event is ranked among the largest GLEs since the beginning of neutron monitor records with gigantic relative count rate increases at the south-polar neutron monitor stations McMurdo (almost 3000%), Terre Adélie (4500%), and South Pole (more than 5000%). The GLE lasted for several hours and showed an extreme North-South anisotropy during the initial phase that was seen in the observations of polar neutron monitor stations during the first about 30 minutes of this GLE (see Figure 7 and Figure 12). About one and a half hour after the onset of the event, the relative count rate increases for sea-level neutron monitor stations at northern and southern polar latitudes were comparable (in the order of 70%). Afterwards the intensity could be considered as approximately isotropic, and the relative NM count rate increases remained above 10% until about 7 hours after onset.

The large differences in the NM count rate increases during the initial phase of the event, and the strong temporal dependence of the intensity of the solar energetic particles suggest that a precise analysis of the event in terms of radiation exposure at aviation altitudes can only be achieved with an accurate treatment of the geographical and temporal characteristics of the event. Several publications exist in literature describing this extraordinary GLE both in terms of solar energetic particle spectra and the effect on the radiation exposure in aviation. A list of such publications is given in Appendix 4 and was also provided to the groups participating in this inter-comparison. It was left to the participants to select one or a number of publications to derive the characteristics of the event needed for a calculation of the radiation exposure on the selected, representative flights (Appendix 3).

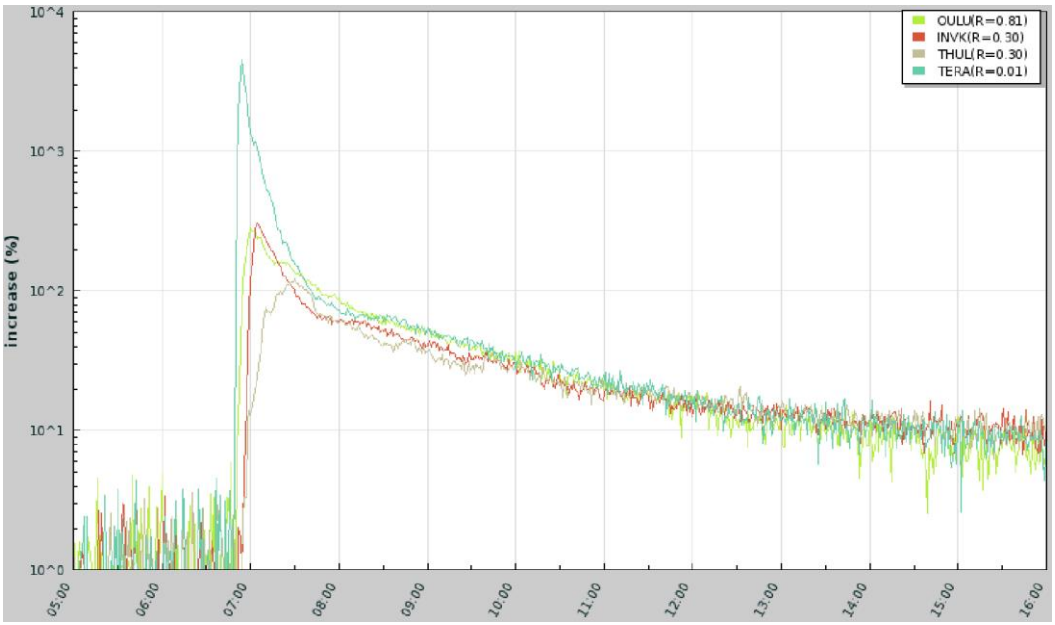

Figure 12: Relative neutron monitor count rate increases of selected stations during GLE69 provided by www.NMBD.eu Responses of neutron monitors in Antarctica, Terre Adélie (TERA), recorded significantly different intensities than stations on the northern hemisphere, Oulu (OULU), Inuvik (INVK) and Thule (THUL).

In the following, we illustrate the effect of the anisotropic solar cosmic ray flux during the onset and main phase of GLE69 on the total (i.e. due to GCR and solar particles) radiation dose rate and radiation dose at flight altitude. In addition to the real, anisotropic case, we show also the simulated global dose rates for the assumed scenario of a fully isotropic near-Earth solar particle flux.

As an example Figure 13 shows the calculated effective dose rate at atmospheric depth of 250 g/cm^2 (ca. 10.5 km) over the northern hemisphere (left) and over the southern hemisphere (right) during the maximum phase of GLE69 based on the GLE characteristics as determined with the data of the worldwide network of neutron monitors (Bütikofer, 2007; Bütikofer 2008). At about 70°S, 135°E the calculated effective dose rate caused by solar cosmic ray was at about 5000 µSv/h for some minutes, whereas the effective dose rate was only about 10 µSv/h near the North Pole during that time.

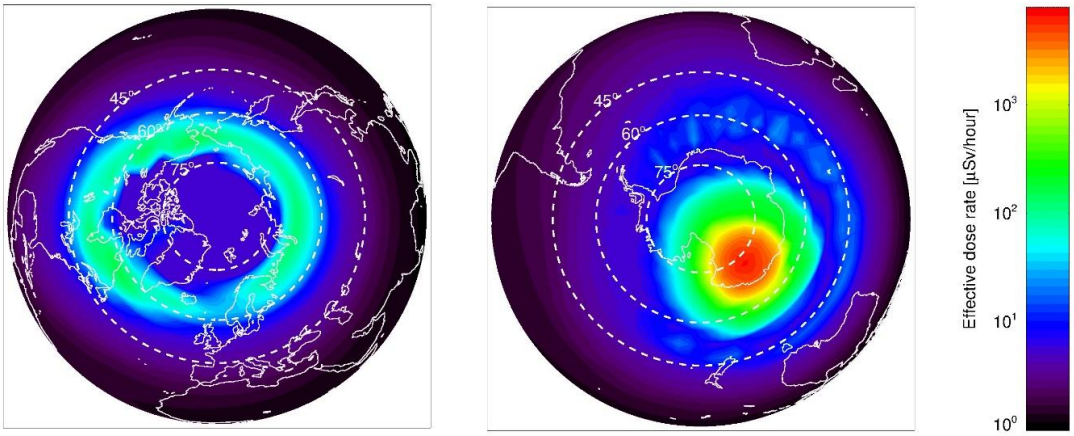

Figure 13: Calculated effective dose rate at 250 g/cm² (ca. 10.5 km, 34 000 ft) over the northern hemisphere (left) and over the southern hemisphere (right) during the maximum phase of GLE69 based on GLE parameters determined from the data of the worldwide network of NM stations.

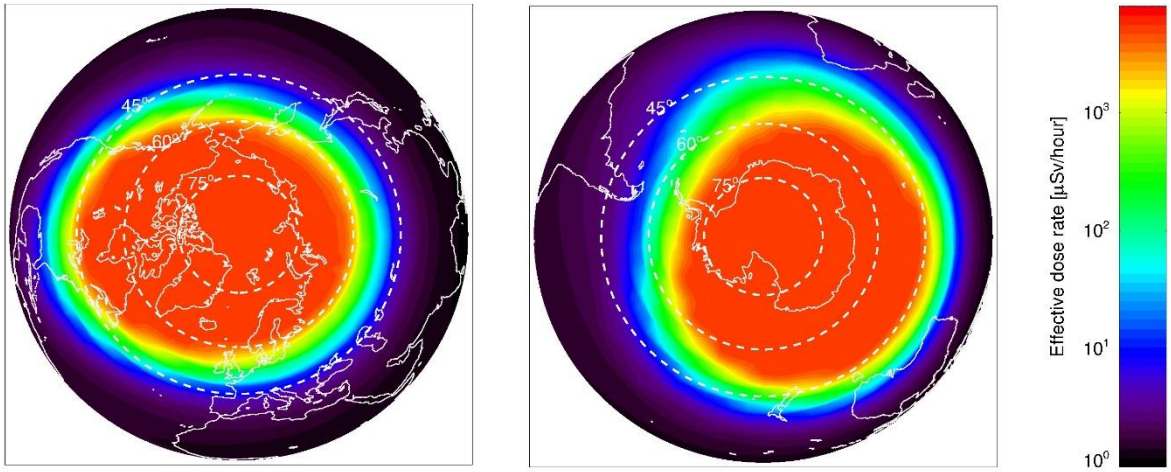

Figure 14: Calculated effective dose rate at 250 g/cm² over the North hemisphere (left) and over the South hemisphere (right) during the maximum phase of GLE69 with the assumption of isotropic solar cosmic ray flux near Earth.

Figure 14 shows the corresponding results assuming a fully isotropic solar cosmic ray flux near Earth. As can be concluded from the comparison with Figure 13, anisotropy effects during energetic solar particle events can be significant. However, in the course of a GLE the flux of the solar particles usually becomes more and more isotropic. This effect is illustrated in Figure 15. There, we show the effect of anisotropy of the solar cosmic ray flux during GLE69 on the ambient dose equivalent rate at an atmospheric depth of 250 g/cm² during the course of the event above the south polar region NM station Terre Adélie (66.65°S, 140.01°E) and above the north polar region NM station Thule (76.50°N, 291.30°E).

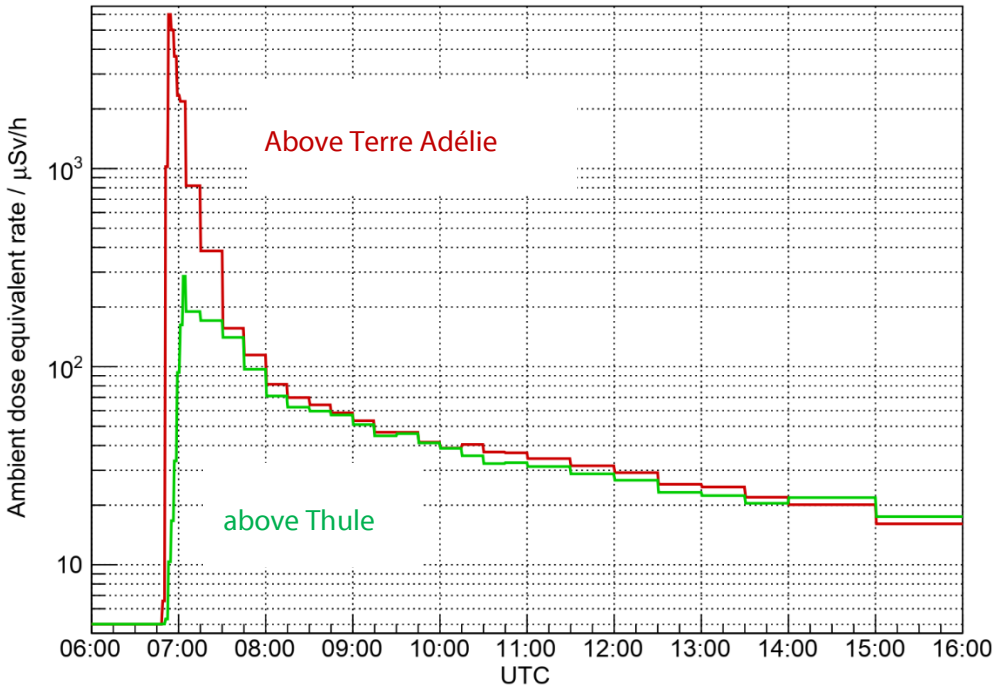

Figure 15: Time evolution of the ambient dose equivalent rate above the neutron monitor stations Terre Adélie (66.65°S, 140.01°E) and Thule (76.50°N, 291.30°E) at an atmospheric depth of 250 g/cm^2 during the GLE on 20 January 2005 based on GLE parameters as determined from the data of the worldwide network of NM stations.

5.2 Characteristics of selected flight routes

5.2.1 Selection of the flight routes

For the comparison, three representative routes flown by passenger aircraft were selected, comparable to the routes used in the EURADOS Report on "Comparison of Codes Assessing Radiation Exposure of Aircraft Crew due to Galactic Cosmic Radiation" (EURADOS, 2012). The route from San Francisco to Paris represents a typical transatlantic flight. The second flight from Chicago to Beijing represents a polar flight route on the northern hemisphere. The third flight from Sydney to Johannesburg represents a polar flight route on the southern hemisphere. The corresponding routes are shown in Figure 16. Two of the routes are classified as ultra-long range flights with durations of more than 13 hours (see Table 4).

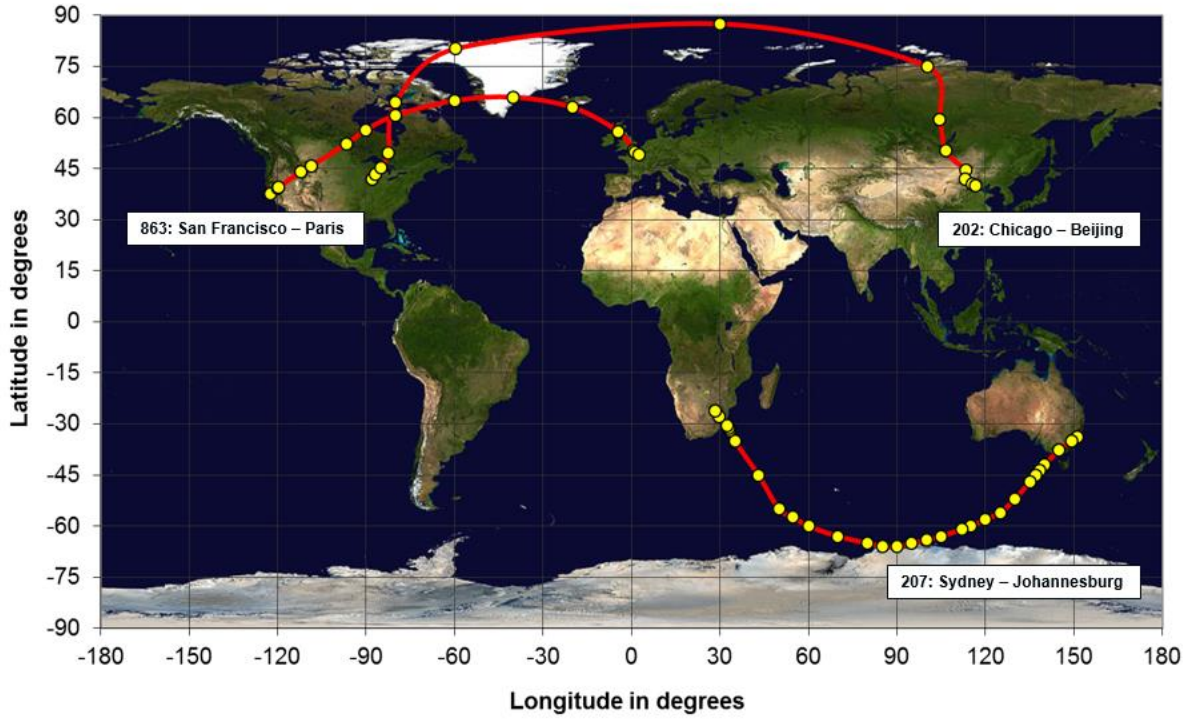

Figure 16: The selected flight routes of the 3 flights investigated (863: San Francisco-Paris, 202: Chicago-Beijing, and 207: Sydney-Johannesburg). Yellow dots denote waypoints with given latitude, longitude, altitude, and time of flight. The solid lines guide the eye between the waypoints. (Map: Courtesy ESA)

Table 4: The three flights investigated with flight durations and maximum altitudes. Detailed flight route data are given in Appendix 2 and Appendix 3.

Flight #	Departure airport (ICAO code)	Destination airport (ICAO code)	Flight duration (hh:mm)	Max. altitude (km)
00863	San Francisco (KSFO)	Paris (LFPG)	09:15	11.9
00202	Chicago (KORD)	Beijing (ZBAA)	13:11	11.3
00207	Sydney (YSSY)	Johannesburg (FAJS)	13:45	11.9

5.2.2 Flight route data

The flight data files for three selected flight routes (see Figure 16) were distributed to the participants in the specific format described below (see also Appendix 2 and Appendix 3).

Each flight data file contains in the first line – the so-called info-line – general information about the flight such as flight number, departure and destination airports in the four-letter alphanumeric code defined by the International Civil Aviation Organization (ICAO), and date and time of scheduled take-off and touch-down in Universal Time Coordinated (UTC). All values are separated by semicolons. As

an example, the first line for flight number 00863 from San Francisco to Paris is shown, with an explanation of the format in Table 5:

```
00863;KSFO;LFPG;29/09/1989;10:20;29/09/1989;19:35;
```

Table 5: Explanations of fields used in the info-line for flight number 00863 from San Francisco to Paris

Field	Explanation
00863	Flight number
KSFO	ICAO code of the departure airport
LFPG	ICAO code of the destination airport
29/09/1989	Take-off date (UTC) (dd/mm/yyyy)
10:20	Take-off time (UTC) (hh:mm)
29/09/1989	Touch-down date (UTC) (dd/mm/yyyy)
19:35	Touch-down time (UTC) (hh:mm)

The following lines – so-called waypoint lines – start with the flight number, followed by air navigation data, separated by semicolons. There are three types of waypoint lines. The first and the last line in the block of waypoint lines are labelled as AER (aerodrome) to indicate the departure or arrival airport. The second and the last-but-one waypoints denote top of climb (TOC) and top of descent (TOD), respectively. Between the TOC and TOD waypoints there are several intermediate waypoint lines (INT) depending on the flight route. Each waypoint flag (AER, TOC, TOD, and INT) is followed by the flight level or elevation, elapsed time, and geographic position (see Appendix 2 and Appendix 3). The flight level (FL) and elevation of airports are defined as barometric altitude in feet divided by 100. The elevation of all airports was set to zero "000". Elapsed time is given in hh:mm format and always begins with 00:00 in the departure waypoint. The geographic coordinates are defined by North (N) and South (S) latitude (lat) in degrees, minutes, and seconds in DDMMSS format, and West (W) and East (E) longitude (long) in DDDMMSS format, respectively. As an example, the line with the common waypoint (INT) is shown below, with an explanation in Table 6.

```
00863;INT;330;00:24;393154N;1193924W;
```

Table 6: Explanations of fields used in the waypoint lines for flight number 00863 from San Francisco to Paris.

Field	Explanation
00863	Flight number
INT	Waypoint flag
330	Altitude (FL)
00:24	Elapsed time (hh:mm)
393154N	Geographical latitude (DDMMSS)
1193924W	Geographical longitude (DDDMMSS)

Apart from the flight route and altitude profile, route radiation doses during a GLE highly depend on the flight times with respect to the time profile of the GLE event. For this investigation, therefore, the departure dates and times of the flights were suitably adjusted to the temporal evolution of GLE42 (Appendix 2) and GLE69 (Appendix 3). Figure 17 and Figure 18 illustrate the situation for GLE42 and GLE69, respectively.

The participants were asked to calculate the total route dose as well as the local dose rates at the given waypoints in terms of $H^*(10)$ and E, separately for GCR and SCR.

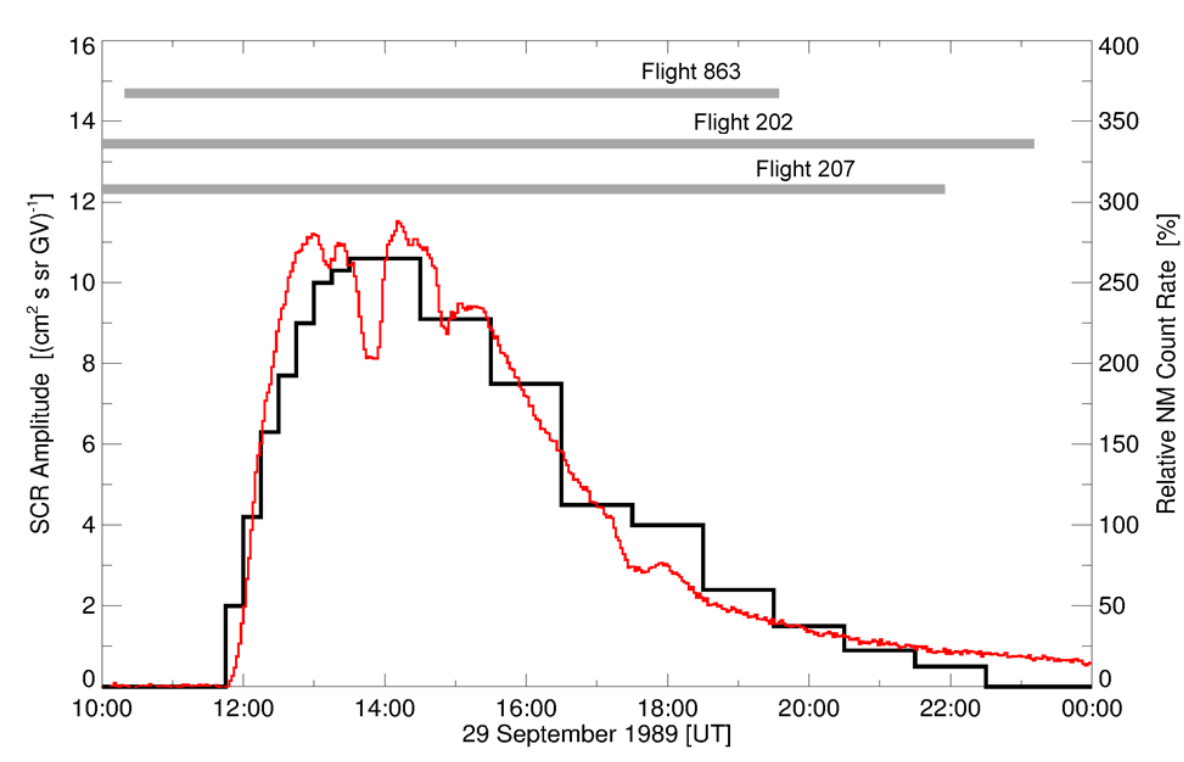

Figure 17: Amplitude of the solar cosmic ray flux at 1 GV as defined for the study of the simplified GLE42 on 29 September 1989, 10:00-24:00 UT (black line, see chapter 5.1.1). The horizontal grey bars indicate the adjusted flight times of the three investigated flights (for details see Appendix 2). For illustration the five-minute pressure corrected relative count rate of the neutron monitor at McMurdo, Antarctica, is also shown (red line, data source: NMDB).

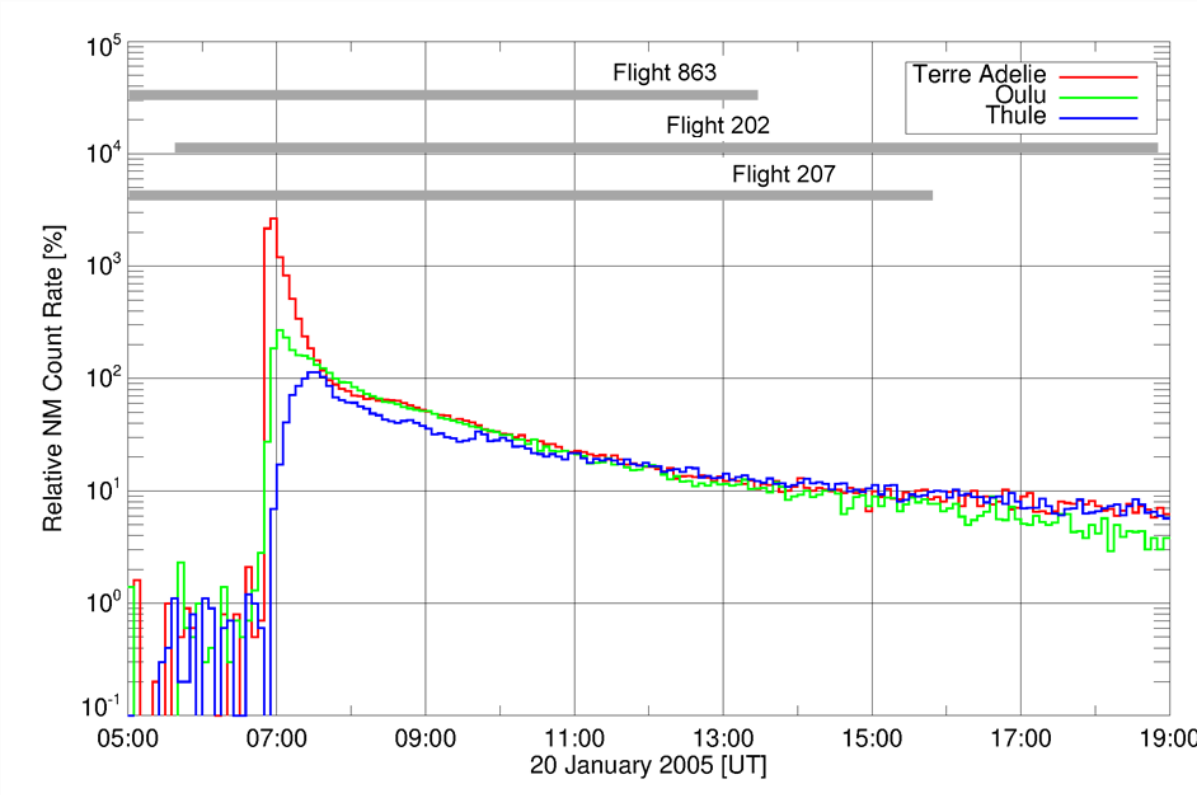

Figure 18: Five-minute pressure corrected relative count rates (in logarithmic scale) of the neutron monitors Terre Adélie, Antarctica (red line), Oulu, Finland (green line), and Thule, Greenland (blue line) for GLE69 on 20 January 2005, 05:00-19:00 UT. NM data source: NMDB. The horizontal grey bars indicate the adjusted flight times of the three investigated flights (for details see Appendix 3).

5.3 Results of dose data comparison

The results in this report are presented in an anonymous way. It is not intended to recommend any of the participating codes in particular for radiation protection services.

Comparisons of calculations for the three selected flight profiles and two investigations ("simplified GLE42" and GLE69) were performed in total with nine computer codes in terms of operational quantity ambient dose equivalent, $H^*(10)$, and radiation protection quantity effective dose, E, for both flight route doses and dose rates. However, it must be noted, that not all codes provide both types of quantities. In addition, not all codes were used to analyse both the "simplified GLE42" and the GLE69 investigations. Therefore, the number of data-points varies from figure to figure.

For both investigations, results are presented in a similar manner. First, route doses are presented in terms of effective dose, E, and ambient dose equivalent, $H^*(10)$, in chapters 5.3.1.1 for "simplified GLE42" and chapter 5.3.2.1 for GLE69. Next, in order to analyse the influence of temporal changes in SCR flux, ambient dose equivalent rates and effective dose rates are presented as a function of time – chapter 5.3.1.2 for "simplified GLE42" and chapter 5.3.2.2 for GLE69.

5.3.1 Investigation 1 (GLE42)

5.3.1.1 Route dose in terms of effective dose, E and ambient dose equivalent, $H^*(10)$

Figure 19 shows an anonymous comparison of the route ambient dose equivalent due to galactic cosmic radiation for the three selected flight routes – 863, 202, and 207. Figure 20 shows an anonymous comparison for the sum of GCR and SCR for the same flights. Results for effective dose for the same conditions are presented in Figure 21 and Figure 22. In most cases, the contribution of solar energetic particles (as assumed in this scenario) increases the median of the effective dose and ambient dose equivalent by factor of about 3 to 4. For the individual codes, however, this factor varies over a larger range between 2 to about 5.

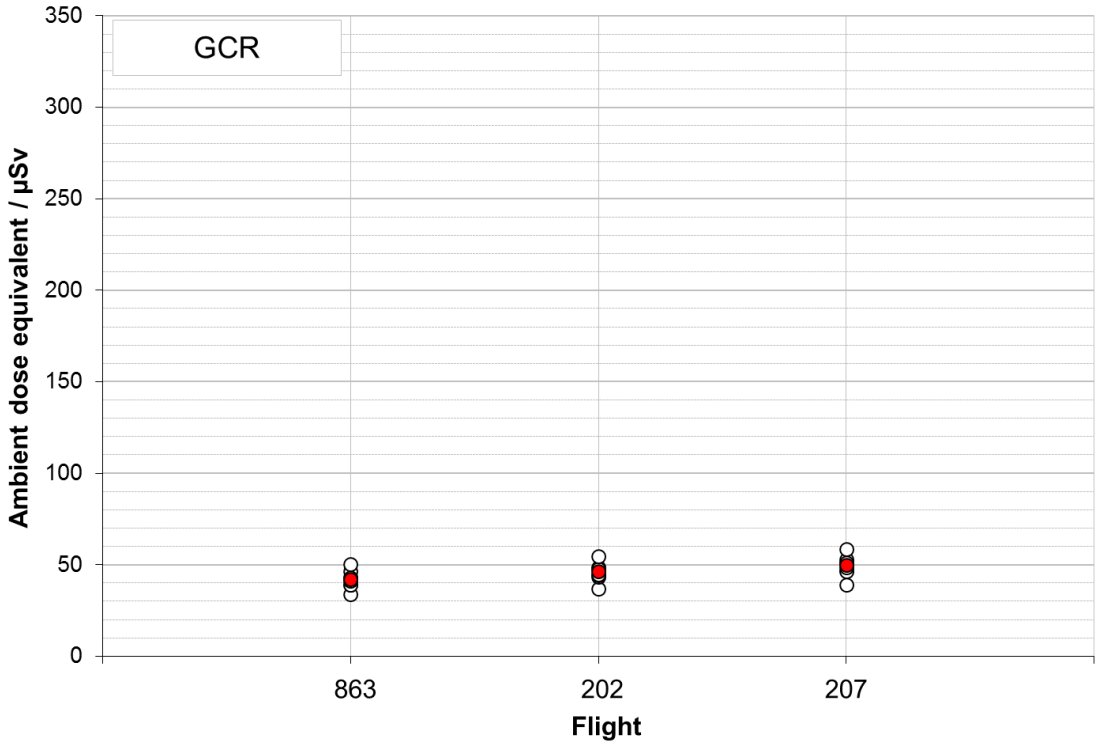

Figure 19: Comparison of route ambient dose equivalent for galactic cosmic radiation (GCR) calculated for selected flights (white) presented with the median (red).

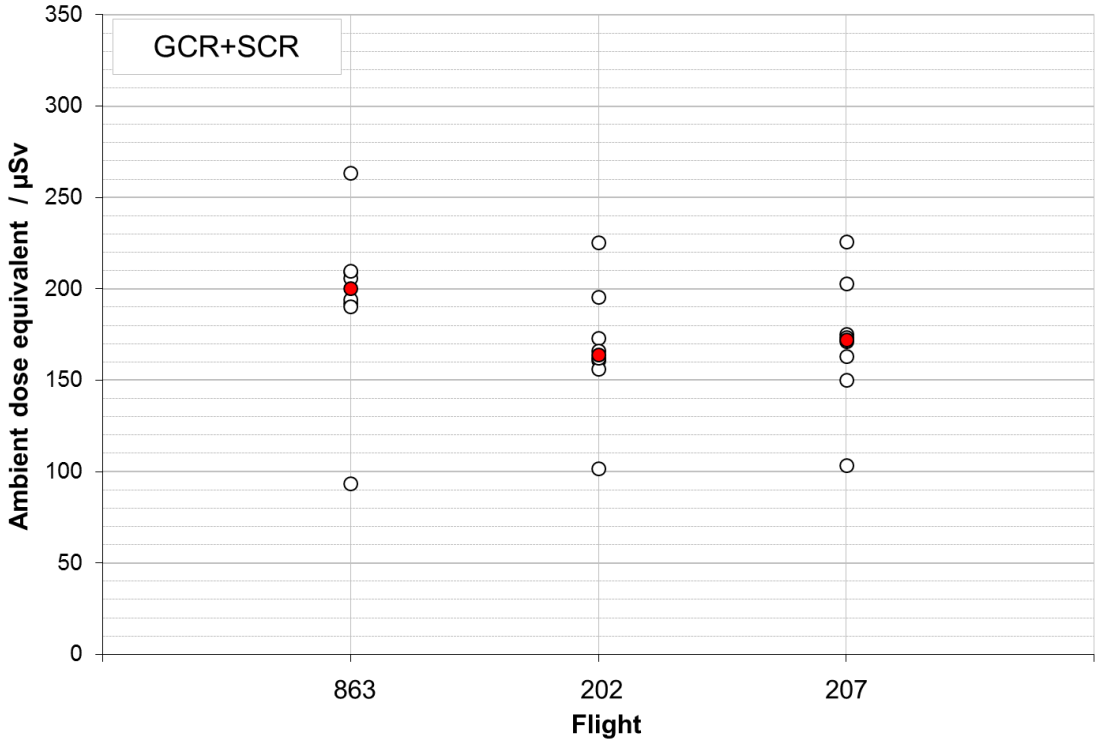

Figure 20: Comparison of route ambient dose equivalent of the sum of galactic cosmic radiation (GCR) and "simplified GLE42" event (SCR) calculated for selected flights (white) presented with the median (red).

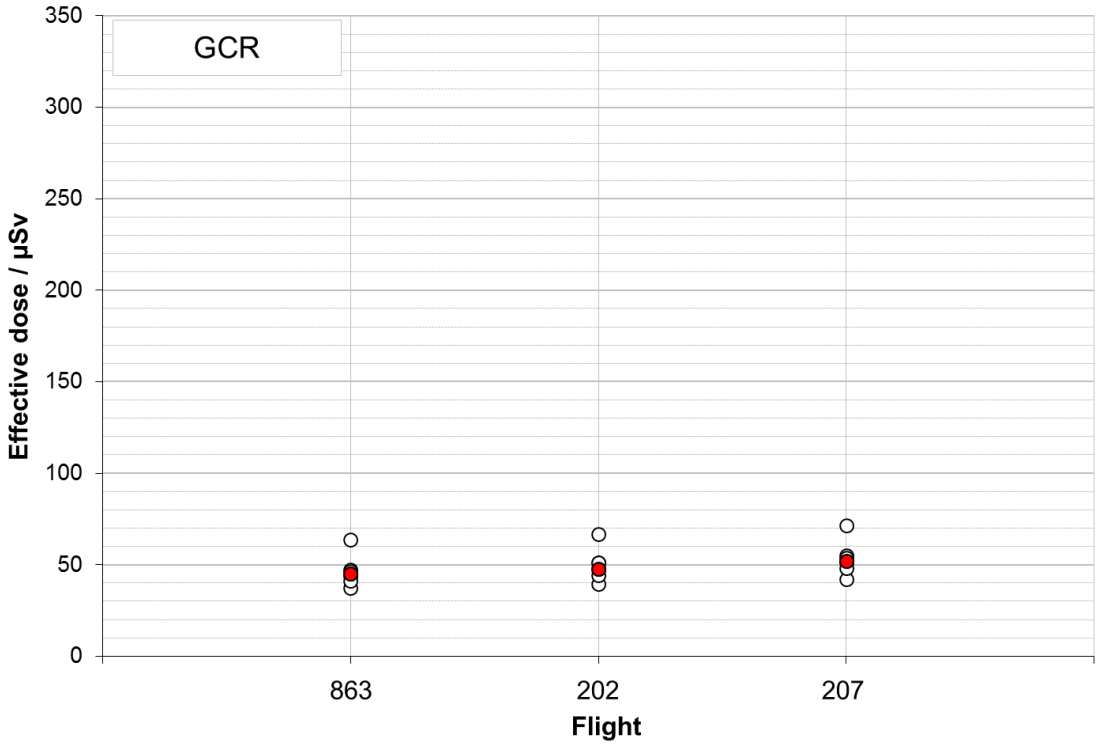

Figure 21: Comparison of route effective dose for galactic cosmic radiation (GCR) calculated for selected flights (white) presented with the median (red).

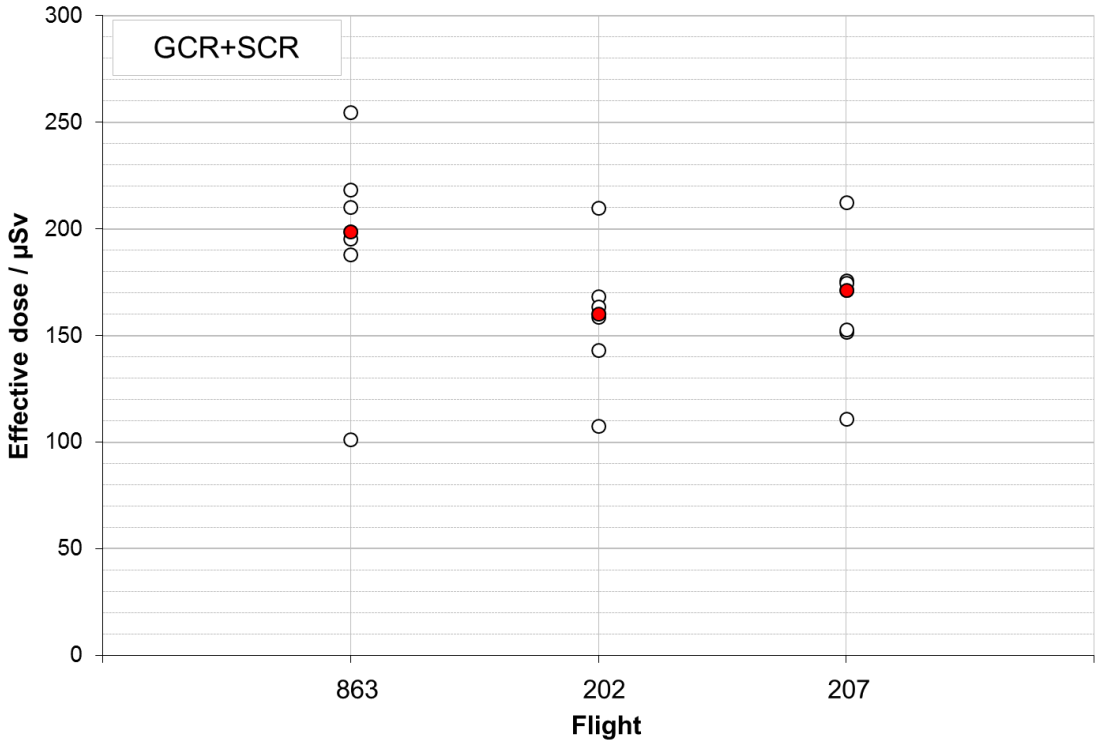

Figure 22: Comparison of route effective dose of the sum of galactic cosmic radiation (GCR) and "simplified GLE42" event (SCR) calculated for selected flights (white) presented with the median (red).

5.3.1.2 Dose rate profile over flight time

Dose rate profiles over flight time allow for analysis that is more detailed. Since in this "simplified GLE42" scenario the SCR angular distribution was on purpose defined as isotropic, such dose rate profiles allow to investigate the influence of temporal changes in SCR intensity.

Flight 863: San Francisco–Paris

The flight profile 863 is listed in Appendix 2 and illustrated in Appendix 3. Figure 23 presents an anonymous comparison of ambient dose equivalent rate as a function of flight time for galactic cosmic rays (GCR) only, while Figure 24 presents the sum of galactic cosmic rays (GCR) and solar cosmic radiation (SCR). Figure 24 presents also amplitude of the temporal evolution of solar protons flux as defined in this scenario. Analogous figures but for effective dose are Figure 25 and Figure 26. The influence of temporal evolution of solar proton flux is evident. While ambient dose equivalent rate values for GCR only are around 5 µSv/h for the whole cruising flight phase, the dose rate increases by a factor of around 7 for median in the peak SRC intensity (between 13:00 and 15:00) when both components GCR and SCR are considered. The lowest calculated dose rate in the SCR peak is about 25 µSv/h (factor 5 larger compared to GCR), the highest – twice more – about 50 µSv/h (factor 10 larger compared to GCR). Similar factors were obtained for effective dose (see Figure 25 and Figure 26).

Flight 202: Chicago–Beijing

Data for flight 202 Chicago-Beijing (for full flight profile see Appendix 2 and Appendix 3) are presented similarly to the previous flight. Figure 27 presents an anonymous comparison of ambient dose equivalent rate as a function of flight time for galactic cosmic rays (GCR) only, while Figure 28 presents the sum of galactic cosmic rays (GCR) and solar cosmic radiation (SCR) with the amplitude of solar proton flux as defined in this scenario. Analogously for effective dose rate, see: Figure 29 and Figure 30.

In this case, the flight profile does not contain a waypoint at the time of the maximum SCR flux. This draws attention to a practical aspect for those who attempt to assess radiation exposure during SCR events – since these events may take from minutes to hours, flight profiles should have a reasonably short time steps, particularly when altitude or position (cutoff rigidity) of the aircraft changes rapidly. If the exact information is lacking, assumptions on aircraft location will have to be made and those may contribute to the uncertainty of the calculated route doses.

Figure 28 shows that ambient dose equivalent rates around the maximum SCR flux increased by factor of about 5 to 6 for the median, however no information is available for the peak-time itself. The lowest calculated dose rate around the SCR peak is about 20 µSv/h (factor 5 larger compared to GCR-median), the highest – almost 40 µSv/h (about factor 8 larger compared to GCR-median). Similar factors are observed for effective dose rate – see Figure 29 and Figure 30.

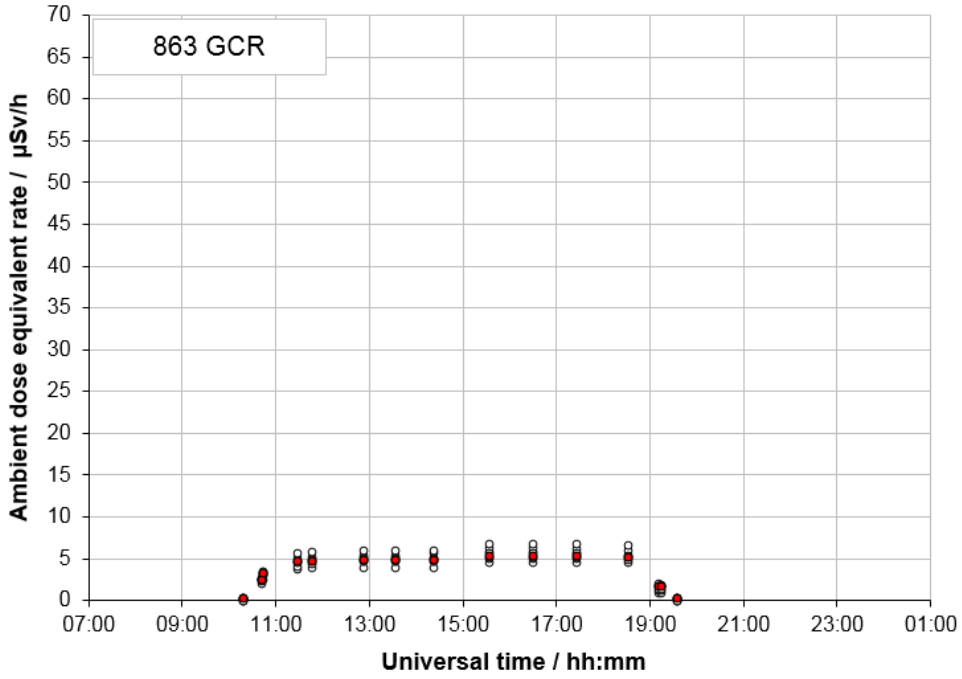

Figure 23: Comparison of ambient dose equivalent rate for galactic cosmic radiation (GCR) calculated for selected flight profile (863: San Francisco–Paris) by different codes (white) presented with median (red).

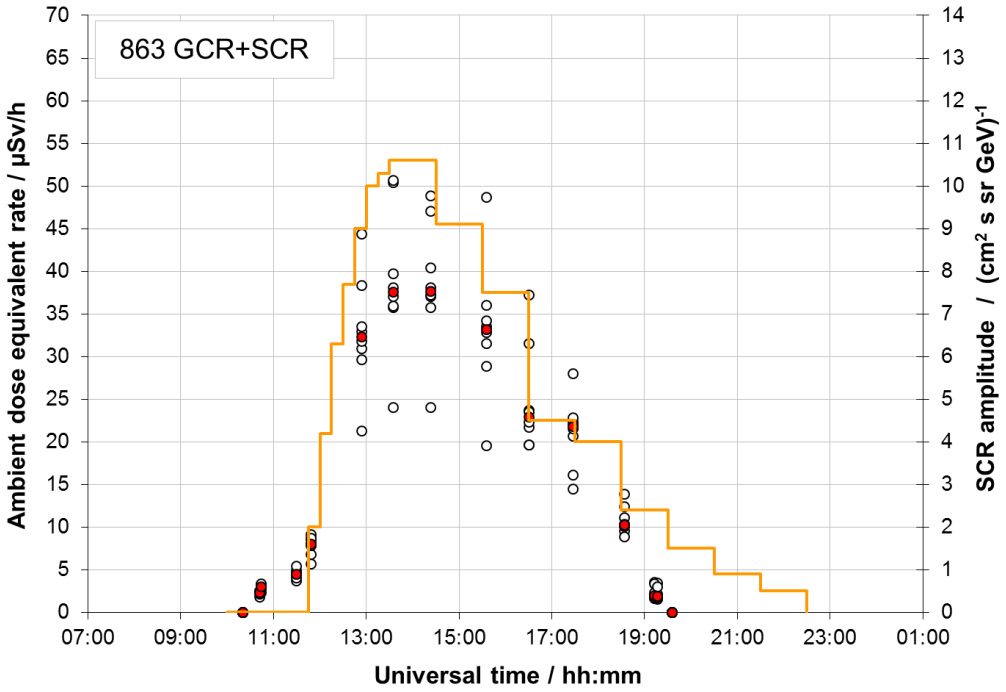

Figure 24: Comparison of ambient dose equivalent rate for the sum of galactic cosmic radiation (GCR) and "simplified GLE42" event (SCR) calculated for selected flight profile (863: San Francisco–Paris) by different codes (white, left axis) presented with median (red, left axis). In addition, we show the time profile of GLE42 event (orange, right axis) for solar protons with an energy of 1 GeV near Earth, outside the geomagnetosphere as defined in Table 2.

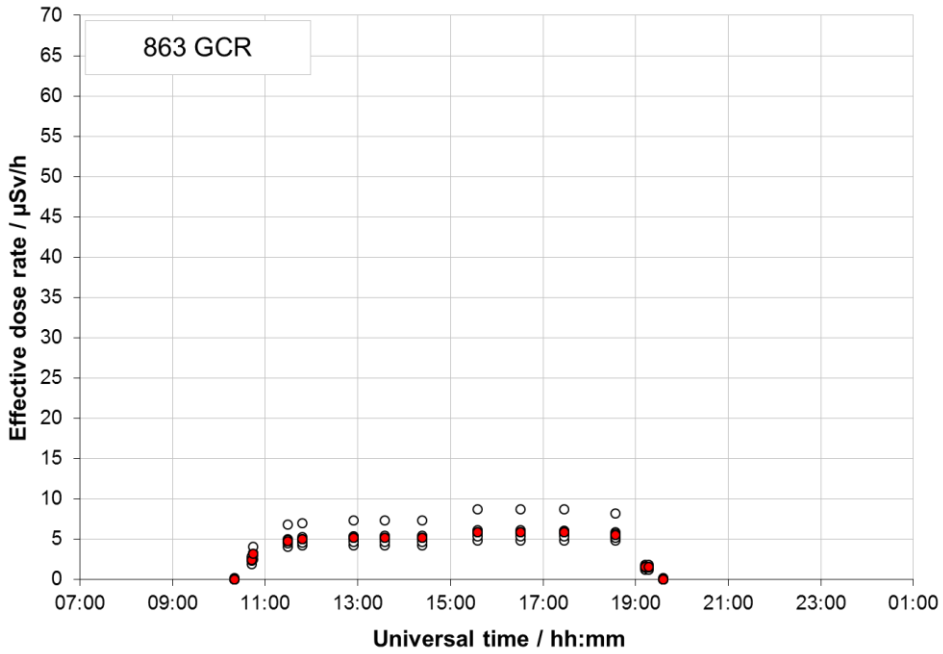

Figure 25: Comparison of effective dose rate for galactic cosmic radiation (GCR) calculated for selected flight profile (863: San Francisco–Paris) by different codes (white) presented with median (red).

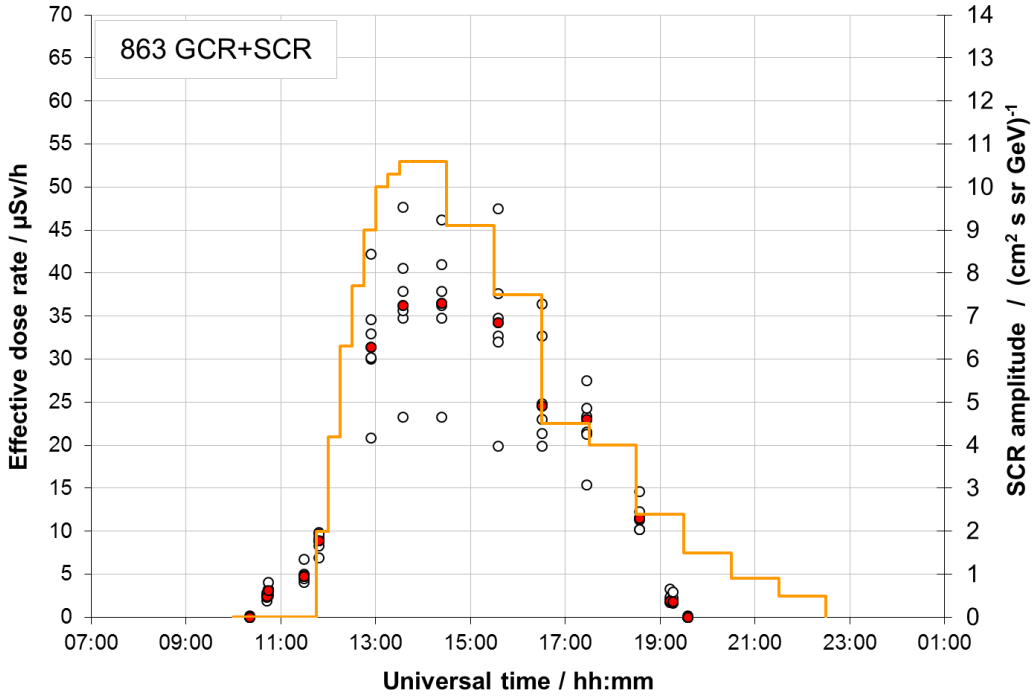

Figure 26: Comparison of effective dose rate for the sum of galactic cosmic radiation (GCR) and "simplified GLE42" event (SCR) calculated for selected flight profile (863: San Francisco–Paris) by different codes (white, left axis) presented with median (red, left axis). In addition, we show the time profile of GLE42 event (orange, right axis) for solar protons with an energy of 1 GeV near Earth, outside the geomagnetosphere as defined in Table 2.

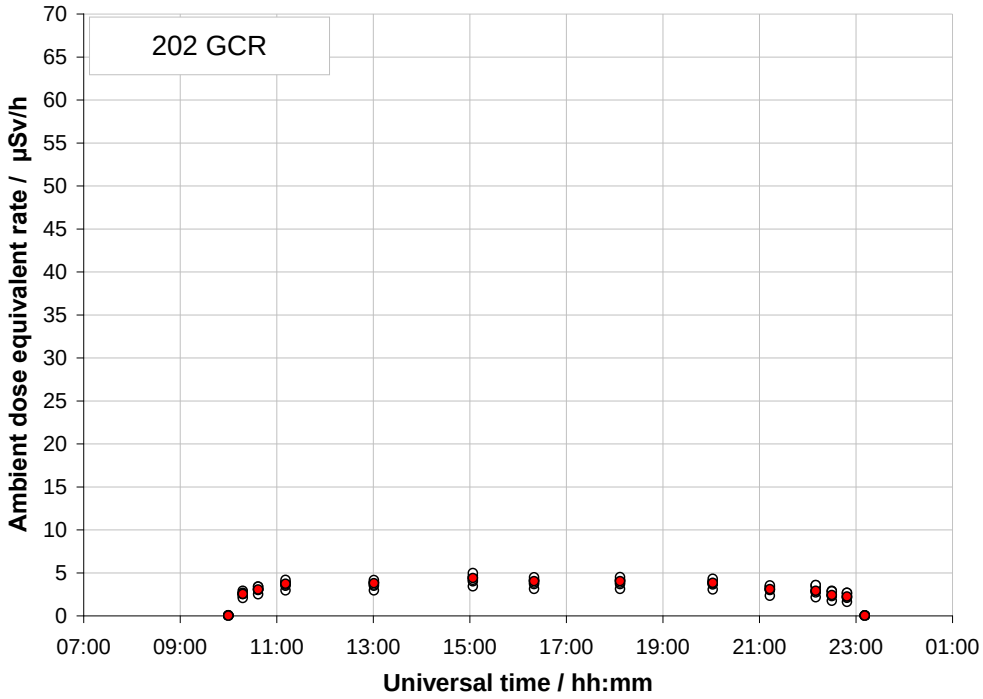

Figure 27: Comparison of ambient dose equivalent rate for galactic cosmic radiation (GCR) calculated for selected flight profile (202: Chicago–Beijing) by different codes (white) presented with median (red).

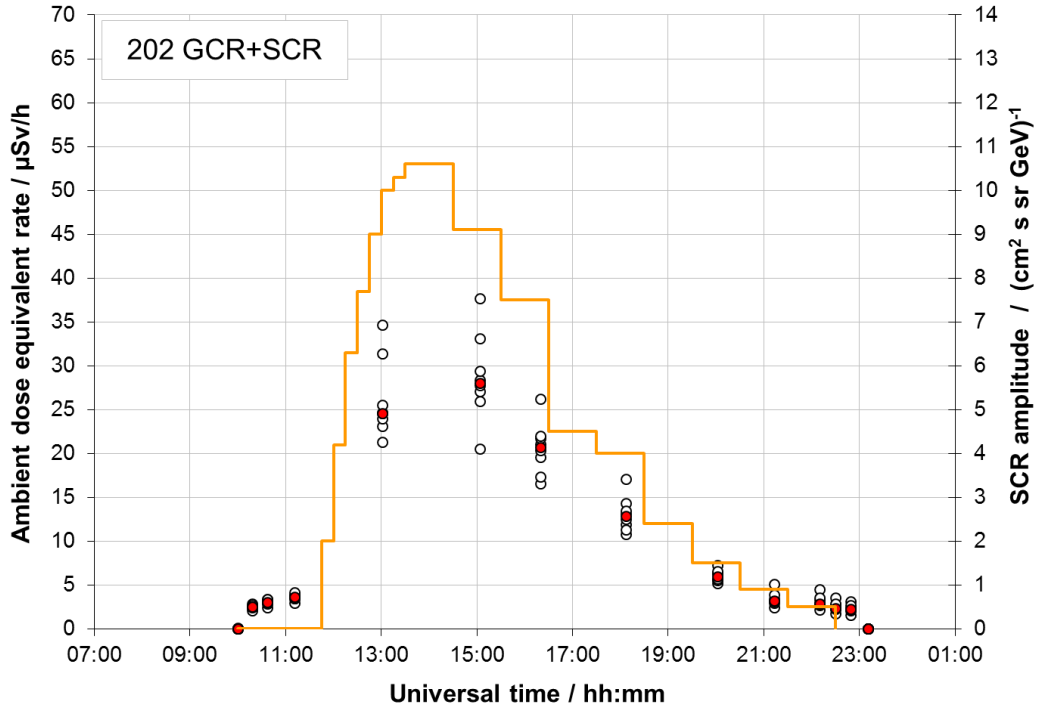

Figure 28: Comparison of ambient dose equivalent rate for the sum of galactic cosmic radiation (GCR) and "simplified GLE42" event (SCR) calculated for selected flight profile (202: Chicago–Beijing) by different codes (white, left axis) presented with median (red, left axis). In addition, we show the time profile of GLE42 event (orange, right axis) for solar protons with energies of 1 GeV near Earth, outside the geomagnetosphere as defined in Table 2.

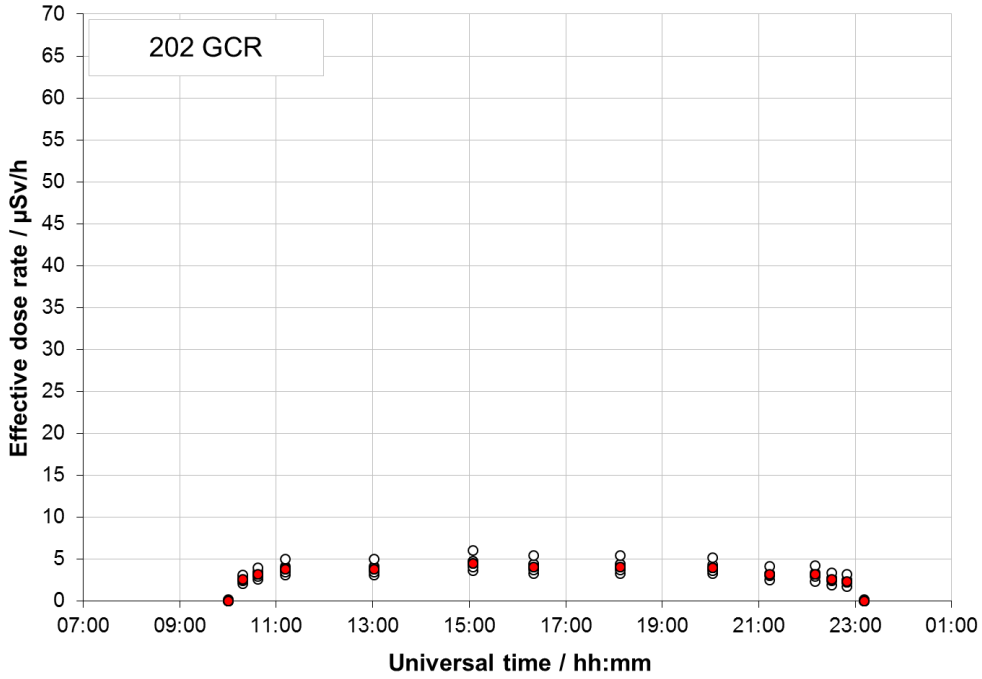

Figure 29: Comparison of effective dose rate for galactic cosmic radiation (GCR) calculated for selected flight profile (202: Chicago–Beijing) by different codes (white) presented with median (red).

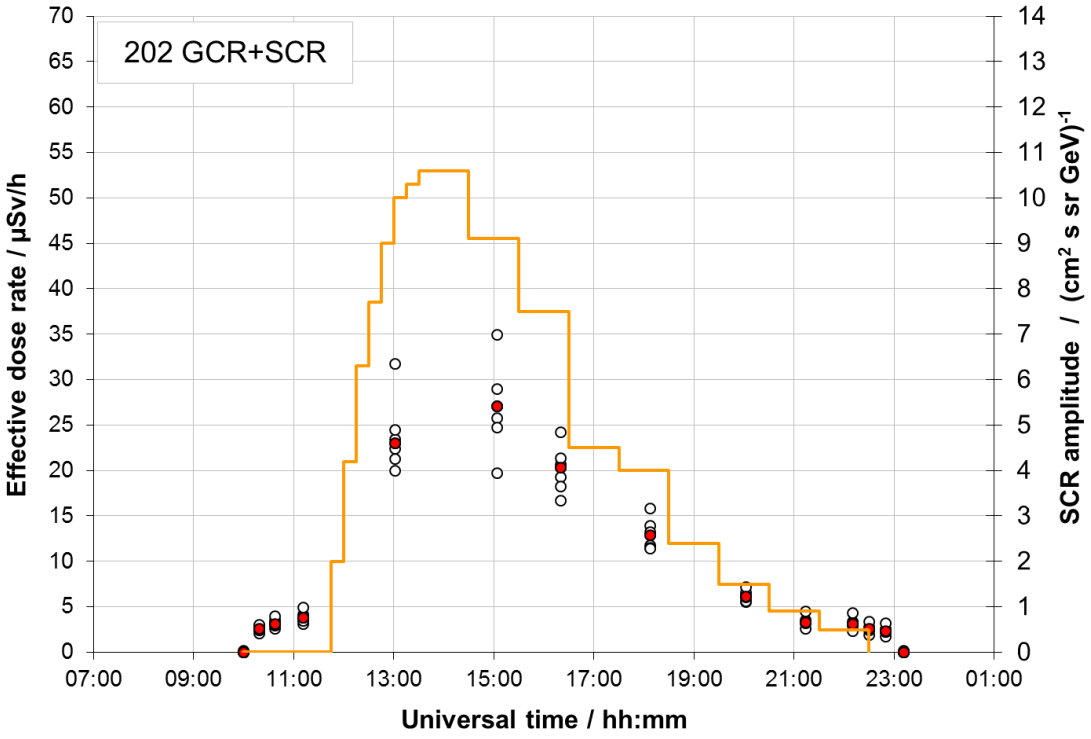

Figure 30: Comparison of effective dose rate for the sum of galactic cosmic radiation (GCR) and "simplified GLE42" event (SCR) calculated for selected flight profile (202: Chicago–Beijing) by different codes (white, left axis) presented with median (red, left axis). In addition, we show the time profile of GLE42 event (orange, right axis) for solar protons with energies of 1 GeV near Earth, outside the geomagnetosphere as defined in Table 2.

Flight 207: Sydney–Johannesburg

Data for flight 207 Sydney – Johannesburg (for full flight profile see Appendix 2 and Appendix 3) are presented similarly to the previous flights. Figure 31 presents the comparison of ambient dose equivalent rate as a function of flight time for GCR. Figure 32 presents the same for the sum of the effects due to GCR and SCR, and the amplitude of solar protons flux as defined in this scenario. Analogously for effective dose rate, see: Figure 33 and Figure 34.

Figure 32 shows that the median of ambient dose equivalent rate values around the SCR peak increased by factor of about 6 with respect to the median of ambient dose equivalent rate values for GCR as shown in Figure 31. A comparison of Figure 31 and Figure 32 further shows that the lowest calculated ambient dose equivalent rate around the SCR peak is between 20 µSv/h and 25 µSv/h, i.e. a factor of about 5 larger compared to GCR-median. The highest ambient dose equivalent rate value is about 45 µSv/h, i.e. about a factor 9 larger compared to GCR-median. Similar factors are observed for effective dose rate (see Figure 33 and Figure 34).

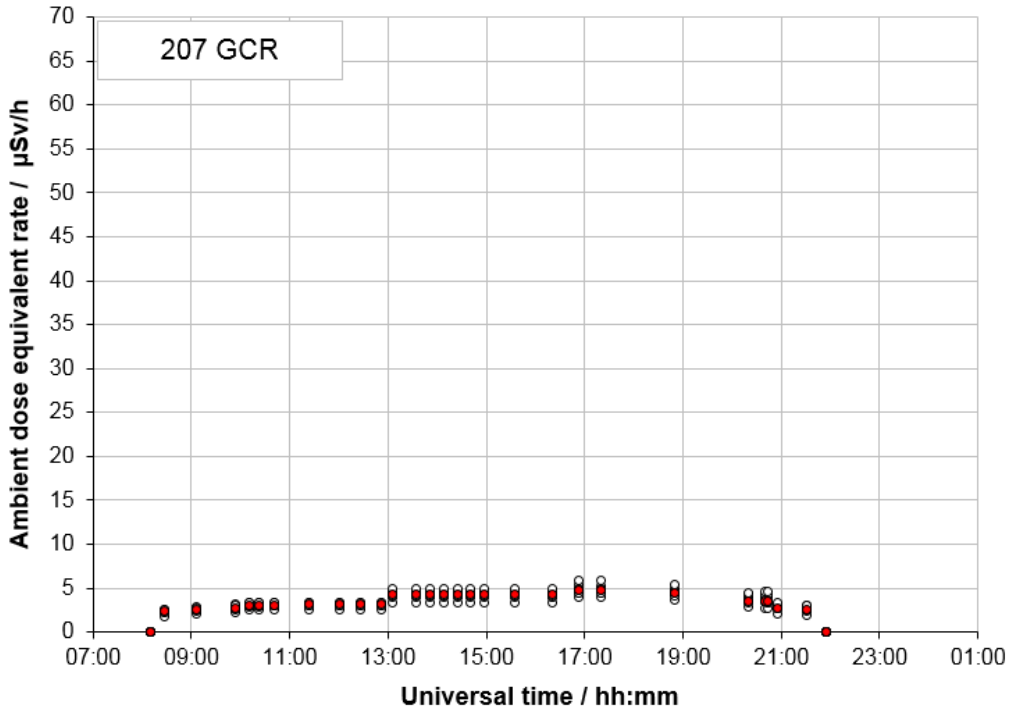

Figure 31: Comparison of ambient dose equivalent rate for galactic cosmic radiation (GCR) calculated for selected flight profile (207: Sydney–Johannesburg) by different codes (white) presented with median (red).

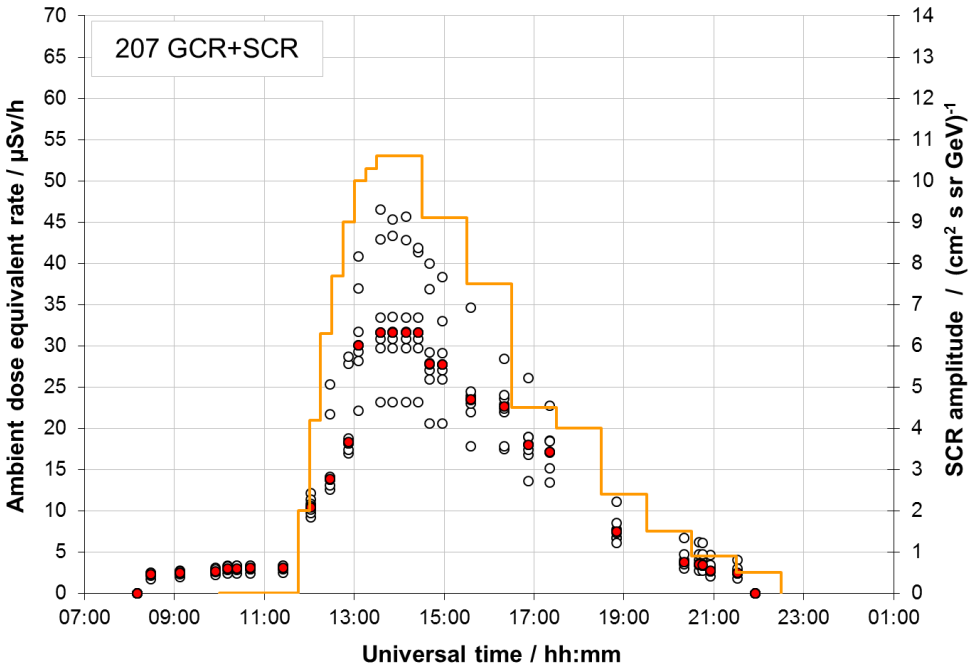

Figure 32: Comparison of ambient dose equivalent rate for the sum of galactic cosmic radiation (GCR) and "simplified GLE42" event (SCR) calculated for selected flight profile (207: Sydney–Johannesburg) by different codes (white, left axis) presented with median (red, left axis). In addition, we show the time profile of GLE42 (orange, right axis) event for solar protons with energies of 1 GeV near Earth, outside the geomagnetosphere as defined in Table 2.

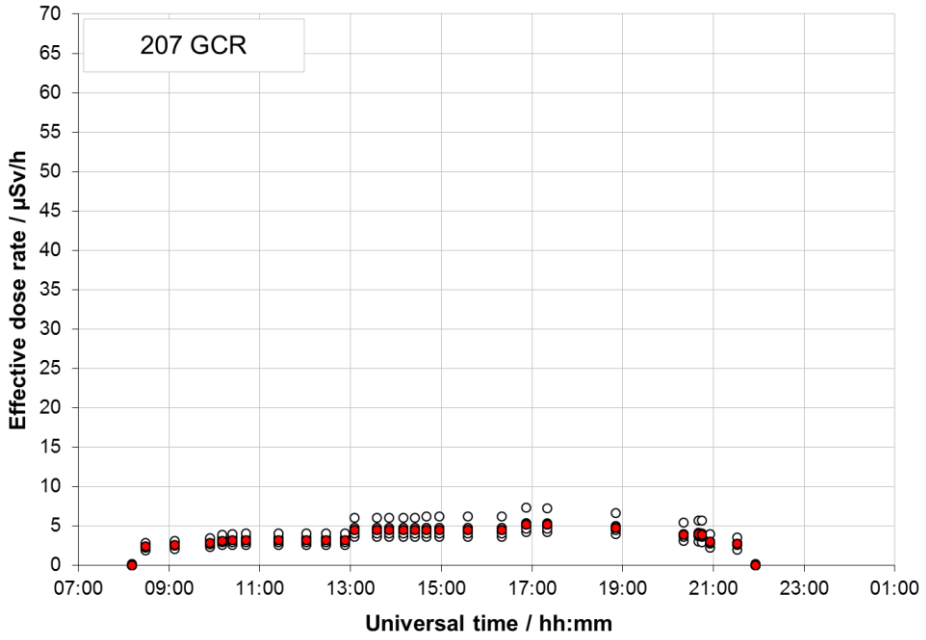

Figure 33: Comparison of effective dose rate for galactic cosmic radiation (GCR) calculated for selected flight profile (207: Sydney–Johannesburg) by different codes (white) presented with median (red).

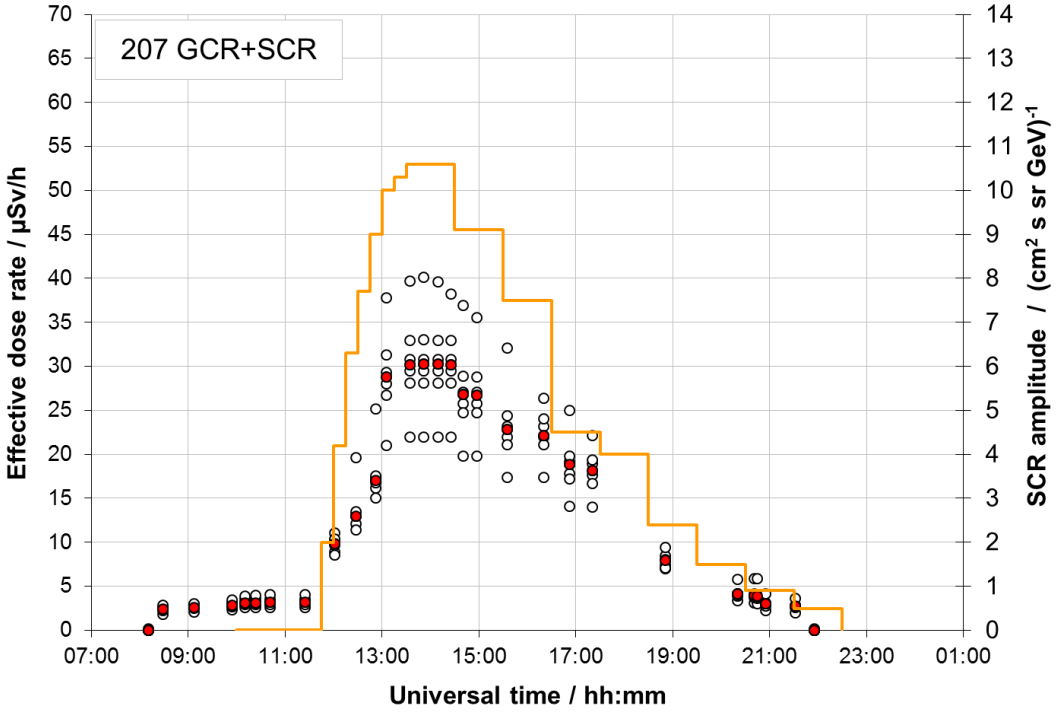

Figure 34: Comparison of effective dose rate for the sum of galactic cosmic radiation (GCR) and "simplified GLE42" event (SCR) calculated for selected flight profile (207: Sydney–Johannesburg) by different codes (white, left axis) presented with median (red, left axis). In addition, we show the time profile of GLE42 (orange, right axis) event for solar protons with energies of 1 GeV near Earth, outside the geomagnetosphere as defined in Table 2.

5.3.2 Investigation 2 (GLE69)

5.3.2.1 Route dose in terms of ambient dose equivalent $H^*(10)$ and effective dose E

Figure 35 shows the comparison of route ambient dose equivalent, $H^*(10)$, as a function of flight time for GCR. The median route $H^*(10)$ due to GCR for the flight 863 (San Francisco–Paris) is 55 µSv; the minimum value is about 45 µSv and maximum is about 65 µSv. For the flight 202 (Chicago–Beijing) the median $H^*(10)$ is 60 µSv; with similar minimum and maximum values compared to flight 863. The median $H^*(10)$ for the flight 207 (Sydney–Johannesburg) is 65 µSv; the minimum value is about 55 µSv and maximum is about 70 µSv.

Figure 36 presents the comparison for the sum of the effects due to GCR and SCR. For the flight 863 the median $H^*(10)$ is about 375 µSv; minimum is about 175 µSv and maximum about 600 µSv. For the flight 202 the median $H^*(10)$ is 300 µSv; minimum is about 100 µSv and maximum about 425 µSv. For the flight 207 the median $H^*(10)$ is about 450 µSv; minimum is about 150 µSv and maximum about 575 µSv.

For route effective dose, Figure 37 and Figure 38 present the corresponding comparison for GCR and for the sum of GCR and SCR, respectively. Figure 38 shows that for the flight 863 the median E is about 400 µSv; minimum is about 250 µSv and maximum about 475 µSv. For the flight 202 the median E is 260 µSv; minimum is about 180 µSv and maximum about 320 µSv. For the flight 207 the median E is about 440 µSv; minimum is about 300 µSv and maximum about 460 µSv.

As for effective dose, the spread of route dose values for GCR is roughly the same as for ambient dose equivalent, while it is not the case for the sum of GCR and SCR. It must be noted that not all codes provide both results in terms of ambient dose equivalent and effective dose.

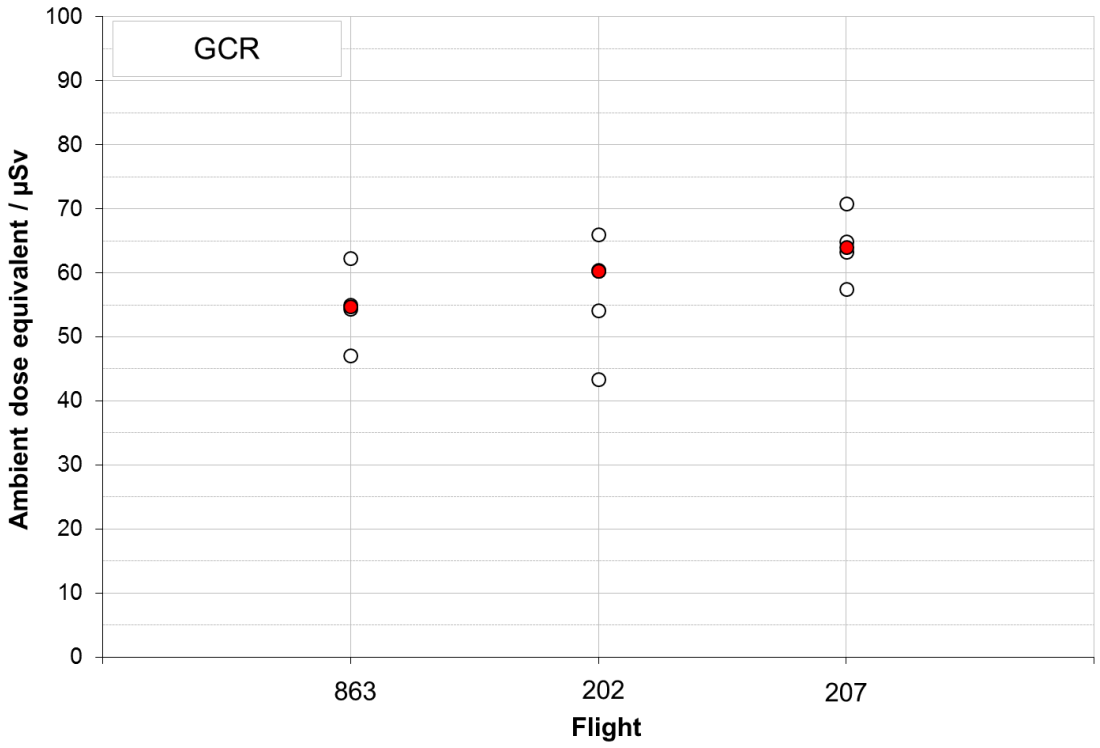

Figure 35: Comparison of route ambient dose equivalent for galactic cosmic radiation (GCR) calculated with 1-minute resolution for selected flights (white) presented with the median (red).

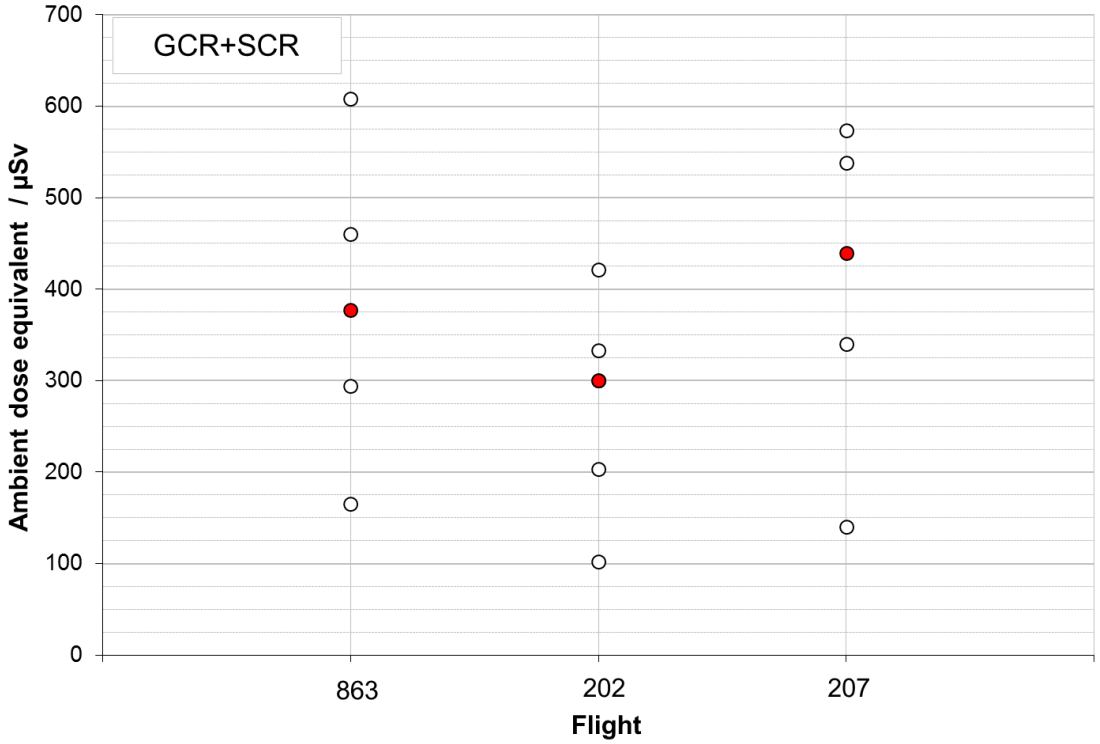

Figure 36: Comparison of route ambient dose equivalent of the sum of galactic cosmic radiation (GCR) and GLE69 event (SCR) calculated with 1-minute resolution for selected flights (white) presented with the median (red).

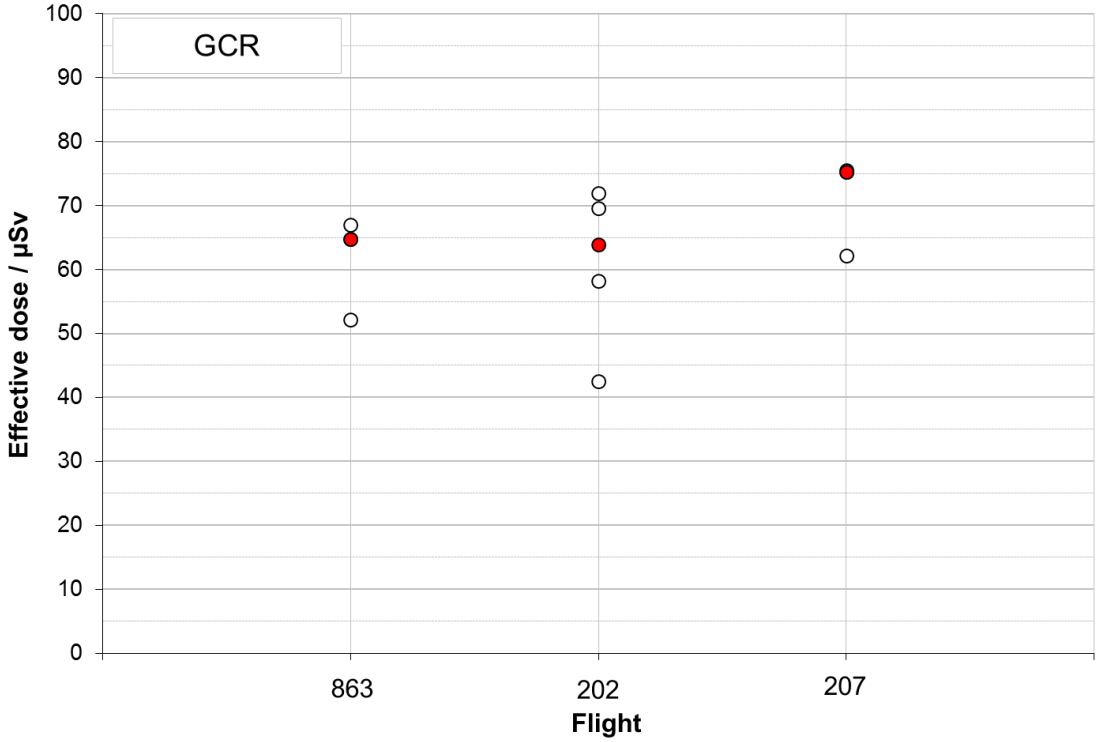

Figure 37: Comparison of route effective dose for galactic cosmic radiation (GCR) calculated with 1-minute resolution for selected flights (white) presented with the median (red).

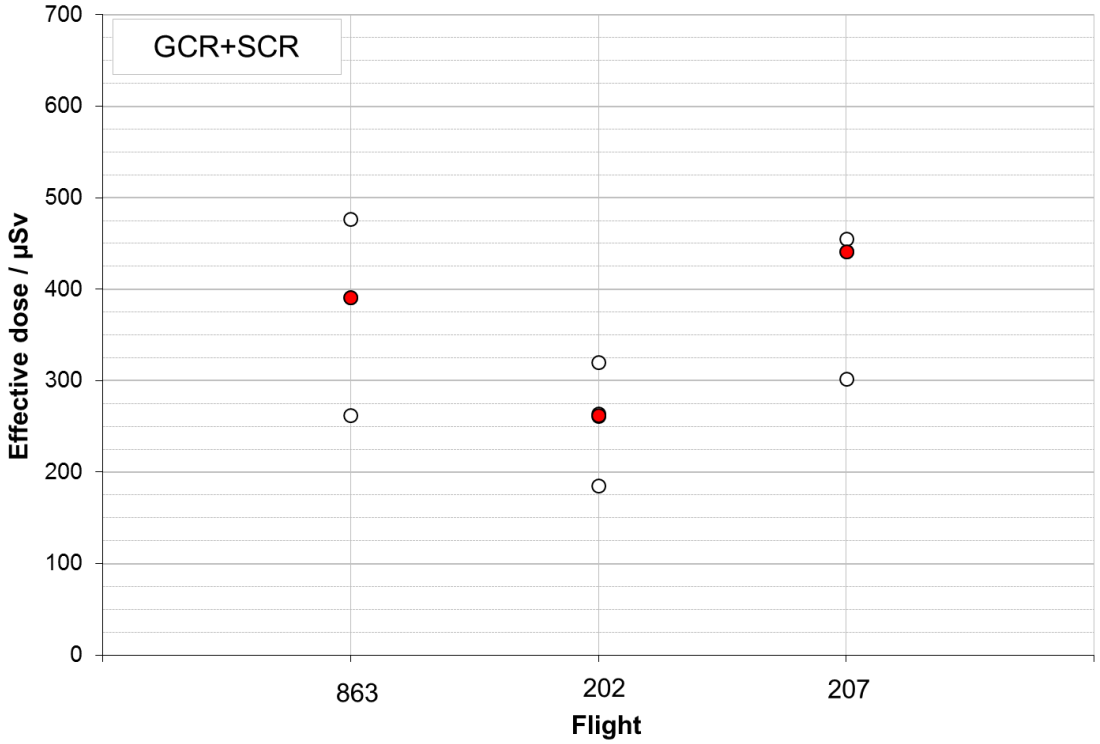

Figure 38: Comparison of route effective dose of the sum of galactic cosmic radiation (GCR) and GLE69 event (SCR) calculated with 1-minute resolution for selected flights (white) presented with the median (red).

5.3.2.2 Dose rate profile over flight time

Figure 39 until Figure 50 present calculated data of dose rate profiles over flight time. The corresponding flight time with respect to the time profile of the GLE event is given in Figure 18. Contrary to corresponding figures in chapter 5.3.1.2, here no median values are presented as the calculations for this investigation were done at various timestamps by different codes.

Figure 39 presents the comparison of ambient dose equivalent rate for GCR conditions calculated for San Francisco – Paris flight (flight 863). Figure 40 presents the comparison for the same quantity calculated for the same flight but for both GCR and SCR conditions. While the maximum calculated ambient dose equivalent rate for GCR conditions is roughly 8 µSv/h, the peak calculated ambient dose equivalent rate for GCR and SCR is about 550 µSv/h. The phase of the flight when ambient dose equivalent rate is above 100 µSv/h takes 1 – 2 hours, depending on the code. Similar observations can be done for effective dose (Figure 41 and Figure 42). For GCR, the maximum effective dose rates are slightly higher than ambient dose equivalent rate – 9 µSv/h, but the peak calculated effective dose rate is lower than previously - about 400 µSv/h. This may come from the fact, that not all codes give both quantities.

For flight 202, Chicago – Beijing, ambient dose equivalent rates are presented in Figure 43 for GCR and Figure 44 for the sum of GCR and SCR. Effective dose rates are presented in Figure 45 for GCR and Figure 46 for the sum of GCR and SCR. The maximum calculated ambient dose equivalent rate for GCR is slightly more than 6 µSv/h and about 550 µSv/h for the sum of SCR and GCR. Similarly, for effective dose rate: maximum value for GCR is about 7 µSv/h and some 425 µSv/h for the sum of SCR and GCR. The phase with dose rates (both, ambient dose equivalent and effective dose) above 100 µSv/h lasts about 1 hour.

The same sequence of figures is presented for flight 207, Sydney–Johannesburg: Figure 47 for ambient dose equivalent rate due to GCR, Figure 48 for ambient dose equivalent rate due to SCR and GCR, Figure 49 for effective dose rate due to GCR and finally Figure 50 for effective dose rate due to both GCR and SCR. The maximum ambient dose equivalent rate due to GCR is about 7 µSv/h (Figure 47) and maximum effective dose rate is 8 µSv/h (Figure 49). For the sum of GCR and SCR, the maximum values are 1.5 mSv/h for ambient dose equivalent rate (Figure 48) and 1.1 mSv/h for effective dose rate (Figure 50). In both cases, however, the maximum lasts some minutes, while the phase with dose rates above 100 µSv/h is up to 2 hours. Compared to the two other flights, calculations performed for this flight showed the largest peak dose rate values. That can be attributed to the north-south anisotropy during the initial and main phase of the SPE and the different flight profiles.

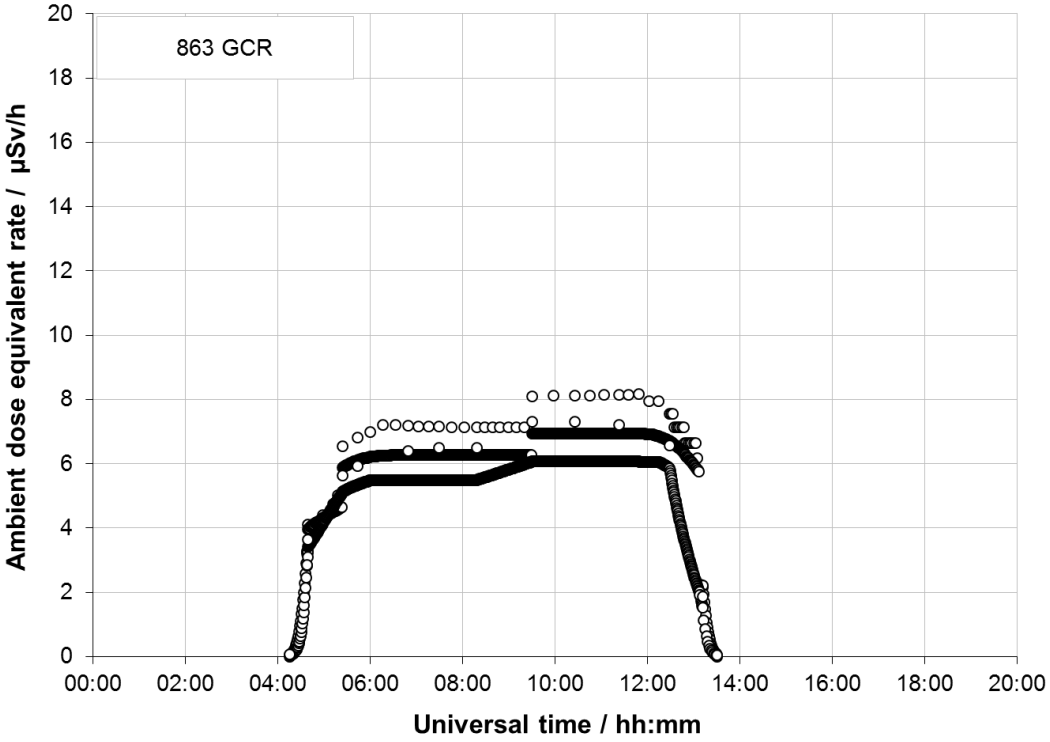

Figure 39: Comparison of ambient dose equivalent rate for galactic cosmic radiation (GCR) calculated for selected flight profile (863: San Francisco–Paris) by four codes.

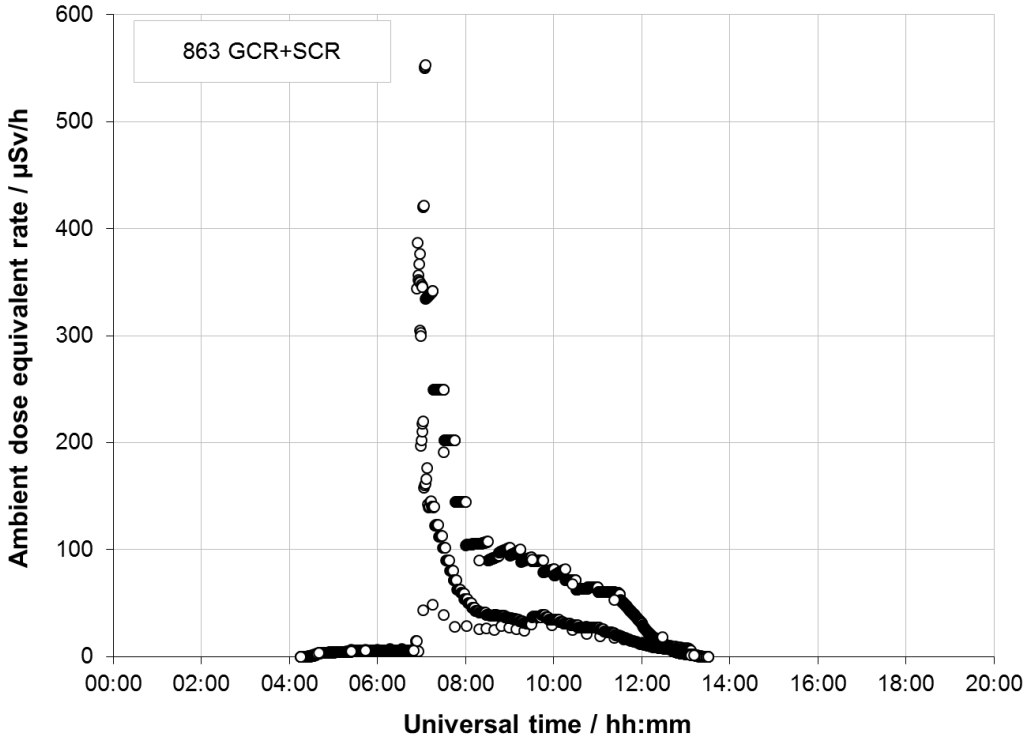

Figure 40: Comparison of ambient dose equivalent rate for the sum of galactic cosmic radiation (GCR) and GLE69 event (SCR) calculated for selected flight profile (863: San Francisco–Paris) by four codes.

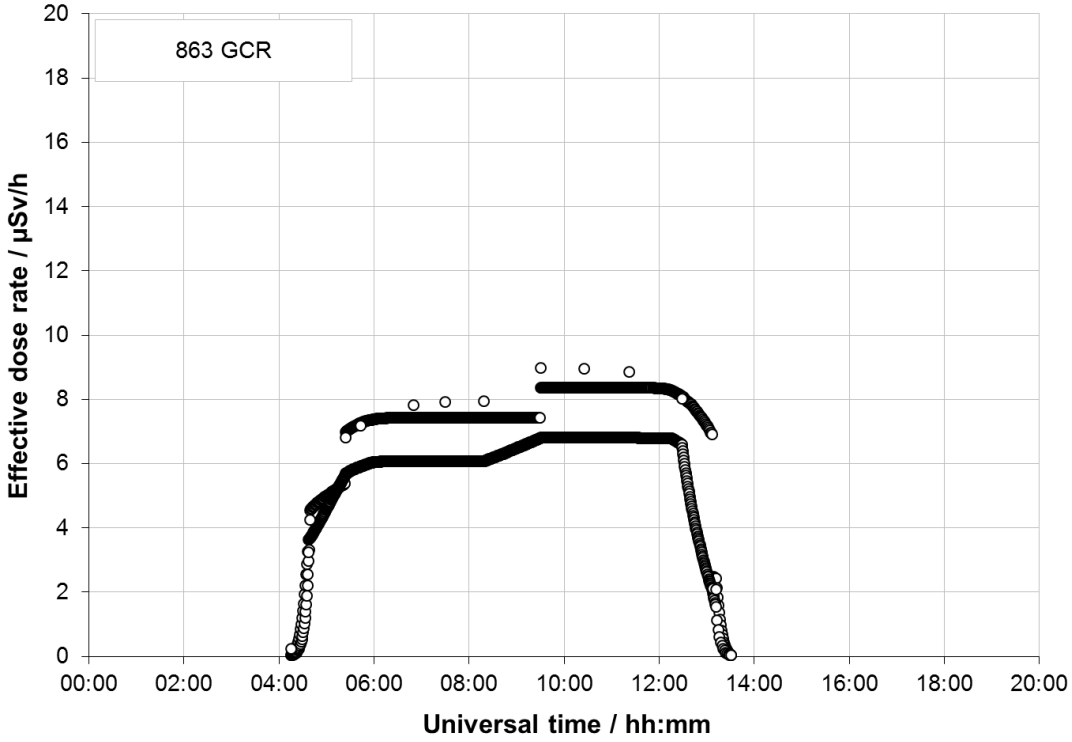

Figure 41: Comparison of effective dose rate for galactic cosmic radiation (GCR) calculated for selected flight profile (863: San Francisco–Paris) by three codes.

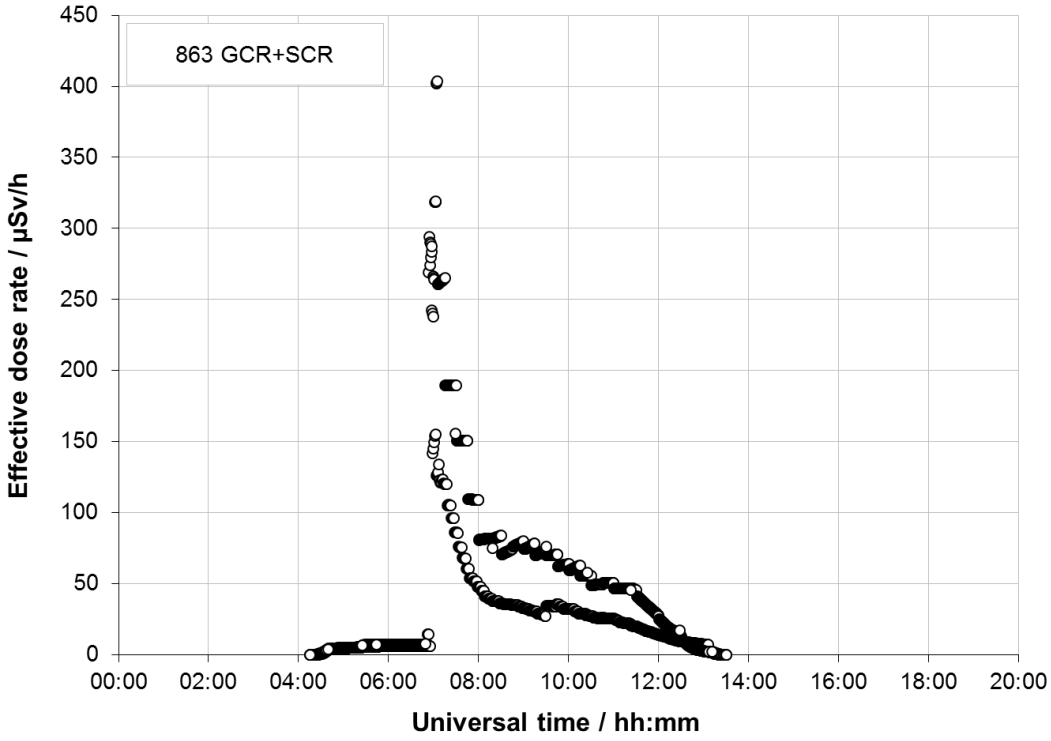

Figure 42: Comparison of effective dose rate for the sum of galactic cosmic radiation (GCR) and GLE69 event (SCR) calculated for selected flight profile (863: San Francisco–Paris) by three codes.

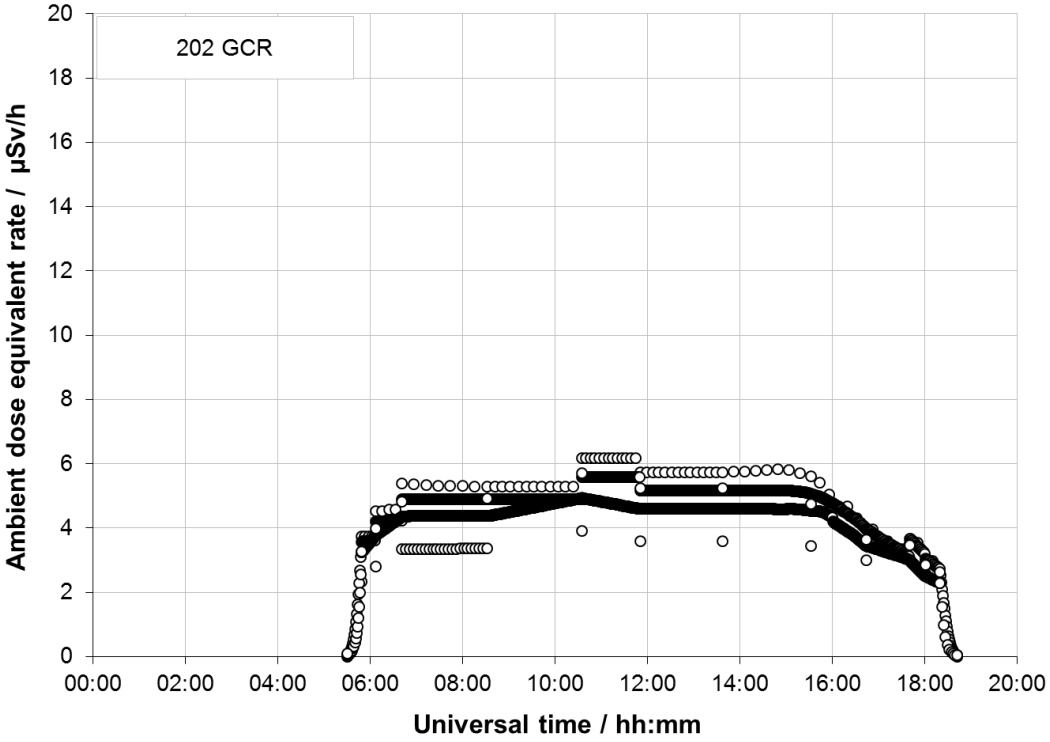

Figure 43: Comparison of ambient dose equivalent rate for galactic cosmic radiation calculated for selected flight profile (202: Chicago–Beijing) by five codes.

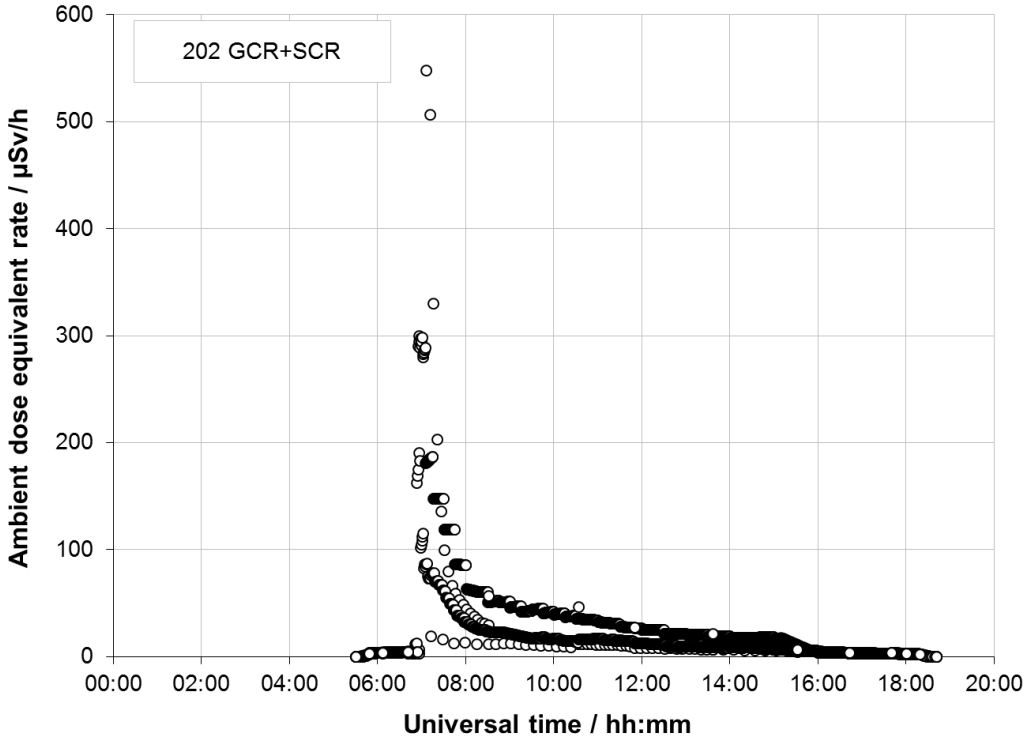

Figure 44: Comparison of ambient dose equivalent rate for the sum of galactic cosmic radiation and GLE69 event calculated for selected flight profile (202: Chicago–Beijing) by five codes.

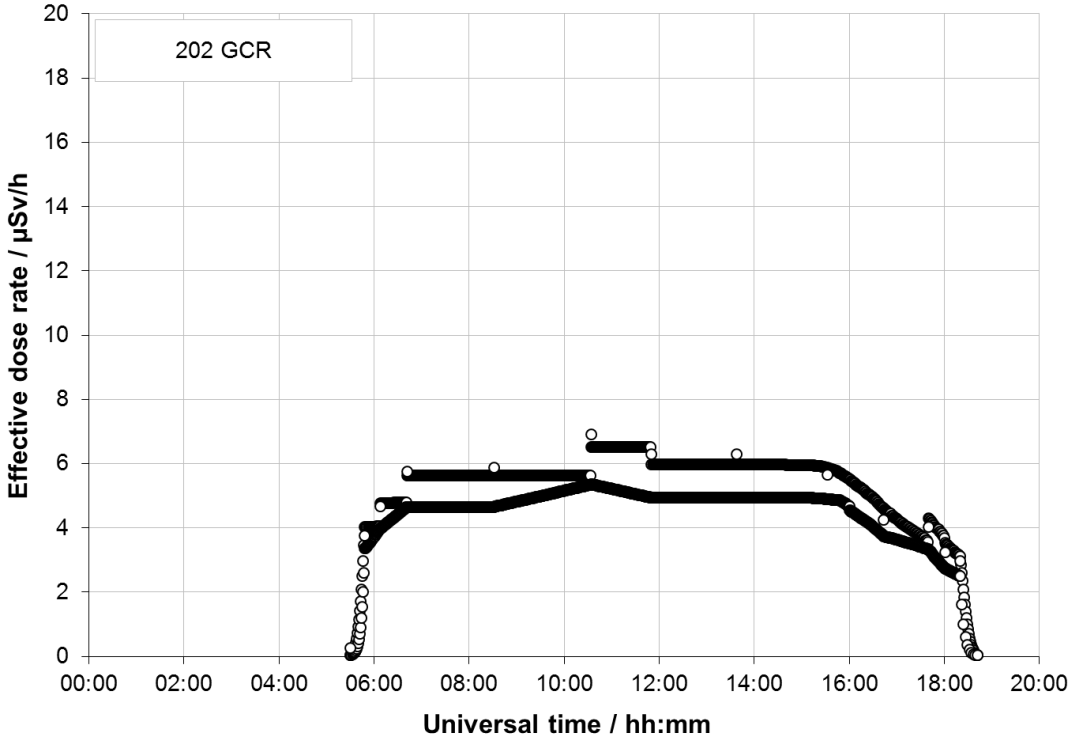

Figure 45: Comparison of effective dose rate for galactic cosmic radiation (GCR) calculated for selected flight profile (202: Chicago–Beijing) by four codes.

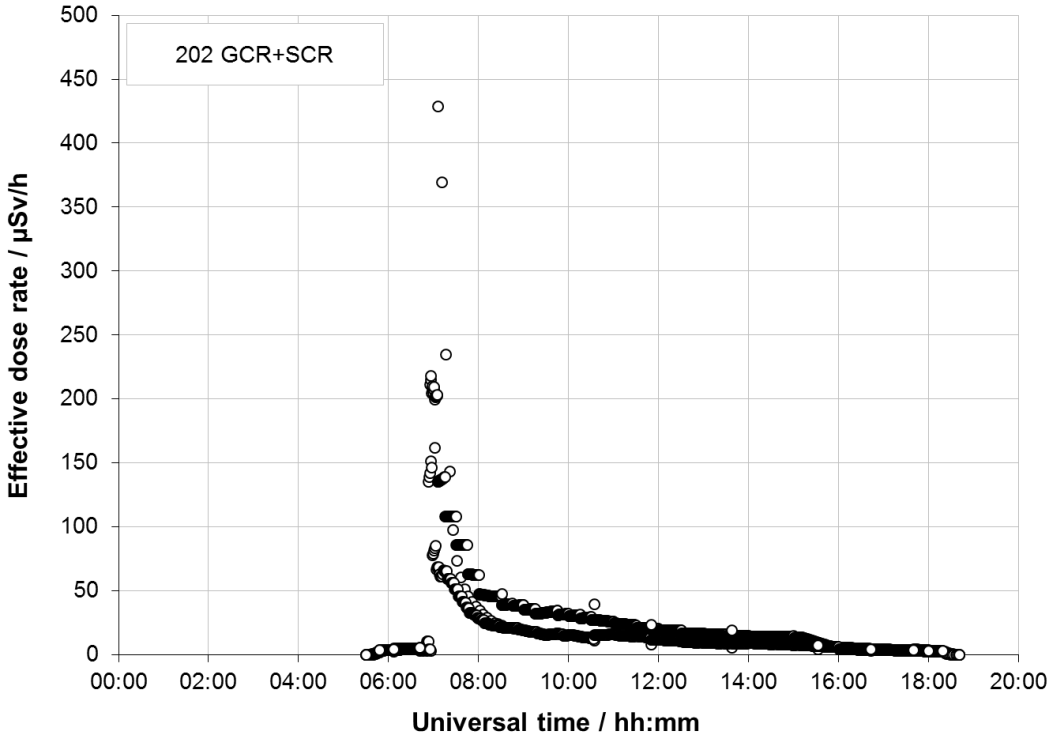

Figure 46: Comparison of effective dose rate for the sum of galactic cosmic radiation (GCR) and GLE69 event (SCR) calculated for selected flight profile (202: Chicago–Beijing) by four codes.

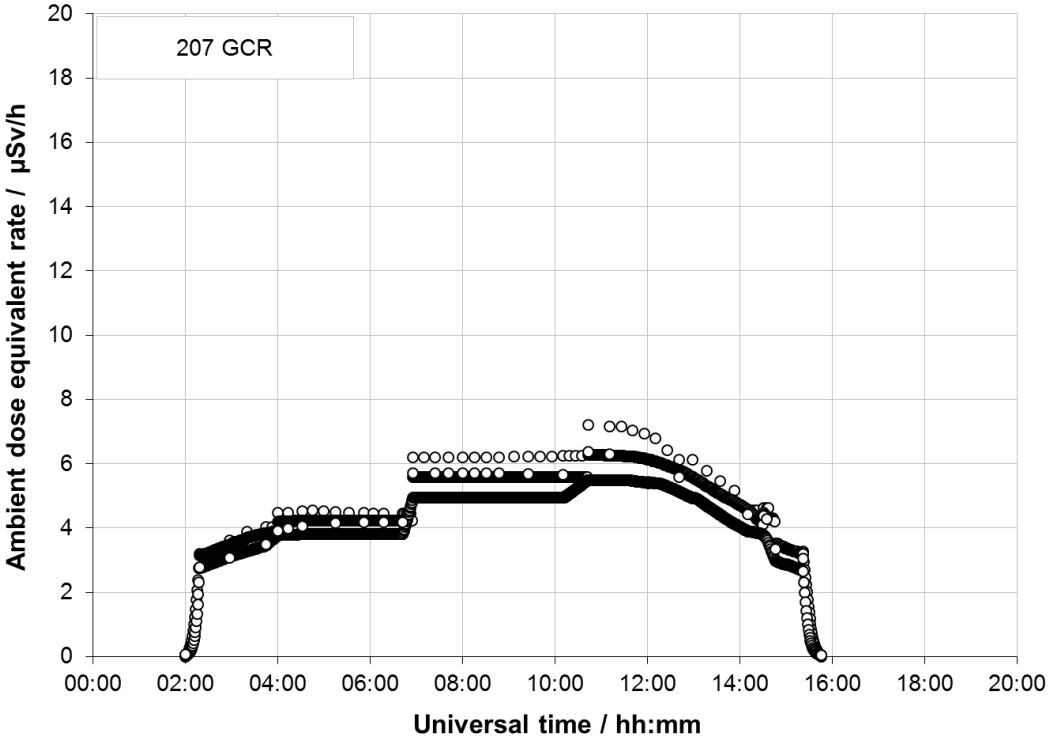

Figure 47: Comparison of ambient dose equivalent rate for galactic cosmic radiation (GCR) calculated for selected flight profile (207: Sydney–Johannesburg) by four codes.

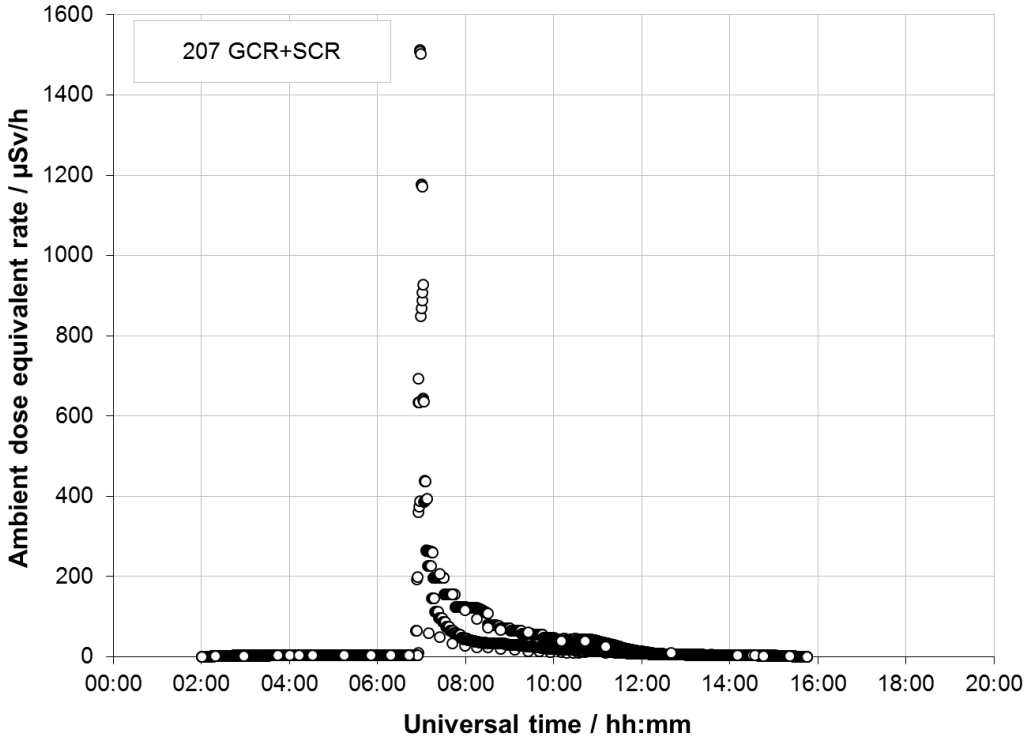

Figure 48: Comparison of ambient dose equivalent rate for the sum of galactic cosmic radiation (GCR) and GLE69 event (SCR) calculated for selected flight profile (207: Sydney–Johannesburg) by four codes.

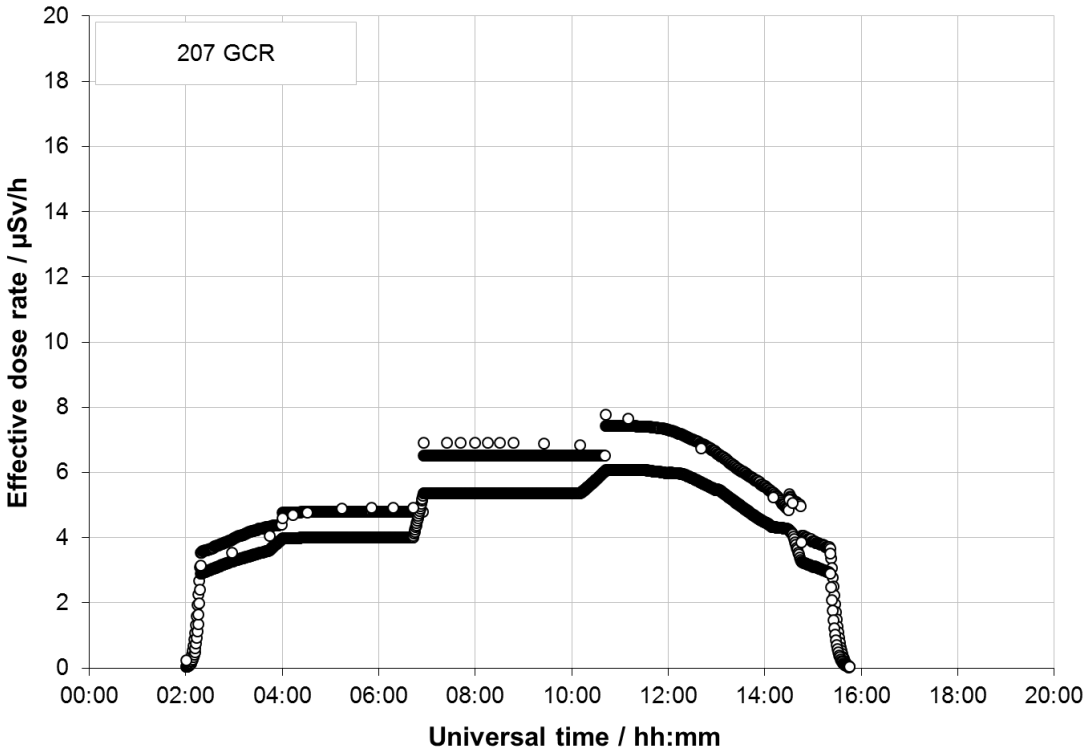

Figure 49: Comparison of effective dose rate for galactic cosmic radiation (GCR) calculated for selected flight profile (207: Sydney–Johannesburg) by three codes.

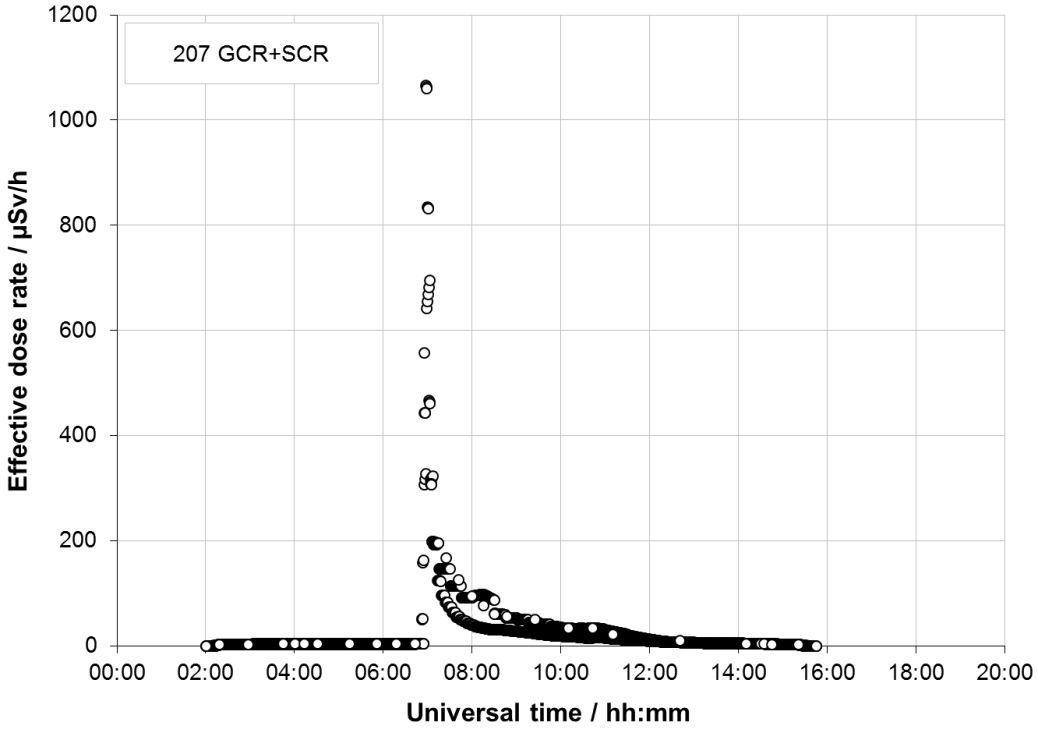

Figure 50: Comparison of effective dose rate for the sum of galactic cosmic radiation (GCR) and GLE69 event (SCR) calculated for selected flight profile (207: Sydney–Johannesburg) by three codes.

6. Discussion

Figure 19 to Figure 22 and Figure 35 to Figure 38 summarize the results obtained for the calculated route doses by the different codes for the selected flights, both in terms of ambient dose equivalent, $H^*(10)$, and effective dose, E, for the investigation of the ground level enhancement GLE42 and of GLE69. All codes result in the expected dose due to GCR as well as the increased dose during both ground level enhancements. As expected, the GCR dose data agree quite well, while the dose comparisons for GLE42 and GLE 69 show larger dose differences than for GCR.

To compare all calculated route dose results, H_{calc}, the median of the route dose results, H_{median}, is determined for each flight for the condition GCR, SCR, and GCR+SCR separately. Figure 51 and Figure 52 show the relative deviation $(H_{calc} - H_{median})/H_{median}$ for the three conditions and the three flights. There is obviously a significant spread in the dose ratios for the SCR but not for GCR. The reason for this could have several causes and can only be partially discussed in this report. It would require a detailed description of all mathematical procedures by all code providers. Since quite good agreement of codes has already been demonstrated between the codes for the assessment of doses and dose rates caused by GCR, one reason might be the different handling of the time dependent spectrum and anisotropy of the solar energetic protons. To clarify the influence of these parameters on the deviation of different codes to their median, investigations of two different GLEs with different approaches have been carried out in this study. While in the investigation of GLE42, a defined solar proton input spectrum has been provided, in the investigation of GLE69 the information on SCR input spectrum was provided by references to published data. In fact, we have observed different results for both investigations, which we will discuss in more detail.

For GLE42, the median values for $H^*(10)$ due to GCR calculated for the different flights are 42 µSv, 46 µSv and 50 µSv. The maximum deviation from the median is on the order of 20% which corresponds to a factor of about 1.5 between the lowest and the highest calculated route dose. The median values of the calculated route doses for $H^*(10)$ for the contribution of SCR are 161 µSv, 123 µSv and 123 µSv which means that on average the dose due to SCR on these routes was estimated to be between 2.5 to 4 times higher than the GCR dose. The model predictions for the SCR dose show a much broader distribution than the GCR doses with maximum deviations from the median of up to 70%. The highest estimates for the SCR route dose are factors of 4 to 5 greater than the lowest estimates. The large spread in the SCR data is somewhat diluted in the total route doses containing both GCR and SCR contributions; here the maximum deviations from the median are on the order of 40% to 50% and the ratio between the highest and the lowest estimated route dose is between 2 and 3. For the effective dose, the results are similar but with a somewhat higher maximum deviation of 40% from the median for the estimated effective dose due to GCR.

For GLE69, the GCR contribution is greater by about 15% due to the lower solar activity at the time of the event and the spread in the estimate of $H^*(10)$ is slightly higher but comparable to GLE42 (maximum deviations from the median between 10% and 30%). For SCR alone, however, the distribution is even broader than for GLE42 with maximum deviations above 80% of the median. The most extreme differences occur for the northern flight route from Chicago to Beijing (flight 202) for which the highest estimate is more than a factor of 10 greater than the lowest estimate. For the total route doses containing both GCR and SCR this translates to maximum deviations from the median between 60% and 70% and factors of about 4 between the lowest and the highest estimate.

Figure 53 shows frequency distributions based on the data from Figure 51 and Figure 52 for the relative deviations $(H_{calc} - H_{median})/H_{median}$ for both the ambient dose equivalent, $H^*(10)$ and effective

dose, *E*. The results of the comparison for the various codes that calculated the route doses for the GCR show a standard deviation from the median of 17%. This confirms the result that has been already published earlier on comparison of codes assessing radiation exposure of aircraft crew due to galactic cosmic radiation (EURADOS Report 2012-03). Figure 53 shows further for the SCR and GLE42 a standard deviation from the median of about 30% for both $H^*(10)$ and *E*. For GLE69 the corresponding standard deviation from the respective median is 50% for $H^*(10)$ and 25% for *E*.

The set of codes used for calculation of $H^*(10)$ and *E* was not the same. So, the reason for the differences of the standard deviations from the medians cannot be explained without going in the details of the different codes and compromising the anonymity.

As already mentioned above, the main difference between the dose assessments for GLE42 and for GLE69 is that different SCR input data were used: precisely defined data for GLE42 and literature values for GLE69. For GLE42 an isotropic SCR flux was assumed whereas the modelling characteristics of GLE69 were defined by each participant and had to reflect the large anisotropy during the initial and maximum phase of the SCR event as reported in the literature. Therefore, we conclude that one of the major reasons for the different results of both investigations is the different treatment of the SCR characteristics in the different codes.

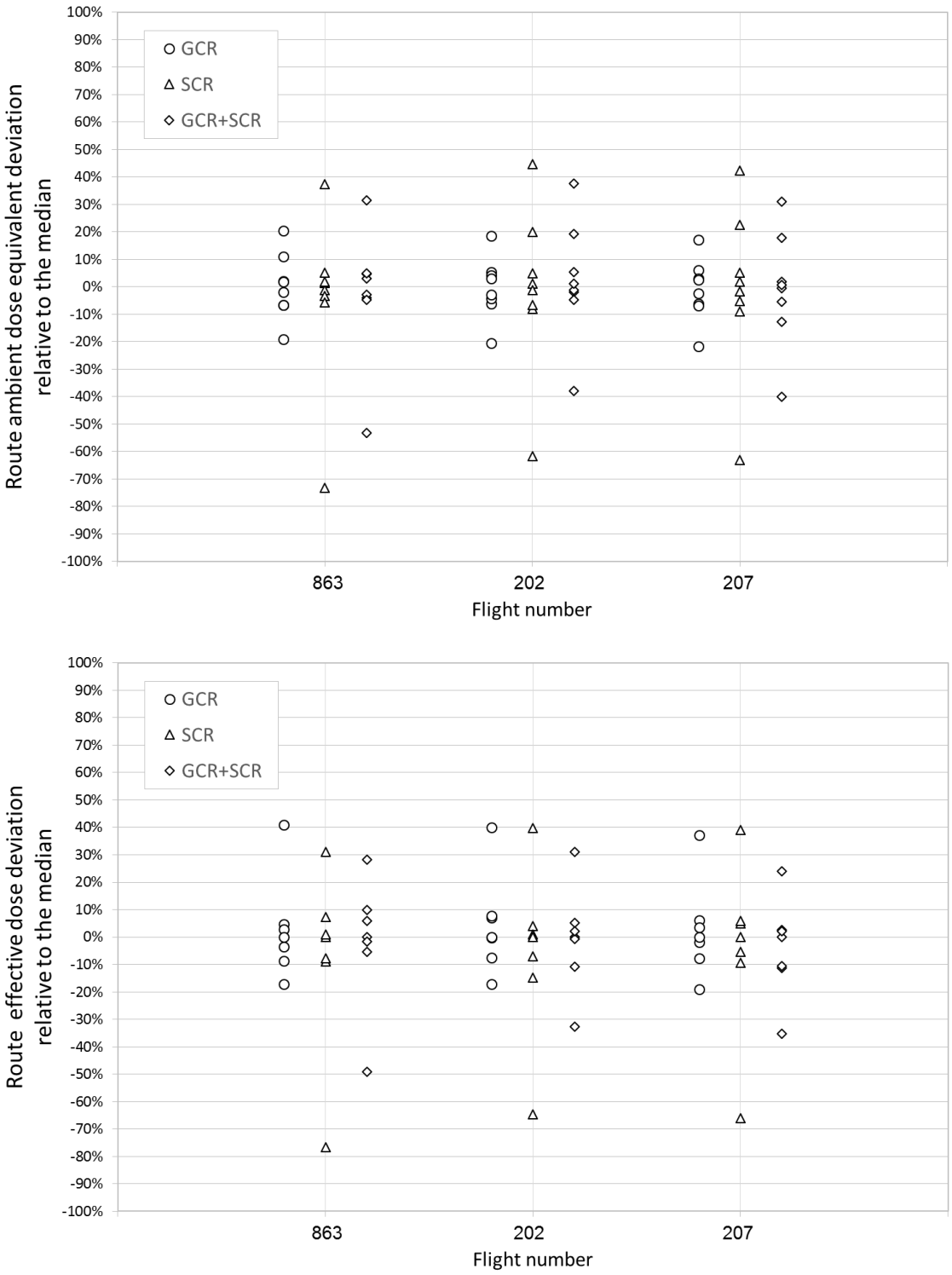

Figure 51: Comparison of the deviations for the route ambient dose equivalent, $H^*(10)$, (upper diagram) and route effective dose, E, (lower diagram) for GCR, SCR and the sum GCR+SCR for the investigation of GLE42.

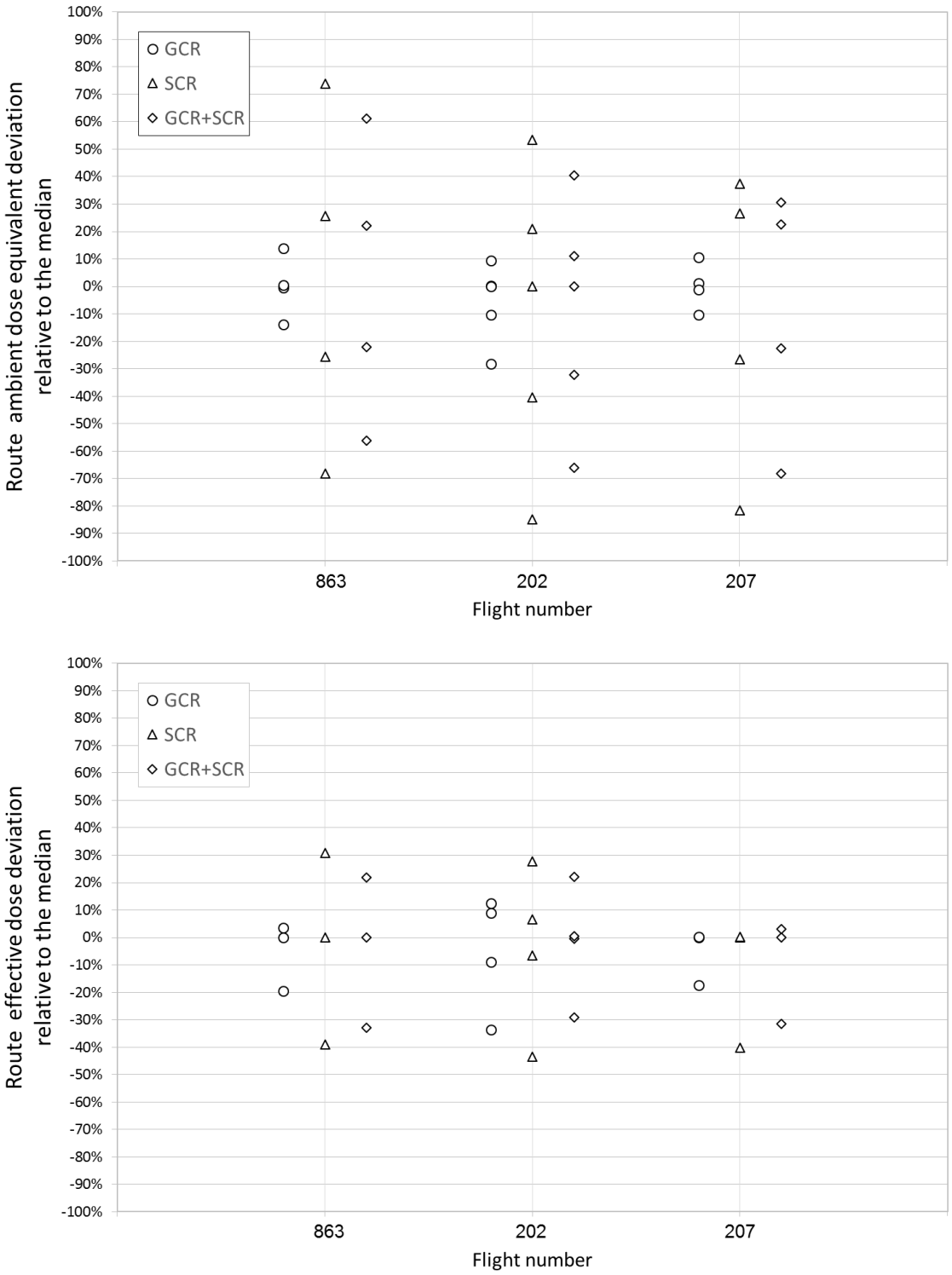

Figure 52: Comparison of the deviations of the route ambient dose equivalent, $H^*(10)$, (upper diagram) and the route effective dose, E, (lower diagram) and for GCR, SCR and the sum GCR+SCR for the investigation of GLE69.

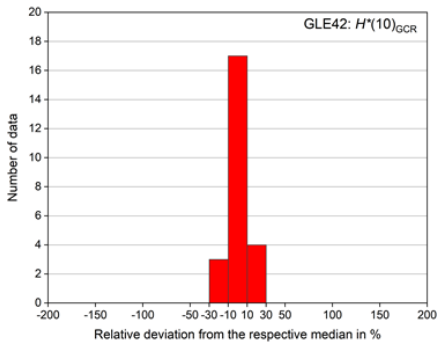

GLE42: GCR, $H^*(10)$, 11% (1σ)

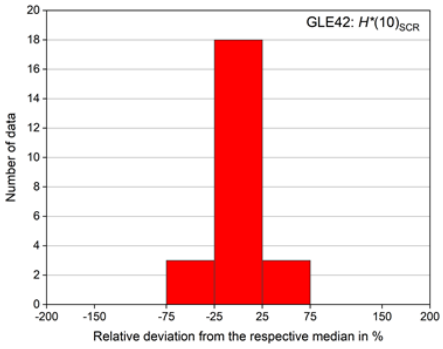

GLE42: SCR, $H^*(10)$, 29% (1σ)

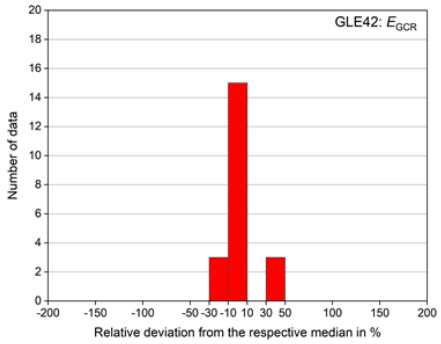

GLE42: GCR, E, 17% (1σ)

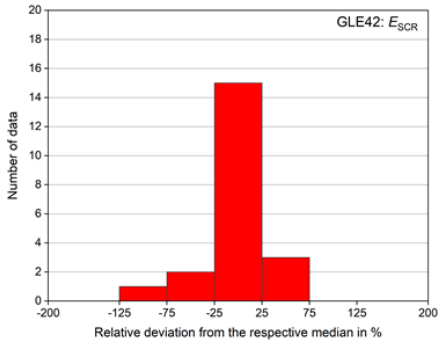

GLE42: SCR, E, 30% (1σ)

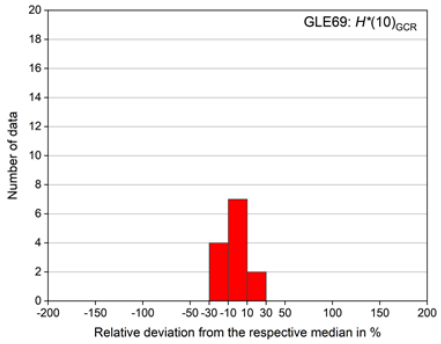

GLE69: GCR, $H^*(10)$, 11% (1σ)

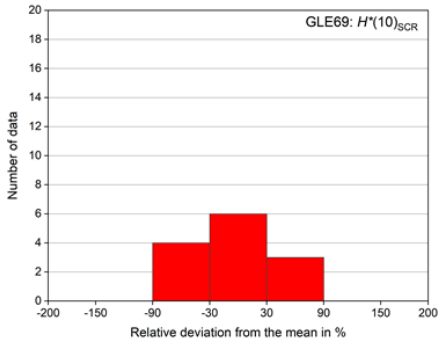

GLE69: SCR, $H^*(10)$, 50% (1σ)

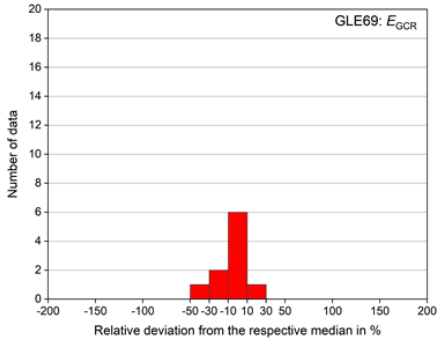

GLE69: GCR, E, 14% (1σ)

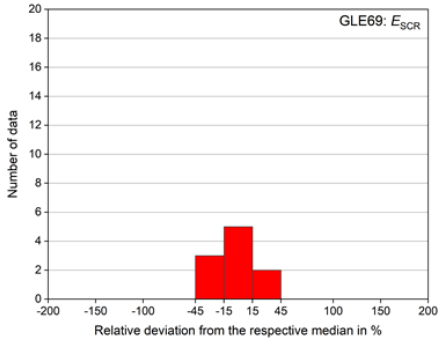

GLE69: SCR, E, 25% (1σ)

Figure 53: Relative deviation of all calculated route ambient dose equivalent values $H^*(10)$ and effective dose values E from their respective medians. Data presented for GCR (left) and SCR (right) for both investigations for GLE42 (top) and GLE69 (bottom).

7. Conclusions

Nine codes have been used for the assessment of radiation exposure in typical flight altitudes in a comparison exercise organised by the EURADOS Working Group 11 on High Energy Radiation Fields on harmonization of aviation dosimetry practices in European countries. Some of these codes are based on simulation of the secondary field of cosmic radiation by Monte Carlo techniques, while others use a semi-empirical solution based on a fit to experimental data.

Although the results of the report show estimates of the route doses due to GCR that are consistent and fairly in line with those given in the previous EURADOS report on GCR dose (EURADOS Report 2012-03), the spread in the reported route doses due to SCR is significantly larger. The maximum deviation from the median of the route doses calculated by individual codes reaches values of more than 70% for GLE42 for which the definition of the primary spectrum was pre-defined and should not provide a source of uncertainty to the model results. This large spread in the SCR route dose results based on a pre-defined spectrum cannot be explained by this report without compromising the anonymity of the codes. For GLE69, for which no specific primary proton characteristics were provided, the maximum deviation of the SCR route doses from the median reaches values above 80% and factors up to about 10 between the lowest and highest route dose value, which reduce to factors of about 4 if the total route doses include GCR and SCR.

Summarizing the results for all flights for the SCR, for GLE42 a standard deviation from the median of about 30% for both $H^*(10)$ and E is obtained. For GLE69 the corresponding standard deviation from the respective median is 50% for $H^*(10)$ and 25% for E.

We conclude that one of the major reasons for the significant spreading of the SCR route dose results obtained by the different codes is the identification and handling of the solar proton characteristics. Therefore, we strongly suggest developing a traceable method to identify and handle the solar proton characteristics (spectrum, anisotropy, time evolution) related to ground level enhancements.

In addition, we recommend that any code to be used for dose assessment of radiation exposure due to solar cosmic radiation at aviation altitudes should be validated by experimental data. This of course calls for on-board measurements during GLE events. Given the unpredictable nature of such events, this requires carefully planned, long-term measurement strategies.

8. References

(Agostinelli, 2003) Agostinelli, S., Allison, J., Amako, K. , Apostolakis, J., Araujo, H., Arce, P., Asai, M., Axen, D., Banerjee, S., Barrand, G., Behner, F., Bellagamba, L., Boudreau, J., Broglia, L., Brunengo, A., Burkhardt, H., Chauvie, S., Chuma, J., Chytracek, R., Cooperman, G., Cosmo, G., Degtyarenko, P., Dell'Acqua, A., Depaola, G., Dietrich, D., Enami, R., Feliciello, A., Ferguson, C., Fesefeldt, H., Folger, G., Foppiano, F., Forti, A., Garelli, S., Giani, S., Giannitrapani, R., Gibin, D., Gómez Cadenas, J.J., González, I., Gracia Abril, G., Greeniaus, G., Greiner, W., Grichine, V., Grossheim, A., Guatelli, S., Gumplinger, P., Hamatsu, R., Hashimoto, K., Hasui, H., Heikkinen, A., Howard, A., Ivanchenko, V., Johnson, A., Jones, F.W., Kallenbach, J., Kanaya, N., Kawabata, M., Kawabata, Y., Kawaguti, M., Kelner, S., Kent, P., Kimura, A., Kodama, T., Kokoulin, R., Kossov, M., Kurashige, H., Lamanna, E., Lampén, T., Lara, V., Lefebure, V., Lei, F., Liendl, M., Lockman, W., Longo, F., Magni, S., Maire, M., Medernach, E., Minamimoto, K., Mora de Freitas, P., Morita, Y., Murakami, K., Nagamatu, M., Nartallo, R., Nieminen, P., Nishimura, T., Ohtsubo, K., Okamura, M., O'Neale, S., Oohata, Y., Paech, K., Perl, J., Pfeiffer, A., Pia, M.G., Ranjard, F., Rybin, A., Sadilov, S., Di Salvo, E., Santin, G., Sasaki, T., Savvas, N., Sawada, Y., Scherer, S., Sei, S., Sirotenko, V., Smith, D., Starkov, N., Stoecker, H., Sulkimo, J., Takahata, M., Tanaka, S., Tcherniaev, E., Safai Tehrani, E., Tropeano, M., Truscott, P., Uno, H., Urban, L., Urban, P., Verderi, M., Walkden, A., Wander, W., Weber, H., Wellisch, J.P., Wenaus, T., Williams, D.C., Wright, D., Yamada, T., Yoshida, H., and Zschiesche, D., Geant4 – a simulation toolkit, Nuclear Instruments and Methods in Physics Research A, 506(3), 250-303 (2003).

(Allison, 2006) Allison, J., Amako, K., Apostolakis, J., Araujo, H., Arce Dubois, P., Asai, M., Barrand, G., Capra, R., Chauvie, S., Chytracek, R., Cirrone, G.A.P., Cooperman, G., Cosmo, G., Cuttone, G., Daquino, G.G., Donszelmann, M., Dressel, M., Folger, G., Foppiano, F., Generowicz, J., Grichine, V., Guatelli, S., Gumplinger, P., Heikkinen, A., Hrivnacova, I., Howard, A., Incerti, S., Ivanchenko, V., Johnson, T., Jones, F., Koi, T., Kokoulin, R., Kossov, M., Kurashige, H., Lara, V., Larsson, S., Lei, F., Link, O., Longo, F., Maire, M., Mantero, A., Mascialino, B., McLaren, I., Mendez Lorenzo, P., Minamimoto, K., Murakami, K., Nieminen, P., Pandola, L., Parlati, S., Peralta, L., Perl, J., Pfeiffer, A., Pia, M.G., Ribon, A., Rodrigues, P., Russo, G., Sadilov, S., Santin, G., Sasaki, T., Smith, D., Starkov, N., Tanaka, S., Tcherniaev, E., Tome, B., Trindade, A., Truscott, P., Urban, L., Verderi, M., Walkden, A., Wellisch, J.P., Williams, D.C., Wright, D., and Yoshida, H., Geant4 Developments and Applications, IEEE Transactions on Nuclear Science, 53(1), 270–278 (2006).

(Badhwar, 1994) Badhwar, G.D. and O'Neill, P.M., Long-term modulation of galactic cosmic radiation and its model for space exploration, Advances in Space Research, 14(10), 749–757 (1994).

(Badhwar, 1996) Badhwar, G.D. and O'Neill, P.M., Galactic Cosmic Radiation Model and its Applications, Advances in Space Research, 17(2), 7–17 (1996).

(Badhwar, 1997) Badhwar, G. D., The radiation environment in low-Earth orbit, Radiat. Res. 148(5), 3–10 (1997).

(Badhwar, 2001) Badhwar, G.D., O'Neill, P.M., and Troung, A.G., Galactic cosmic radiation environmental model, AIP Conference Proceedings, 552, 1179-1184 (2001).

(Balabin, 2013) Balabin, Yu.V., Germanenko, A.V., Vashenyuk, E.V., and Gvozdevsky, B.B., The First GLE of the New 24th Solar Cycle, 33rd International Cosmic Ray Conference, Rio de Janeiro, 2, 1467-1470 (2013).

(Beck, 1999) Beck, P., Ambrosi, P., Schrewe, U., and O'Brien, K., ACREM, Aircrew Radiation Exposure Monitoring, ARC Seibersdorf Research Report OEFZS-G-0008 (1999).

(Beck, 2007) Beck, P., Latocha, M., Dorman, L., Pelliccioni, M., and Rollet, S., Measurements and simulations of the radiation exposure to aircraft crew workplaces due to cosmic radiation in the atmosphere, Radiat. Prot. Dosim. 126(1-4), 564-567 (2007).

(Beck, 2008) Beck, P., Bartlett, D.T., Bilski, P., Dyer, C., Flückiger, E., Fuller, N., Lantos, P., Reitz, G., Rühm, W., Spurný, F., Taylor, G., Trompier, F., and Wissmann, F., Validation of modelling the radiation exposure due to solar particle events at aircraft altitudes, Radiat. Prot. Dosim. 131(1), 51-58 (2008).

(Beck, 2009a) Beck, P., Bottollier, J.F., Reitz, G., Rühm, W., and Wissmann, F., Cosmic Radiation and Aircrew Exposure, EURADOS Workshop, Braunschweig, January 29-30, 2009, Radiat. Prot. Dosim. 136(4), 231-328 (2009). doi.org/10.1093/rpd/ncp230

(Beck, 2009b) Beck, P., Dyer, C., Fuller, N., Hands, A., Latocha, M., Rollet, S., and Spurný, F., Overview of on-board measurements during solar storm periods, Radiat. Prot. Dosim. 136(4), 297-303 (2009).

(Behrens, 2010) Behrens, R., Uncertainties in external dosimetry: analytical vs. Monte Carlo method, Radiat. Prot. Dosim. 138(4), 346-352 (2010).

(Bombardieri, 2007) Bombardieri, D.J., Michael, K.J., Duldig, M.L., and Humble, J.E., Relativistic proton production during the 2001 April 15 solar event, The Astrophysical Journal, 665(1), 813-823, doi: 10.1086/519514 (2007).

(Bombardieri, 2008) Bombardieri, D.J., Duldig, M.L., Humble, J.E., and Michael, K.J., An Improved Model for Relativistic Solar Proton Acceleration Applied to the 2005 January 20 and Earlier Events, Astrophysical Journal, 682, 1315-1327, doi: 10.1086/589494 (2008).

(Bottollier, 2003) Bottollier-Depois, J.F., Biau, A., Blanchard, P., Clairand, I., Dessarps, P., Lantos, P., Saint-Lô, D., and Valero, M., Assessing exposure to cosmic radiation aboard aircraft: the SIEVERT system, Radioprotection, 38(3), 357-366 (2003).

(Bottollier, 2007) Bottollier-Depois, J.F., Blanchard, P., Clairand, I., Dessarps, P., Fuller, N., Lantos, P., Saint-Lô, D., and Trompier. F., An operational approach for aircraft crew dosimetry: the SIEVERT system, Radiat. Prot. Dosim. 125(1-4), 421-424 (2007).

(Burger, 2000) Burger, R.A., Potgieter, M.S., and Heber, B., Rigidity dependence of cosmic ray proton latitudinal gradients measured by the Ulysses spacecraft: Implications for the diffusion tensor, Journal of Geophysical Research (Space Physics), 105(A12), 27447–27455 (2000).

(Bütikofer, 2007) Bütikofer, R., Flückiger, E.O., Desorgher, L., and Moser, M.R., The extreme solar cosmic ray particle event on 20 January 2005 and its influence on the radiation dose rate at aircraft altitude, Science of The Total Environment, 391(2-3), 177-183, doi:10.1016/j.scitotenv.2007.10.021, Online (2007).

(Bütikofer, 2008) Bütikofer, R., Flückiger, E.O. , Desorgher, L., and Moser, M.R., The extreme solar cosmic ray particle event on 20 January 2005 and its influence on the radiation dose rate at aircraft altitude, Science of The Total Environment 391(2-3), 177-183, doi:10.1016/j.scitotenv.2007.10.021, Printed (2008).

(Bütikofer, 2013) Bütikofer, R., Flückiger, E., Balabin, Y., and Belov A., The reliability of GLE analysis based on neutron monitor data – a critical review, Proc. 33rd International Cosmic Ray Conference, Rio de Janeiro, 3, 1509-1512 (2013).

(Caballero, 2004) Caballero-Lopez, R.A. and Moraal, H., Limitations of the force field equation to describe cosmic ray modulation, Journal of Geophysical Research (Space Physics) 109, A01101, doi:10.1029/2003JA010098 (2004).

(Cooke, 1991) Cooke, D. J., Humble, J. E., Shea, M. A., Smart, D. F., Lund, N., Rasmussen, I. L., Byrnak, B., Goret, P., and Petrou, N., On cosmic-ray cut-off terminology, Il Nuovo Cimento C, 14(3), 213-234, doi: 10.1007/BF02509357 (1991).

(Cramp, 1997) Cramp, J.L. Duldig, M.L., Flückiger, E.O., Humble, J.E., Shea, M.A., and Smart, D.F, The October 22, 1989, solar cosmic ray enhancement: An analysis of the anisotropy and spectral characteristics, Journal of Geophysical Research, 102(A11), 24237-24248, doi: 10.1029/97JA01947 (1997).

(Debrunner, 1980) Debrunner, H. and Lockwood, J.A., The spatial anisotropy, rigidity spectrum, and propagation characteristics of the relativistic solar particles during the event on May 7, 1978, Journal of Geophysical Research (Space Physics), 85(A12), 6853-6860 (1980).

(Desorgher, 2005) Desorgher, L., PLANETOCOSMICS Software Users' Manual, 2005. cosray.unibe.ch/~laurent/planetocosmics, last access January 2021.

(Desorgher, 2006) Desorgher, L., Flückiger, E.O., and Gurtner, M. The PLANETOCOSMICS Geant4 application, 36th COSPAR Scientific Assembly (2006); www.spenvis.oma.be/help/models/planetocosmics.html, last access January 2021.

(Drouet, 2012) Drouet, F. and Michelet, M., EAN request on radiation protection of aircraft crew - Final - 7th February 2012, https://www.eu-alara.net/index.php/activities/ean-documents-and-publications/docman-menu/survey/85-aircraft-crew/file.html, last access May 2020.

(Dyer, 2003a) Dyer, C. S., Lei, F., Clucas, S. N., Smart, D. F., and Shea, M. A., Calculations and observations of solar particle enhancements to the radiation environment at aircraft altitudes, Adv. Space Res. 32(1), 81-93 (2003).

(Dyer, 2003b) Dyer, C. S., Lei, F., Clucas, S. N., Smart, D. F., and Shea, M. A., Solar particle enhancements of single event effect rates at aircraft altitudes, IEEE Trans. Nucl. Sci. 50(6), 2038-2045, doi: 10.1109/TNS.2003.821375 (2003).

(Dyer, 2007) Dyer, C.S., Lei, F., Hands, A., and Truscott, P., Solar particle events in the QinetiQ Atmospheric Radiation Model, IEEE Trans. Nucl. Sci. 54(4), 1071-1075, doi: 10.1109/TNS.2007.893537 (2007).

(Ellison, 1985) Ellison, D.C. and Ramaty, R., Shock acceleration of electrons and ions in solar flares, Astrophys. J. 298, 400–408 (1985)

(EU, 1996) European Union, Council Directive 96/29/Euratom of 13 May 1996 laying down basic safety standards for the protection of the health of workers and the general public against the dangers arising from ionising radiation, Official Journal of the European Communities, L159, 29 June 1996 (1996).

(EU, 1997) European Commission, European Radiation Dosimetry Group: Exposure of Air Crew to Cosmic Radiation. A Report of EURADOS Working Group 11, EURADOS Report 1996.01. European Commission Report Radiation Protection 85, ECSC-EC-EAEC, Brussels, Luxembourg (1997).

(EU, 2000) European Commission, European Community Council Directive 2000/79/EC of 27 November 2000 concerning the European Agreement on the Organisation of Working Time of Mobile Workers in Civil Aviation concluded by the Association of European Airlines (AEA), the European Transport Workers' Federation (ETF), the European Cockpit Association (ECA), the European Regions Airline Association (ERA) and the International Air Carrier Association (IACA), Official Journal of the European Communities, L302, 57 (2000).

(EU, 2004) European Commission, European Radiation Dosimetry Group WG5 Report Cosmic Radiation Exposure of Aircraft Crew: Compilation of Measured and Calculated Data, European Commission, Radiation Protection, 140, European Commission,

Luxembourg, (2004). https://ec.europa.eu/energy/sites/default/files/documents/140.pdf last access January 2021

(EU, 2014) European Union, Council Directive 2013/59/EURATOM of 5 December 2013 laying down basic safety standards for the protection of the health of workers and the general public against the dangers arising from ionising radiation, Official Journal of the European Union, L13, 17 January 2014 (2014).

(EURADOS, 2004) The European Radiation Dosimetry Group (EURADOS), Cosmic radiation exposure of aircraft crew - Compilation of measured and calculated data, European Commission, Radiation Protection Issue No 140 (ISBN 92-894-8448-9) (2004), Editors: L. Lindborg, D. T. Bartlett, P. Beck, I. R. McAulay, K. Schnuer, H. Schraube and F. Spurný (2004).

(EURADOS, 2012) The European Radiation Dosimetry Group (EURADOS), Comparison of Codes Assessing Radiation Exposure of Aircraft Crew due to Galactic Cosmic Radiation, (ISBN 978-3-943701-02-9) (2012), Editors: Bottollier-Depois, J.F., Beck, P., Latocha, M., Mares, V., Matthiä, D., Rühm, W., and Wissmann, F. (2012).

(FAA, 2014) FAA, Advisory Circulars (ACs), 120-61B, In-flight Radiation Exposure (11-21-2014), https://www.faa.gov/regulations_policies/advisory_circulars/ last access January 2021

(Ferrari, 2005) Ferrari, A., Sala, P.R., Fasso, A., and Ranft, J., FLUKA: a multi-particle transport code, Report CERN-2005-010, INFN-TC-2005-11, SLAC-R-773 (2005).

(Finlay, 2010a) Finlay, C., S. Maus, C. Beggan, M. Hamoudi, F. Lowes, N. Olsen, and E. Thebault, Evaluation of candidate geomagnetic field models for IGRF-11. Earth Planets and Space, 62(10):787–804. doi:10.5047/eps.2010.11.005 (2010).

(Finlay, 2010b) Finlay, C., S. Maus, C. D. Beggan, T. N. Bondar, A. Chambodut, T. A. Chernova, A. Chulliat, Golovkov, V. P., Hamilton, B., Hamoudi, M., Holme, R., Hulot, G., Kuang, W., Langlais, B., Lesur, V., Lowes, F. J., Lühr, H., Macmillan, S., Mandea, M., McLean, S., Manoj, C., Menvielle, M. Michaelis, I., Olsen, N., Rauberg, J., Rother, M., Sabaka, T. J., Tangborn, A., Tøffner-Clausen, L., Thébault, E., Thomson, A. W. P., Wardinski, I., Wei, Z., Zvereva, T. I., International Geomagnetic Reference Field: the eleventh generation. Geophysical Journal International, 183(3):1216–1230. doi:10.1111/j.1365-246X.2010. 04804 (2010).

(Friedberg, 1993) Friedberg, W., Duke, F. E., Snyder, L., Faulkner, D. N., O'Brien, K., Darden Jr., E. B., and Parker D. E., The Cosmic Radiation Environment at Air Carrier Flight Altitudes and Possible Associated Health Risks, Radiat. Prot. Dosimetry, 48(1), 21-25 (1993).

(Gaisser, 2001) Gaisser, T. K., Honda, M., Lipari, P., and Stanev, T., Primary spectrum to 1 TeV and beyond, Proc. 27th International Cosmic Ray Conference (ICRC 2001), Hamburg, Germany, 1643-1646, (2001).

(Garcia, 1975) Garcia-Munoz, M., Mason, G.M., and Simpson, J.A., The anomalous He-4 component in the cosmic-ray spectrum at below approximately 50 MeV per nucleon during 1972-1974, Astrophysical Journal, 202, 265-275 (1975).

(GEANT4, 2009a) GEANT4 Collaboration, Physics Reference Manual, Technical Report GEANT4v.9.3, CERN (2009).

(GEANT4, 2009b) GEANT4 Collaboration, User's Guide for Application Developers, Technical Report GEANT4 v.9.3, CERN, (2009).

(Gleeson, 1968a) Gleeson, L.J., Emerging Theories of the Solar Modulation of Cosmic Rays, Proceedings of the Astronomical Society of Australia PASAu, 1(4), 130-132 (1968).

(Gleeson, 1968b) Gleeson, L.J. and Axford, W.I. Solar Modulation of Galactic Cosmic Rays, Astrophys. J. 154, 1011-1026 (1968).

(Grechnev, 2008) Grechnev, V.V., Kurt, V.G., Chertok, I.M., Uralov, A.M., Nakajima, H., Altyntsev, A.T., Belov, A.V., Yushkov, B.Yu., Kuznetsov, S.N., Kashapova, L.K., Meshalkina, N.S., and Prestage, N.P., An Extreme Solar Event of 20 January 2005: Properties of the Flare and the Origin of Energetic Particles, Solar Physics, 252(1), 149-177, DOI: 10.1007/s11207-008-9245-1 (2008).

(Grieder, 2001) Grieder, P. K. F., Cosmic rays at earth: Researcher's reference manual and data book, Elsevier, 2001, ISBN 0-444-50710-8 (2001).

(Hands, 2017) Hands, A., Lei, F., Ryden, K., Dyer, C., Underwood, C., and C. Mertens, New Data and Modelling for Single Event Effects in the Stratospheric Radiation Environment, IEEE Trans. Nucl. Sci. 64(1), 587 – 595, doi:10.1109/TNS.2016.2612000 (2017).

(Heinrich, 1999) Heinrich, W., Roesler, S., and Schraube, H., Physics of Cosmic Radiation Fields, Radiat. Prot. Dosimetry, 86(4), 253–258 (1999).

(http://cosray.unibe.ch) http://cosray.unibe.ch/~laurent/planetocosmics/, last access January 2021; connection is not safe.

(http://inf.infn.it) https://www.lnf.infn.it/lnfadmin/radiation/conversioncoefficient.htm, last access January 2021; connection is not safe.

(http://www.nmdb.eu) NMDB home page: http://www.nmdb.eu, last accessed January 2021; connection is not safe.

(https://gle.oulu.fi) Oulu GLE database: https://gle.oulu.fi, last access January 2021.

(https://mcnpx.lanl.gov) MCNPX home page: https://mcnpx.lanl.gov, last access January 2021.

(https://sievert-system.org) SIEVERT home page: https://www.sievert-system.org, last access January 2021.

(https://www.eurados.org) EURADOS home page: https://eurados.sckcen.be/en, last accessed January 2021.

(https://www.faa.gov/data_research/research/med_humanfacs/aeromedical/media/MV-DATES.zip), last accessed January 2021.

(https://www.helmholtz-muenchen.de/epcardnet) EPCARD.Net Product Home Site: https://www.helmholtz-muenchen.de/epcardnet, last access January 2021.

(https://www.pstep.jp) Project for Solar-Terrestrial Environment Prediction: https://www.pstep.jp/?lang=en, last access January 2021.

(ICRP, 1991) ICRP, International Commission on Radiological Protection, 1990 Recommendations of the International Commission on Radiological Protection, ICRP Publication 60, Ann. ICRP, 21(1-3) (1991).

(ICRP, 1996) ICRP, International Commission on Radiological Protection, Conversion Coefficients for use in Radiological Protection against External Radiation, ICRP Publication 74, Ann. ICRP, 26(3-4) (1996).

(ICRP, 1997) ICRP, International Commission on Radiological Protection, General principles for the radiation protection of workers, ICRP Publication 75, Ann. ICRP, 27(1) (1997).

(ICRP, 2007) ICRP, International Commission on Radiological Protection, The 2007 Recommendations of the International Commission on Radiological Protection, ICRP Publication 103, Ann. ICRP, 37(2-4) (2007).

(ICRP, 2016) ICRP, International Commission on Radiological Protection, Radiological Protection from Cosmic Radiation in Aviation, ICRP Publication 132. Ann. ICRP 45(1), 1–48 (2016).

(ICRU, 1993) Units in Radiation Protection Dosimetry, ICRU Report 51, Journal of the ICRU, os26(2) (1993).

(ICRU, 2010) Reference Data for the Validation of Doses from Cosmic-Radiation Exposure of Aircraft Crew, ICRU Report 84 (prepared jointly with ICRP), Journal of the ICRU, 10(2) (2010).

(Kataoka, 2014) Kataoka, R., Sato, T., Kubo, Y., Shiota, D., Kuwabara, T., Yashiro, S., and Yasuda, H., Radiation dose forecast of WASAVIES during ground-level enhancement, Space Weather, 12(6), 380-386 (2014).

(Kelly, 1999) Kelly, M., Menzel, H.G., Schnuer, K., and Ryan, T. (Eds), Proc. Int. Conf. Cosmic Radiation and Aircrew Exposure, Dublin, July 1-3, 1998, Radiat. Prot. Dosim. 86, 245-356 (1999).

(Klein, 2014) Klein, K.-L., Masson, S., Bouratzis, C., Grechnev, V., Hillaris, A., and Preka-Papadema, P., The relativistic solar particle event of 2005 January 20: origin of delayed particle acceleration, A&A, 572, A4, DOI: 10.1051/0004-6361/201423783 (2014).

(Koi, 2003) Koi , T., Asai, M., Wright D.H., Niita, K., Nara, Y., Amako, K., and Sasaki, T., Interfacing the JQMD and JAM nuclear reaction codes to Geant4, SLAC-PUB 9978 (2003).

(Kubo, 2015) Kubo, Y., Kataoka, R., and Sato, T., Interplanetary particle transport simulation for warning system for aviation exposure to solar energetic particles, Earth, Planets and Space, 67, 117 (2015).

(Kuwabara, 2006) Kuwabara, T., Bieber, J.W., Clem, J., Evenson, P., and Pyle, R., Development of a ground level enhancement alarm system based upon neutron monitors, Space Weather, 4, S10001, doi:10.1029/2006SW000223 (2006).

(Kuznetsov, 2008) Kuznetsov, S.N., Kurt, V.G., Yushkov, B.Yu., and Kudela, K., CORONAS-F satellite data on the delay between the proton acceleration on the Sun and their detection at 1 AU, in: Caballero, R., et al. (eds.) Proc. 30th Int. Cosmic Ray Conf. 1, 121-124 (2008).

(Lantos, 2003a) Lantos, P. and Fuller, N., History of the solar flare radiation doses on-board aeroplanes using a semi-empirical model and Concorde measurements, Radiat. Prot. Dosim. 104(3), 199-210 (2003).

(Lantos, 2003b) Lantos, P., Fuller, N., and Bottollier-Depois, J-F., Methods for Estimating of Radiation Doses Received by Commercial Aircrew, Aviation, Space and Environmental Medicine, 74(7), 746-752 (2003).

(Lantos, 2004) Lantos, P. and Fuller, N., Semi-empirical model to calculate potential radiation exposure on board airplane during solar particle events, IEEE Transactions on Plasma Science, 32(4), 1468-1477 (2004).

(Lantos, 2006) Lantos, P., Radiation doses potentially received on-board aeroplanes during recent solar particle events, Rad. Prot. Dos. 118(4), 363-374 (2006).

(Latocha, 2009) Latocha, M., Beck, P., and Rollet, S., AVIDOS – a software package for European accredited aviation dosimetry, Radiat. Prot. Dos. 136(4) 286-290 (2009).

(Latocha, 2016) Latocha, M. and Beck, P., Cosmic radiation assessment at ESA's space weather portal with AVIDOS, Proceedings of the 16th European Conference on Radiation and Its Effects on Components and Systems (RADECS), Bremen, 2016, pp. 1-4., DOI: 10.1109/RADECS.2016.8093138 (2016).

(Lei, 2004) Lei, F., Clucas, S., Dyer, C., and Truscott, P., An atmospheric radiation model based on response matrices generated by detailed Monte Carlo simulations of cosmic ray interactions, IEEE Trans. Nucl. Sci. 51(6), 3442-3451 (2004).

(Lei, 2006) Lei, F., Hands, A., Dyer, C., and Truscott, P. Improvement to and validations of the QinetiQ Atmospheric Radiation Model (QARM), IEEE Trans. Nucl. Sci. 53(4), 1851-1858 (2006).

(Lewis, 2001) Lewis, B.J., McCall, M.J., Green, A.R., Bennett, L.G., Pierre, M., Schrewe, U.J., O'Brien, K., and Felsberger, E., Aircrew Exposure from Cosmic Radiation on Commercial Airline Routes, Radiat. Prot. Dosim. 93(4), 293-314 (2001).

(Lewis, 2002) Lewis, B.J., Bennett, L.G.I., Green, A.R., McCall, M.J., Ellaschuk, B., Butler A., and Pierre, M., Galactic and Solar Radiation Exposure to Aircrew During a Solar Cycle, Radiat. Prot. Dosim. 102(3), 207-228 (2002).

(Lewis, 2004) Lewis, B.J., Desormeaux, M., Green, A.R., Bennett, L.G.I., Butler, A., McCall, M., and Saez Vergara, J.C., Assessment of Aircrew Radiation Exposure by Further Measurements and Model Development, Radiat. Prot. Dosim. 111(2), 151-171 (2004).

(Lillhök, 2007) Lillhök, J., Beck ,P., Botollier-Depois, J.F., Latocha, M., Lindborg, L., Roos, H., Roth, J., Schraube, H., Spurny, F., Stehno, G., Trompier, F., and Wissman, F., A Comparison of ambient dose equivalent meters and dose calculations at constant flight conditions, Radiat. Meas. 42(3), 323-333 (2007).

(Lindborg, 2004) Lindborg, L., Bartlett, D., Beck, P., McAulay, I., Schnuer, K., Schraube, H., and Spurny, F., Cosmic radiation exposure of aircraft crew: compilation of measured and calculated data, doi.org/10.1093/rpd/nch232, Radiat Prot Dosim. 110(1-4), 417-422 (2004).

(Macmillan, 2011) Macmillan, S. and C. Finlay, The International Geomagnetic Reference Field. In Mandea, M., M. Korte, and B. Hultqvist (editors), Geomagnetic Observations and Models, volume 5 of IAGA Special Sopron Book Series, pages 265–276. Springer Netherlands. doi: 10.1007/978-90-481-9858-0_10 (2011).

(Mares, 2004) Mares, V., Roesler, S., and Schraube, H., Averaged particle dose conversion factors in air crew dosimetry, Radiat. Prot. Dosim. 110(1-4), 371-376 (2004).

(Mares, 2009) Mares, V., Maczka, T., Leuthold, G., and Rühm, W., Air crew dosimetry with a new version of EPCARD, Radiat. Prot. Dosim. 136(4), 262-266 (2009).

(Masson, 2009) Masson, S., Pariat, E., Aulanier, G., and Schrijver, C. J., The Nature of Flare Ribbons in Coronal Null-Point Topology, The Astrophysical Journal, 700(1), 559-578, DOI: 10.1088/0004-637X/700/1/559 (2009).

(Matthiä, 2009) Matthiä, D., The radiation environment in the lower atmosphere: a numerical approach, PhD Thesis, Christian-Albrechts-Universität zu Kiel, Germany (2009).

(Matthiä, 2009a) Matthiä, D., Heber, B., Reitz, G., Meier, M., Sihver, L., Berger, T., and Herbst, K., Temporal and spatial evolution of the solar energetic particle event on 20 January 2005 and resulting radiation doses in aviation, J. Geophys. Res. 114, A08104, doi:10.1029/2009JA014125 (2009).

(Matthiä, 2009b) Matthiä, D., Heber, B., Reitz, G., Sihver, L., Berger, T., and Meier, M., The Ground Level Event 70 on December 13th, 2006 and Related Effective Doses at Aviation Altitudes, Radiat. Prot. Dosim. 136(4), 304-310 (2009).

(Matthiä, 2013) Matthiä, D., Berger, T., Mrigakshi, A.I., and Reitz, G., A ready-to-use galactic cosmic ray model, Advances in Space Research, 51(3), 329-338 (2013).

(Matthiä, 2014) Matthiä, D., Meier, M.M., and Reitz, G., Numerical calculation of the radiation exposure from galactic cosmic rays at aviation altitudes with the PANDOCA core model, Space Weather, 12(3), 161-171, doi:10.1002/2013SW001022 (2014).

(Maus, 2005) Maus, S., Macmillan, S., Chernova, T., Choi, S., Dater, D., Golovkov, V., Lesur, V., Lowes, F., Lühr, H., Mai, W., McLean, S., Olsen, N., Rother, M., Sabaka, T., Thomson, A., and Zvereva, T., International Association of Geomagnetism and Aeronomy (IAGA), Division V, Working Group VMOD: Geomagnetic Field Modeling, The 10th-Generation International Geomagnetic Reference Field, Geophysical Journal International, 161(3), 561-565, doi: 10.1111/j.1365-246X.2005.02641.x (2005).

(Mavromichalaki, 2011) Mavromichalaki, H., Papaioannou, A., Plainaki, C., Sarlanis, C., Souvatzoglou, G., Gerontidou, M., Papailiou, M., Eroshenko, E., Belov, A., Yanke, V., Flückiger, E.O., Bütikofer, R., Parisi, M., Storini, M., Klein, K.-L., Fuller, N., Steigies, C.T., Rother, O.M.,

Heber, B., Wimmer-Schweingruber, R.F., Kudela, K., Strharsky, I., Langer, R., Usoskin, I., Ibragimov, A., Chilingaryan, A., Hovsepyan, G., Reymers, A., Yeghikyan, A., Kryakunova, O., Dryn, E., Nikolayevskiy, N., Dorman, L., and Pustil'nik, L., Applications and usage of the real-time Neutron Monitor Database, Advances in Space Research 47(12), 2210-2222, doi.org/10.1016/j.asr.2010.02.019 (2011).(Mavromichalaki, 2011) Mavromichalaki, H., Papaioannou, A., Plainaki, C., Sarlanis, C., Souvatzoglou, G., Gerontidou, M., Papailiou, M., Eroshenko, E., Belov, A., Yanke, V., Flückiger, E.O., Bütikofer, R., Parisi, M., Storini, M., Klein, K.-L., Fuller, N., Steigies, C.T., Rother, O.M., Heber, B., Wimmer-Schweingruber, R.F., Kudela, K., Strharsky, I., Langer, R., Usoskin, I., Ibragimov, A., Chilingaryan, A., Hovsepyan, G., Reymers, A., Yeghikyan, A., Kryakunova, O., Dryn, E., Nikolayevskiy, N., Dorman, L., and Pustil'nik, L., Applications and usage of the real-time Neutron Monitor Database, Advances in Space Research 47(12), 2210-2222, doi.org/10.1016/j.asr.2010.02.019 (2011).

(Mavromichalaki, 2011) Mavromichalaki, H., Papaioannou, A., Plainaki, C., Sarlanis, C., Souvatzoglou, G., Gerontidou, M., Papailiou, M., Eroshenko, E., Belov, A., Yanke, V., Flückiger, E.O., Bütikofer, R., Parisi, M., Storini, M., Klein, K.-L., Fuller, N., Steigies, C.T., Rother, O.M., Heber, B., Wimmer-Schweingruber, R.F., Kudela, K., Strharsky, I., Langer, R., Usoskin, I., Ibragimov, A., Chilingaryan, A., Hovsepyan, G., Reymers, A., Yeghikyan, A., Kryakunova, O., Dryn, E., Nikolayevskiy, N., Dorman, L., and Pustil'nik, L., Applications and usage of the real-time Neutron Monitor Database, Advances in Space Research 47(12), 2210-2222, doi.org/10.1016/j.asr.2010.02.019 (2011).

(McCracken, 2008) McCracken, K.G., Moraal, H., and Stoker, P.H., Investigation of the multiple-component structure of the 20 January 2005 cosmic ray ground level enhancement, J. Geophys. Res. 113, A12101, doi:10.1029/2007JA012829 (2008).

(Meier, 2019) Meier, M.M. and Matthiä, D., Dose assessment of aircrew: the impact of the weighting factors according to ICRP 103, Journal of Radiological Protection, 39(3), 698-706, doi: 10.1088/1361-6498/ab178d (2019).

(Mewaldt, 2005) Mewaldt, R.A., Looper, M. D., Cohen, C.M.S., Mason, G.M., Haggerty, D.K., Desai, M.I., Labrador, A.W., Leske, R.A., and Mazur, J.E., Solar-Particle Energy Spectra during the Large Events of October-November 2003 and January 2005, Proc. 29th International Cosmic Ray Conference, Pune, ICRC 1, 111-114 (2005).

(Mishev, 2013) Mishev, A.L., Usoskin, I.G., and Kovaltsov, G.A., Neutron monitor yield function: New improved computations, doi: 10.1002/jgra.50325, J. Geophys. Res., Space Physics, 118(6), 2783-2788 (2013).

(Mottl, 2001) Mottl, D., Nymmik, R., and Sladkova, A., Spectra of solar energetic protons derived from statistical analysis of experimental data on large set of events, Proc. 27th International Cosmic Ray Conference, Hamburg, ICRC paper SH030, 3185-3188 (2001).

(NASA, 1976) NOAA, NASA, and USAF, U.S. Standard Atmosphere 1976, *NASA-TM-X-74335* (1976).

(NIST, 2019) NIST, National Institute of Standards and Technology, http://physics.nist.gov/PhysRefData/Star/Text/PSTAR.html, last access May 2020.

(Nymmik, 1992) Nymmik, R.A., Panasyuk, M.I., Pervaja, T.I., and Suslov, A.A., A model of galactic cosmic ray fluxes, Nucl. Tracks and Radiat. Meas. 20(3), 427-429 (1992).

(O'Brien, 1998) O'Brien, K., Friedberg, W., Sauer, H.H. and Smart, D.F., The atmospheric cosmic- and solar energetic particle radiation environment at aircraft altitudes, Adv. Space Res., 21(12), 1739-1748 (1998) (O'Brien, 1998) O'Brien, K., Friedberg, W., Sauer, H.H. and Smart, D.F., The atmospheric cosmic- and solar energetic particle radiation environment at aircraft altitudes, Adv. Space Res., 21(12), 1739-1748 (1998).

(O'Brien, 2000) O'Brien, K., and Sauer, H.H., An adjoint method of calculation of solar-particle-event dose rates. Technology, 7, 449-456 (2000).

(O'Neill, 2006) O'Neill, P.M., Badhwar-O'Neill galactic cosmic ray model update based on advanced composition explorer (ACE) energy spectra from 1997 to present, Adv. Space Res. 37(9), 1727-1733 (2006).

(O'Neill, 2010) O'Neill, P., Badhwar–O'Neill 2010 Galactic Cosmic Ray Flux Model - Revised. IEEE-TNS, 57(6), 3148–3153, doi:10.1109/TNS.2010.2083688 (2010).

(O'Sullivan, 1999) O'Sullivan, D. (1999) Co-ordinator, Study of Radiation Fields and Dosimetry at Aviation Altitudes: Final Report January 1996-June 1999, The Dublin Institute for Advanced Studies School of Cosmic Physics Report 99-9-1, Dublin Institute for Advanced Studies, Dublin, Ireland, (1999).

(Pelliccioni, 2000) Pelliccioni, M., Overview of fluence-to-effective dose and fluence-to-ambient dose equivalent conversion coefficients for high energy radiation calculated using the FLUKA code, Radiat. Prot. Dosim. 88(4), 279–297 (2000).

(Picone, 2002) Picone, J.M., Hedin, A.E., Drob, D.P., and Aikin, A.C., NRMLMSISE-00 empirical model of the atmosphere: Statistical comparisons and scientific issues, J. Geophys. Res. 107(A12), SIA 15-1-SIA 15-16, doi:10.1029/2002JA009430 (2002).

(Pioch, 2012) Pioch, C.D., Measurement and Simulation of the Radiation Environment in the Lower Atmosphere for Dose Assessment, PhD Thesis, TU München (2012).

(Plainaki, 2010) Plainaki, C. , Mavromichalaki, H., Belov, A., Eroshenko, E., Andriopoulou, M., and Yanke, V., A New Version of the Neutron Monitor Based Anisotropic GLE Model: Application to GLE60, Solar Physics, 264, 239-254, doi: 10.1007/s11207-010-9576-6 (2010).

(Poluianov, 2017) Poluianov, S.V., Usoskin, I.G., Mishev, A.L., Shea, M.A., and Smart, D.F., GLE and Sub-GLE Redefinition in the Light of High-Altitude Polar Neutron Monitors, Solar Physics, 292, 176, doi: 10.1007/s11207-017-1202-4 (2017).

(Reames, 2004) Reames, D. V., and Ng, C.K., Heavy Element Abundances in Solar Energetic Particle Events, ApJ, 610(1), 510-522 (2004).

(Reitz, 1991) Reitz, G., Schnuer, K., and Shaw, K., (Eds), Proc. Workshop Radiation Exposure of Civil Aircrew, Luxembourg, June 25-27, 1991, Radiat. Prot. Dosim. 48(1), 3-140 (1993).

(Roesler, 1998) Roesler, S., Heinrich, W., and Schraube, H., Calculation of Radiation Fields in the Atmosphere and Comparison to Experimental Data, Radiation Research, 149(1), 87–97, doi.org/10.2307/3579685 (1998).

(Roesler, 2002) Roesler, S., Heinrich, W., and Schraube, H., Monte Carlo calculation of the radiation field at aircraft altitudes, Radiat. Prot. Dosim. 98(4), 367-388, doi:10.1093/oxfordjournals.rpd.a006728 (2002).

(Sato, 2008) Sato, T., Yasuda, H., Niita, K., Endo, A., and Sihver, L., Development of PARMA: PHITS-based Analytical Radiation Model in the Atmosphere, Radiat. Res. 170(2), 244-259, doi: 10.1667/RR1094.1 (2008).

(Sato, 2009), Sato, T., Endo, A., Zankl, M. Petoussi-Henss, N, and Niita, K., Fluence-to-dose conversion coefficients for neutrons and protons calculated using the PHITS code and ICRP/ICRU adult reference computational phantoms, Physics in Medicine & Biology, Volume 54, Number 7 (2009)

(Sato, 2014) Sato, T., Kataoka, R., Yasuda, H., Yashiro, S., Kuwabara, T., Shiota, D., and Kubo, Y., Air shower simulation for WASAVIES: warning system for aviation exposure to solar energetic particles, Radiat. Prot. Dosim. 161(1-4), 274-278 (2014).

(Schraube, 2002) Schraube, H., Leuthold, G., Heinrich, W., Roesler, S., Mares, V. and Schraube, G., EPCARD – European program package for the calculation of aviation route doses, User's

manual, GSF-National Research Center, Neuherberg, Germany, ISSN 0721 - 1694. GSF-Report 08/02 (2002).

(Schrewe, 2000) Schrewe, U. J., Global measurements of the radiation exposure of civil air crew from 1997 to 1999, Radiat. Prot. Dosim. 91(4), 347-364 (2000).

(Shea, 1990) Shea, M.A. and Smart, D.F., A Summary of Major Solar Proton Events, Solar Phys. 127, 297-320, (1990).

(Shea, 1993) Shea, M.A. and Smart, D.F., Solar proton events: History, statistics and predictions, Proc. Solar-Terrestrial Prediction – IV, 2, 48-70 (1993).

(Shea, 1999) Shea, M.A. and Smart, D.F., Patterns of Solar Proton Events over Four Solar Cycles, Proc. 26th Int. Cosmic Ray Conf. 6, 374-377, (1999).

(SiGLE_RT, 2018) https://previ.obspm.fr/index.php?page=SiGLEevolves

(Simnett, 2006) Simnett, G. M., The timing of relativistic proton acceleration in the 20 January 2005 flare, A&A, 445(2), 715-724, https://doi.org/10.1051/0004-6361:20053503 (2006).

(Simnett, 2007) Simnett, G. M., Erratum: The timing of relativistic proton acceleration in the 20 January2005 flare and other papers, A&A, 472(1), 309 – 310, https://doi.org/10.1051/0004-6361:20053503e (2007).

(Smart, 1971) Smart, D.F., Shea, M.A., and Tanskanen, P.J., A Determination of the Spectra, Spatial Anisotropy, and Propagation Characteristics of the Relativistic Solar Cosmic-Ray Flux on November 18, 1968. Proc. 12th International Conference on Cosmic Rays, 2, 483-488 (1971).

(Smart, 1991) Smart, D.F., Shea, M.A., Wilson, M.D., and Gentile, L.C., Solar Cosmic Rays on 29 September 1989; An Analysis using the World-Wide Network of Cosmic Ray Stations, Proc. 22nd International Conference on Cosmic Rays, ICRC, 3, 97-100 (1991).

(Smart, 1997) Smart, D.F. and Shea, M.A., World grid of cosmic ray vertical cutoff rigidities for Epoch 1990.0. , Proc. 25th International Cosmic Ray Conference, 2, 401-404 (1997).

(Smart, 2000) Smart, D.F., Shea, M.A., and Flückiger, E.O., Magnetospheric models and trajectory computations, Space Science Reviews, 93, 305-333, doi: 10.1023/A:1026556831199 (2000).

(Spurny, 2001) Spurny, F. and Dachev, Ts., Measurement on Board an Aircraft during an Intense Solar Flare, Ground Level Event 60, on April 15, 2001, Radiat. Prot. Dosim. 95(3), 273-275 (2001).

(Takada, 2007) Takada, M., Lewis, B.J., Boudreau, M., Al Anid, H., and Bennett, L.G.I., Modelling of Aircrew Radiation Exposure from Galactic Cosmic Rays and Solar Particle Events, Radiat. Prot. Dosim. 124(4), 289-318 (2007).

(Thierfeldt, 2009) Thierfeldt, S., Haider, C., Hans, P., Kaleve, M., and Neuenfeldt, F., Evaluation of the implementation of radiation protection measures for aircrew in EU member states, Radiat. Prot. Dosim. 136(4), 324–328, doi:10.1093/rpd/ncp170 (2009).

(Tsyganenko, 1989), Tsyganenko, N.A., A magnetospheric magnetic field model with a warped tail current sheet, Planetary and Space Science, 37(1), 5-20 (1989).

(Tylka, 1997) Tylka, A.J., Adams, J.H., Boberg, P.R., Brownstein, B., Dietrich, W.F., Flueckiger, E.O., Petersen, E.L., Shea, M.A., Smart, D.F., and Smith, E.C., CREME96: a revision of the cosmic ray effects on micro-electronics code, IEEE T. Nucl. Sci. 44(6), 2150–2160, doi: 10.1109/23.659030 (1997).

(Usoskin, 2005) Usoskin, I., G., Alanko-Huotari, G., Kovaltsov, A., and Mursula, K., Heliospheric modulation of cosmic rays: Monthly reconstruction for 1951-2004, J. Geophys. Res. 110, A12108, doi: 10.1029/2005JA011250 (2005).

(Usoskin, 2011) Usoskin, I.G., Bazilevskaya, G.A., and Kovaltsov, G.A., Solar modulation parameter for cosmic rays since 1936 reconstructed from ground-based neutron monitors and ionization chambers, J. Geophys. Res. (Space Physics), 116, A02104, doi:10.1029/2010JA016105 (2011).

(Vashenyuk, 2005) Vashenyuk, E.V., Balabin, Yu.V., Gvozdevsky, B.B., Karpov, S.N., Yanke, V.G., Eroshenko, E.A., Belov, A.V., and Gushchina, R.T., Relativistic solar cosmic rays in January 20, 2005 event on the ground based observations, Proc. 29th International Cosmic Ray Conference, ICRC 1, 209-212 (2005).

(Wissmann, 2006) Wissmann, F., Long-term measurements of H*(10) at aviation altitudes in the northern hemisphere, Radiat. Prot. Dosim. 121(4), 347-357 (2006).

(Wissmann, 2010) Wissmann, F., Reginatto, M. and Möller T., The ambient dose equivalent at flight altitudes: a fit to a large set of data using a Bayesian approach, J. Radiol. Prot. 30(3), 513-524, doi: 10.1088/0952-4746/30/3/006 (2010).

(Yasuda, 2011) Yasuda, H., Sato, T., Yonehara, H., Kosako, T., Fujitaka, K., and Sasaki, Y., Management of cosmic radiation exposure for aircrew in Japan, Radiat. Prot. Dosim. 146(1-3), 123-125, doi: 10.1093/rpd/ncr133 (2011).

Appendix 1: Description of Models

A1.1 AVIDOS and SOLARDOS

AVIDOS is based on numerical calculations and an empirical model. Numerical calculations were performed using the FLUKA (Ferrari, 2005) Monte Carlo code. A spatial density profile of the Earth's atmosphere and an updated primary proton energy spectrum (Gaisser, 2001) were taken into account in modelling the Earth environment and galactic cosmic radiation. Resulting fluence rates were converted into ambient dose equivalent rates and into effective dose rates using fluence to dose conversion coefficients (Pelliccioni, 2000) according to the ICRP 60 publication (ICRP, 1991). A multi-parameter model (Beck, 2007) was applied to the results of the FLUKA calculations, allowing the determination of ambient dose equivalent rates and effective dose rates over the full range of vertical cutoff rigidity (Smart, 1997), solar deceleration potential (Badhwar, 1997) and commercially used altitudes. The solution was implemented in a computational code called AVIDOS. Route doses are calculated by integrating dose rates calculated at each waypoint. A waypoint should give information on current flight time, geographical location and altitude. If the travel time between two following waypoints is larger than 5 minutes, sub-waypoints are created assuming constant altitude and route along a great circle. AVIDOS is regularly updated with neutron monitor records to reflect changes in solar activity. AVIDOS is further described by Latocha, et al. (Latocha, 2009). Dose determination of the aircraft crew with AVIDOS is carried out with uncertainties less than ± 30% and in accordance with the laboratory standard EN ISO IEC 17025, which is valid worldwide due to the accreditation of the Austrian accreditation body as a member of the International Laboratory Accreditation Cooperation (ILAC).

SOLARDOS is a module for real-time assessment of radiation exposure at aviation altitudes due to strong solar energetic particles that lead to enhanced radiation levels on ground (GLE). This module together with AVIDOS forms the software package AVIDOS 2.0. The estimation of GLE radiation exposure has few steps. In the first step, a solar proton spectrum is assessed. This is done based on a wide literature study and data from a single neutron monitor station. AVIDOS 2.0 calculates a soft spectrum with lower maximum proton energies and a hard one with higher maximum proton energies for an isotropic incidence scenario. The spectra are propagated through the atmosphere using Mote Carlo numerical simulations results performed with Geant4 (Agostinelli et al., 2003; Allison et al., 2006) application PLANETOCOSMICS (http://cosray.unibe.ch). For ambient dose equivalent and effective dose rates, the ICRP-60 conversion coefficients (Pelliccioni, 2000) are used. In this way, the minimum and the maximum expected dose rates are assessed. In real-time mode, the whole procedure is automatically triggered by a GLE-alert system and during a GLE event, the calculations are done every 5 minutes. A more detailed description is published elsewhere (Latocha, 2016).

An internet version of AVIDOS 2.0 is provided to the public via the ESA Space Weather Portal (http://swe.ssa.esa.int/web/guest/avidos-federated). It is an educational online software and may not be used for radiation dosimetry services. The software has four modes that differ in complexity. In the public mode, simplified calculations are conducted based only on departure, destination and the date/time of the flight. In aircrew mode, one can change cruising altitude and flight duration. In waypoint mode, one can upload a detailed flight profile. Finally, science mode allows for an analysis of radiation dose dependency on different solar proton spectra and flight paths. In 2021, a new version 3.0 of AVIDOS with web technology and improved graphical user interface will be released.

A1.2 EPCARD.Net and GEANT4 – GLE module

A widely used program for monitoring of the effective dose of aircrews is the **E**uropean **P**rogram package for the **C**alculation of **A**viation **R**oute **D**oses[2] (EPCARD). This code was developed at the Helmholtz Zentrum München (former GSF) by (Schraube et al., 2002) together with scientists from the University of Siegen, Germany, and further improved by (Mares et al., 2009) as EPCARD.Net[3]. EPCARD.Net is a completely new object-oriented code which can be run without recompilation on many state-of-the-art operating systems such as Microsoft® Windows NT/2K/XP/Vista/Win7/Win8 /Win10 (using .Net® or Mono® runtime platform) or "UNIX kernel type" operating systems like Linux, Mac OS X or Solaris (using the Mono® runtime platform). The so called "XML-EPCARD application" for input and output guarantees errorless data exchange. It can be implemented in a broad spectrum of usage scenarios like a WEB service, an Operating System scripts component, or as a single standalone application with intuitive Graphic User Interface. All legal requirements for the determination of effective dose along any flight route are fulfilled by this program package. In 2010, EPCARD.Net ver. 5.4.3 Professional was approved for official use for dose assessment of radiation exposure due to secondary cosmic radiation at aviation altitudes by the German Aviation Authority (LBA) and the National Metrology Institute, Physikalisch-Technische Bundesanstalt (PTB).

The basis for the calculation of effective dose, E, and ambient dose equivalent, $H^*(10)$, in EPCARD.Net are secondary particle spectra of neutrons, protons, photons, electrons and positrons, muons, and pions, calculated by (Roesler, 1998, 2002) and (Heinrich, 1999) with FLUKA Monte Carlo code (Ferrari, 2005) at various depths down to sea level for all possible physical circumstances of solar activity and geomagnetic shielding conditions. The primary galactic spectra used in the FLUKA calculations, as well as the modulation potential describing solar activity, and the related impact on the GCR intensity and spectral distribution near Earth ware based on the theory of Badhwar and O'Neill (Badhwar et al., 1994, 1996). This model was designed to derive the solar potential from the Climax Neutron Monitor and it was revised by O'Neill (O'Neill, 2006, 2010). These secondary particle spectra were recently inter-compared and shown to be consistent with new results of Pioch (Pioch, 2012). He has used proton and helium spectra from (Burger et al., 2000) and the model for the heliopsheric modulation developed by (Usoskin et al., 2005, 2011) to calculate secondary particle fluxes, and the corresponding dose quantities with GEANT4 v. 9.3 (Agostinelli et al., 2003; Allison et al., 2006) and the G4NDL data library v. 3.13 (GEANT4, 2009a, 2009b). A similar procedure was used in case of GLE42 using a differential intensity of solar protons as defined by (Smart et al., 1991) and used for this EURADOS inter-comparison. Based on secondary cosmic ray particle spectra calculated with GEANT4, and applying minutely flight profiles calculated with EPCARD.Net, including time, altitude, geographic position, and the related vertical effective cutoff rigidity the dose quantities were estimated. Merging EPCARD.Net with GEANT4 calculations provides the basis for a GLE module in EPCARD.Net package. Deriving the intensity-time profile of a GLE as well as the maximum amplitude from near real-time Neutron Monitor databases (e.g. NMDB[4]), and assuming an isotropic flux of solar protons near Earth allows, in most cases, conservative dose estimation soon after the event, which is favored for radiation protection purposes. However, additional investigations and calculations for different GLEs are required in order to fully develop a GLE module for EPCARD.Net which may be routinely applied in aircrew dosimetry.

[2] https://www.helmholtz-muenchen.de/epcard

[3] https://www.helmholtz-muenchen.de/epcardnet

[4] http://www.nmdb.eu

A1.3 FDOScalc

FDOScalc is based on a mathematical model which provides a fit to the complete dataset of ambient dose equivalent rates measured by PTB. The dataset includes 892 data points measured between 1997 and 1999 with an ionization counter and a modified rem counter (Schrewe, 2000), and 1537 data points measured with a tissue-equivalent proportional counter (TEPC) system between 2003 and 2006 (Wissmann, 2006). The model includes all relevant influencing parameters, such as altitude, vertical cutoff rigidity, and neutron monitor rate. The goal was to have a simple-to-use, functional description of the dose rate distribution for different flight altitudes, geographical locations, and levels of solar activity. Since the problem was approached with Bayesian statistical methods, tools were available to investigate and compare various competing mathematical models that could be used to describe the data; it was also possible to evaluate an uncertainty for each dose rate value calculated with the final model function. In references (Schrewe, 2000; Wissmann, 2006), it was shown that relatively simple relations can be used to describe the measured dose rate as a function of the altitude, geomagnetic latitude, and fluence rate of secondary neutrons at ground level. Since the neutron monitor rate is a direct measure of the fluence rate of primary cosmic ray particles entering into the atmosphere, it can be used to evaluate the change in the dose rate at flight altitudes due to changes in solar activity. The neutron monitor at Oulu, Finland, was selected for monitoring the secondary neutron fluence rate at ground level. The geomagnetic latitude is not the best parameter to describe the influence of the Earth's magnetic field. A better parameter is the vertical cutoff rigidity, r_a, which describes the minimum rigidity required for a charged particle to enter the magnetic field and to reach a certain altitude. It was shown in references (Schrewe, 2000; Wissmann, 2006) that the measured data, when normalized to a common altitude of FL350, smoothly follow a simple function of vertical cutoff rigidity r_c,

$$\dot{H}_{\mathrm{FDOScalc}} = \dot{H}_0 + \dot{H}_1 \, \mathrm{e}^{-(r_c/c)^d}$$

$$\dot{H}_{\mathrm{FDOScalc}} = \dot{H}_0 + \dot{H}_1 \, \mathrm{e}^{-(r_c/c)^d}$$

where $\dot{H}_0$ $\dot{H}_0$ and $\dot{H}_1$ $\dot{H}_1$ are assumed to be constant and c, d are fitting parameters. In FDOScalc, a more general expression in which the coefficients are described by a Taylor expansion was used. A detailed analysis using tools of Bayesian data analysis showed that not all expansion coefficients are necessary to describe the data. This approach prevents over- or under-parameterization of the mathematical model. The final equations used in FDOScalc are (Wissmann, 2010):

$$\begin{aligned}
\dot{H}_0 &= a_{00} + a_{01}(h - h^0) \\
\dot{H}_1 &= a_{00} + b_{10}(N_{\mathrm{NM}} - N^0_{\mathrm{NM}}) + c_{10}(N_{\mathrm{NM}} - N^0_{\mathrm{NM}})^2 + \\
&\quad [a_{11} + b_{11}(N_{\mathrm{NM}} - N^0_{\mathrm{NM}}) + c_{11}(N_{\mathrm{NM}} - N^0_{\mathrm{NM}})^2](h - h^0)
\end{aligned}$$

$$\begin{aligned}
\dot{H}_0 &= a_{00} + a_{01}(h - h^0) \\
\dot{H}_1 &= a_{00} + b_{10}(N_{\mathrm{NM}} - N^0_{\mathrm{NM}}) + c_{10}(N_{\mathrm{NM}} - N^0_{\mathrm{NM}})^2 + \\
&\quad [a_{11} + b_{11}(N_{\mathrm{NM}} - N^0_{\mathrm{NM}}) + c_{11}(N_{\mathrm{NM}} - N^0_{\mathrm{NM}})^2](h - h^0)
\end{aligned}$$

where h is the altitude, N_{NM} is the count rate of the neutron monitor in Oulu, and a_{xx}, b_{xx}, and c_{xx} are fitting parameters. The exponent "0" indicates the reference values. The validity of this function is restricted to the data range of the fitted data. Therefore, only calculations for Oulu neutron monitor count rates N_{NM} between 5700 counts/min and 6500 counts/min and flight levels between FL230 and FL415 are allowed.

A1.4 WASAVIES | JISCARD EX

For GCR calculations, JISCARD EX (Yasuda, 2011, http://www.jiscard.jp/) coupled with a PHITS-based analytical code PARMA (Sato, 2008) is used, while calculations for SEP are done with WASAVIES (Kataoka, 2014; Sato, 2014).

WASAVIES (Warning System for Aviation Exposure to Solar Energetic Particles) is a physics-based forward model for predicting the time profile of radiation dose for aircrews. As of 2015, the basic flow of the model is to:

1 detect GLE by a GLE-Alarm system based on the count rates of several neutron monitors (Kuwabara, 2006),
2 evaluate the appropriate mean free path and the injection profile of the event, using the count rates of several neutron monitors,
3 predict the energy and time dependences of the SEP fluxes outside magnetosphere by solving the focused transport equation using the above parameters (Kubo, 2015),
4 normalize the calculated SEP fluxes using the GOES proton data,
5 determine the SEP fluxes at the top of the atmosphere up to 86 km in altitude, using the proton trace model in the magnetosphere (Kataoka, 2014),
6 calculate the SEP fluxes on flight routes using the database of the air-shower simulation for mono-energetic proton incidences performed by PHITS (Sato, 2014), and
7 convert the calculated fluxes to the effective doses using the dose conversion coefficients given in ICRP publication 116.

It takes approximately 2.5 hours to evaluate the mean free path and the injection profile (step 2) after the detection of GLEs, and thus, the current WASAVIES cannot predict doses during the peak of GLEs. Therefore, the developers are trying to reduce the time for the evaluation. The automatic calculation and broadcast system is also under development in the framework of Project for Solar-Terrestrial Environment Prediction – PSTEP (http://www.pstep.jp) in Japan.

A1.5 PCAIRE

The Predictive Code for AIrcrew Radiation Exposure, known as PCAIRE, is a semi-empirical model to calculate radiation exposure for commercial aircrew and frequent flyers (available online at www.pcaire.com), with one of the world's largest repositories of measured global flights spanning a range of geomagnetic latitudes from -40° to 85° (Lewis, 2001). These flight data have been collected on commercial and military aircrafts by PCAIRE in cooperation with the Royal Military College of Canada, since 1997, with 15-30 instrumented flights flown each year (Lewis, 2002; Lewis, 2004).

A tissue-equivalent proportional counter (TEPC) is used to collect ambient dose equivalent data at one-minute intervals. All data are correlated with the specific altitude and global position and then averaged over five-minute intervals using a standard smoothing technique. An altitude correction function has been developed to account for the effect of altitude. In addition, a theoretical analysis scales the data to account for the smaller effect of varying solar modulation (for a given date). The heliocentric potential and altitude correction functions are then used to normalize all of the data. The final result is a single correlation of all dose rate data versus vertical cutoff rigidity. This relationship allows the dose rate for any global position, altitude and date to be interpolated. PCAIRE provides a total ambient dose equivalent, $H^*(10)$, estimate by integrating this dose rate function over a given flight path, accounting for altitude and heliocentric potential effects.

PCAIRE requires user input for the flight duration time, altitudes and time flown at these altitudes, departure and destination locations and the date of the flight. The code provides a rapid route-dose output in total ambient dose equivalent and/or effective dose (using either a FLUKA or LUIN conversion function). PCAIRE maintains complete crew profiles and can associate individuals with flights flown, allowing exposure to be reported on a per-crew basis; likewise, PCAIRE can report a per-flight exposure which can be exported in a format acceptable to HR systems. PCAIRE can be run on corporate servers, via the internet, on an iPhone or on a laptop.

To estimate the additional contributions from Solar Energetic Particles (SEPs), a special model was developed using a Monte-Carlo radiation transport code, MCNPX. The model transports an extrapolated particle spectrum based on satellite measurements through the atmosphere using the MCNPX analysis. This code produces the estimated flux at a specific altitude where radiation dose conversion coefficients are applied to convert the particle flux into effective and ambient dose-equivalent rates. A cut-off rigidity model accounts for the shielding effects of the Earth's magnetic field.

Comparisons were made between the SEP model predictions and actual flight measurements taken with various types of instruments used to measure the mixed radiationfield during Ground Level Enhancements 60 and 65. An anisotropy analysis that uses neutron monitor responses and the pitch angle distribution of energetic solar particles was used to identify particle anisotropy for a solar event in December 2006.

A1.6 PANDOCA

The PANDOCA (Professional AviatioN DOse CAlculator) code was developed at the German Aerospace Center (DLR) at the Institute of Aerospace Medicine. Different versions of the model exist which are capable of calculating the effective dose after recommendations given in ICRP, Report 60 and ICRP Report 103, respectively. The version used in this comparison is described below. It calculates the effective dose after ICRP, Report 60. The most recent version, approved for the dose assessment of aircrew in Germany provides the effective dose following recommendations given in ICRP, Report 103. The impact of the corresponding updated weighting factors on the model was investigated and published in *Meier and Matthiä*, (2019).

The radiation exposure is calculated using the GEANT4 version 4.9.1 Monte Carlo code (Agostinelli, 2003) in combination with the model of the atmosphere (Picone, 2002) and the magnetic field of the Earth (Maus, 2005) provided by the PLANETOCOSMICS tool (http://cosray.unibe.ch). Galactic cosmic hydrogen and helium are considered as primary particles in the energy range from 100 MeV to 1.5 TeV (hydrogen) and 100 MeV to 850 GeV (helium). The primary particle energy spectra as described by Matthiä et al. (2013) are used. The GEANT4 interface to the JAM/JQMD model by Koi et al. (Koi, 2003) is used to calculate the helium transport at energies larger than 10 GeV/n. The resulting energy spectra of secondary protons, neutrons, photons, electrons, positrons, muons and pions at a given altitude are converted to effective dose and ambient dose equivalent using fluence-to-dose conversion factors (http://inf.infn.it).

The geomagnetic shielding effect was taken into account using the effective vertical cutoff rigidity calculated with PLANETOCOSMICS on a two-times-three degree grid in geographic latitude and longitude. The calculations of effective cutoff rigidity are based on the IGRF model of the geomagnetic field for 2005. In order to account for geomagnetic shielding, the geographic location is then converted to cutoff rigidity and the corresponding cutoff energy by interpolating between

the calculated values on the coordinate grid. For a given flight profile, the model provides the effective dose rate dE/dt and the ambient dose equivalent $dH^*(10)/dt$ at each waypoint and the resulting flight-integrated values of E and $H^*(10)$. Details about the PANDOCA model are published in Matthiä et al. (2014).

In case of a ground level enhancement, data from the neutron monitor network is used to derive the temporal evolution of the primary spectrum of the solar energetic particles. Using asymptotic viewing directions of the different neutron monitor stations, the angular distribution of the event is described. Typically, data of about 30 neutron monitor stations is used for this analysis. For the calculation of the radiation exposure on a specific flight route, the asymptotic viewing direction at each waypoint is calculated, the primary energy spectrum is derived and the dose rates at the given location are calculated. The procedure is described in detail in Matthiä et al. (2009 a,b). During solar events without sufficient information from ground based neutron monitors, data from satellite (e.g. GOES) measurements is used.

A1.7 PLANETOCOSMICS - Bern Model

With the Bern model, the radiation dose rates in the Earth's atmosphere due to solar and galactic cosmic radiation are computed in individual steps:

In a first step the near-Earth galactic and solar cosmic radiation flux outside the geomagnetosphere must be determined. The galactic cosmic ray spectrum is described by the heliocentric potential as based on the work of Gleeson and Axford (Gleeson, 1968b), Garcia-Munoz et al. (Garcia-Munoz, 1975), and Caballero-Lopez and Moraal (Caballero-Lopez and Moraal, 2004). The characteristics of the solar cosmic ray flux are determined based on the the measurements of the worldwide network of neutron monitors during the SEP. Neutron monitors are sensitive in the energy range ~500 MeV to ~20 GeV, which includes the majority of the high-energy solar cosmic rays. As neutron monitors are positioned on different geomagnetic latitudes, they have different cutoff energies and are therefore sensitive to different energy ranges. Due to their longitudinal spread, the neutron monitors of the worldwide network differ also in the acquisition directions of primary cosmic rays, i.e. information on the anisotropy of the solar cosmic ray flux can be determined. From the recordings of the worldwide network of neutron monitors, the characteristics of the solar proton flux near Earth during a SPE can be determined by using the method developed by Smart et al. (1971) and Debrunner and Lockwood (1980). With this method the count rate increases of the neutron monitors are simulated by using reasonable assumptions of the specific solar cosmic ray flux, the pitch angle distribution, and the apparent source position near Earth. With a trial and error procedure, the SEP characteristics can be determined by minimizing the difference between the calculated and the observed neutron monitor increases for the set of selected neutron monitor data. With this model it is therefore possible to determine the spectral shape, amplitude, and anisotropy of the solar cosmic ray flux near Earth in the energy range ~500 MeV to ~ 15 GeV. For energies below 500 MeV cosmic ray fluxes near Earth are evaluated from direct measurements of space based detectors.

In a second step the vertical cutoff rigidities, i.e. the minimum rigidity needed so that a cosmic radiation particle can reach the top of the atmosphere in the vertical direction, are computed at the grid points of a 5° X 5° network in geographic coordinates. Here, the Earth's magnetic field is described by the IGRF model for the internal field and by the Tsyganenko89 magnetic field model for the magnetic field caused by variable external sources subject to the dynamic interactions of the solar wind with the geomagnetosphere. For these computations the software suite PLANETOCOSMICS (Desorgher 2005; Desorgher, 2006) is used. PLANETOCOSMICS is based on the Geant4 software, a platform for simulating passage of particles through matter using Monte Carlo

methods (https://geant4.web.cern.ch). The PLANETOCOSMICS application allows to simulate the propagation of charged particles in the planetary magnetic field, and/or the hadronic and electromagnetic interactions of cosmic radiation with the environment of Earth, Mars, or Mercury, including the planet's atmosphere and soil. Possible outputs of the program are the fluence rate of particles at user-defined altitudes or the energy deposited by atmospheric shower particles in the atmosphere. Applications of the PLANETOCOSMICS code include albedo fluence rate estimates, solar particle fluence rate studies, computation of the ionization rate in the atmosphere by cosmic radiation, and the study of energetic electron precipitation events at high latitudes.

The cutoff rigidities and the near-Earth cosmic radiation fluence rate are the basis for the third step, computing the cosmic radiation fluence rate at the top of the Earth's atmosphere for the 5° X 5° grid. In the fourth step, the secondary cosmic radiation fluence rate in the atmosphere at specified altitudes is processed at each grid point. Finally, the radiation dose rates are calculated for selected atmospheric depths at the specified locations from the secondary particle fluence rate, using the fluence-to-dose conversion factors based on FLUKA calculations by Pelliccioni (Pelliccioni, 2000). The Bern model is non-commercial and is only used for scientific purposes.

A1.8 QARM

The QinetiQ Atmospheric Radiation Model (QARM) (Lei, 2004; Dyer, 2007) employs atmospheric response functions generated by Monte Carlo radiation transport codes, in conjunction with cosmic radiation and solar particle spectra and computed particle cutoff rigidities, to generate the radiation field in the atmosphere at any given location and time. In the current version (available through the website http://qarm.space.qinetiq.com), the solar-modulated cosmic radiation spectra for both protons and alpha particles are generated from the Badhwar and O'Neill model (O'Neill, 2006), while the solar particle spectra are calculated from ground level neutron monitor data in conjunction with spacecraft data as described in (Dyer, 2003a; Dyer, 2003b). In the current version the response functions are calculated for both protons and alpha particles using the MCNPX code (http://mcnpx.lanl.gov). The radiation along a flight path may be calculated using either a nominal great circle route or actual flight coordinates. Both directionality and all significant particle species are modelled and the outputs can be used to estimate integral properties of the environment such as ambient dose equivalent to aircrew, using the conversion coefficients of Pelliccioni (Pelliccioni, 2000), and rates of single event effects (SEEs) in avionics, using either measured input cross-sections for neutrons and protons or Weibull fits to such data. The geomagnetic cutoff rigidity can be computed using the latest model of the magnetic field, including both internal and external source terms from the International Geomagnetic Reference Field (IGRF) and the Tsyganenko model respectively. Hence, allowance can be made for both long-term variations and short-term disturbances during geomagnetic storms.

The successor to QARM is the Model of Atmospheric Ionising Radiation Effects (MAIRE), which is currently being updated to include solar energetic particle events, has been validated at high altitudes using balloon-borne radiation detectors (Hands, 2017).

A1.9 SiGLE | SIEVERT

SIEVERT (Bottollier-Depois 2003, 2007) has been jointly developed by the French civil aviation authority (DGAC), the Institute for Radiological Protection and Nuclear Safety (IRSN), the Paris Observatory, the French Institute for Polar Research (IPEV) and Air France as operational adviser. This

tool, which assists airlines in the application of French regulation, has been operational since September 2001. SIEVERT is managed and operated by IRSN and receives support from SiGLE model (Paris Observatory) in the case of a GLE.

SIEVERT provides two services: 1) a tool for calculating doses of cosmic radiation received during flights according to the routes; the doses are made available to companies on a server restricted to professionals; 2) a website for information on exposure to cosmic radiation, used to estimate the dose received during a flight (www.sievert-system.org).

The doses are evaluated, according to flight characteristics, from dosimetric data validated by IRSN. The calculation of the dose received during a flight is based on numerical models which map dose rates of cosmic radiation up to an altitude of 80,000 feet using the EPCARD software (Schraube, 2002) distributed by the Helmholtz Zentrum. In SIEVERT, airspace is split into zones of altitude, longitude and latitude to form a map made up of a mesh of 265,000 cells. A dose rate value is assigned to each cell. The SIEVERT computer evaluates the time spent by the aircraft in each cell and deduces the dose received. Maps are updated every month and, taking into account the trend of the solar cycle, predictive maps can also be drawn up (up to 18 months).

SiGLE is developed and operated by Paris Observatory. It is a semi-empirical model (Lantos, 2003a; Lantos, 2003b; Lantos, 2004; Lantos, 2006) which combines the few available measurements obtained during GLE on board airplanes, with calculations based on particle transport codes for the GLE number 42 (29 September 1989), to compute an estimate of the equivalent dose received by aircrews during a GLE. From the Air France and British Airways Concorde measurements during GLE 42, a linear relationship between ground based neutron monitor GLE time profiles and dose rates at 60,000 feet in altitude is derived for different particle rigidity spectral exponents. The attenuation factor, in relative scale, between the dose rate at 60,000 feet and the dose rate at the aircraft altitude is deduced from theoretical calculations (O'Brien, 1998) and from the measurement on board a Czech Airlines flight from Prague to New York (Spurny, 2001) during the GLE 60 (15 April 2001). Finally, the relative variation of the dose rate with the geomagnetic latitude at subsonic altitudes is estimated using results of dose rate calculations during GLE 42 by O'Brien and Sauer (O'Brien, 2000) and Beck et al. (Beck, 1999) at the Greenwich meridian.

These data are combined in SiGLE to give an estimate of the dose rate at any location in the sky in the course of the event. The rigidity spectrum exponent could be estimated from the ratio between two specific neutron monitors with a good approximation if a more precise determination of the exponent is not available in near real time (with NMDB for example). The reference monitor of SiGLE is located in the Kerguelen Islands at Port-aux-Français. This monitor, operated by IPEV, has a nominal cutoff rigidity of 1.14 GV. Already four GLEs were taken into account in an operational way (14/07/2000, 15/04/2001, 20/01/2005 and 13/12/2006) and corresponding doses included into the SIEVERT maps.

Until 2016, the SiGLE model did not take into account the anisotropy of primary cosmic rays for operations. Nevertheless, a simple approach considering this effect was included in the scientific version, which was used for the intercomparison of the present report (GLE69) conducted in 2013. The updated SiGLE model and its real time version SiGLE_RT (SiGLE_RT, 2018) use the full potential of the worldwide network of neutron monitors to account for the North/South anisotropy of solar particles.

Appendix 2: Flight Data for GLE42

Flight No. 00863: San Francisco (KSFO) – Paris (LFPG)

```
00863;KSFO;LFPG;29/09/1989;10:20;29/09/1989;19:35;
00863;AER;000;00:00;373712N;1222230W;
00863;TOC;300;00:22;392236N;1195554W;
00863;INT;330;00:24;393154N;1193924W;
00863;INT;370;01:09;440518N;1121236W;
00863;INT;370;01:28;454830N;1083730W;
00863;INT;370;02:34;522024N;0964242W;
00863;INT;370;03:14;562424N;0900000W;
00863;INT;370;04:03;603942N;0800000W;
00863;INT;390;05:15;650000N;0600000W;
00863;INT;390;06:10;660000N;0400000W;
00863;INT;390;07:07;630000N;0200000W;
00863;INT;390;08:13;555212N;0042648W;
00863;INT;250;08:52;502106N;0003830E;
00863;TOD;250;08:56;494724N;0011348E;
00863;AER;000;09:15;490036N;0023254E;
```

Flight No. 00202: Chicago (KORD) – Beijing (ZBAA)

```
00202;KORD;ZBAA;29/09/1989;10:00;29/09/1989;23:11;
00202;AER;000;00:00;415800N;0875400W;
00202;TOC;290;00:18;431800N;0865100W;
00202;INT;310;00:37;452400N;0845400W;
00202;INT;330;01:11;494100N;0822400W;
00202;INT;330;03:01;642400N;0800000W;
00202;INT;350;05:04;801100N;0594800W;
00202;INT;338;06:20;873100N;0300000E;
00202;INT;338;08:07;750100N;1001200E;
00202;INT;338;10:02;592600N;1043200E;
00202;INT;338;11:13;502000N;1062800E;
00202;INT;372;12:10;442700N;1131400E;
00202;INT;363;12:30;415000N;1130900E;
00202;TOD;363;12:49;402300N;1152900E;
00202;AER;000;13:11;400500N;1163500E;
```

Flight No. 00207: Sydney (YSSY) – Johannesburg (FAJS)

```
00207;YSSY;FAJS;29/09/1989;08:10;29/09/1989;21:55;
00207;AER;000;00:00;335600S;1511000E;
00207;TOC;300;00:18;350600S;1491200E;
00207;INT;300;00:57;374200S;1444800E;
00207;INT;300;01:44;420000S;1400000E;
00207;INT;310;02:00;434200S;1381800E;
00207;INT;310;02:13;450000S;1370000E;
00207;INT;310;02:31;470000S;1350000E;
00207;INT;310;03:14;520000S;1300000E;
00207;INT;310;03:51;560000S;1250000E;
00207;INT;310;04:17;580000S;1200000E;
00207;INT;310;04:42;600000S;1150000E;
00207;INT;350;04:55;605400S;1115400E;
00207;INT;350;05:24;630000S;1050000E;
00207;INT;350;05:41;640000S;1000000E;
00207;INT;350;05:59;650000S;0950000E;
00207;INT;350;06:15;660000S;0900000E;
00207;INT;350;06:30;660000S;0850000E;
00207;INT;350;06:47;650000S;0800000E;
00207;INT;350;07:25;630000S;0700000E;
00207;INT;350;08:10;600000S;0600000E;
00207;INT;370;08:42;571800S;0544200E;
00207;INT;370;09:10;550000S;0500000E;
00207;INT;370;10:40;450000S;0430000E;
00207;INT;370;12:10;350000S;0350000E;
00207;INT;390;12:30;314800S;0331800E;
00207;INT;390;12:34;311200S;0330000E;
00207;INT;350;12:45;302400S;0321800E;
00207;TOD;350;13:21;274800S;0294800E;
00207;AER;000;13:45;260800S;0281400E;
```

The dashed lines shown in the figures do not represent an actual flight profile but are meant only to guide the eye between the waypoints. The grey line depicts the amplitude of solar cosmic ray flux as assumed for this inter-comparison exercise. Note that the way in which calculations are performed between the waypoints depends on the individual codes.

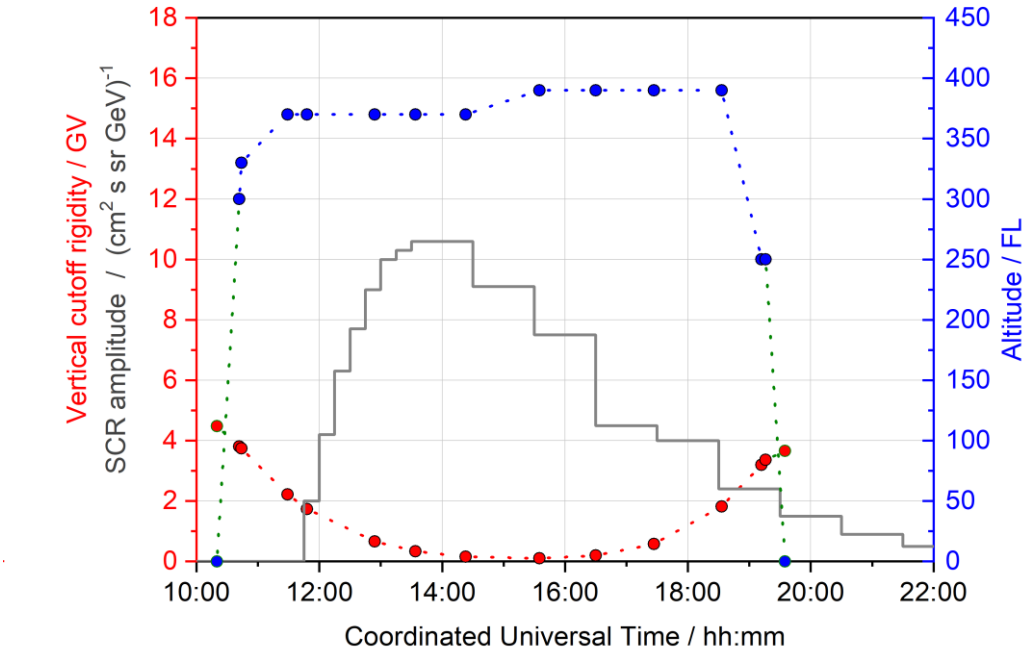

Figure 54: Flight altitude, vertical cutoff rigidity and SCR amplitude for Flight No. 00863 (29/09/1989): San Francisco – Paris

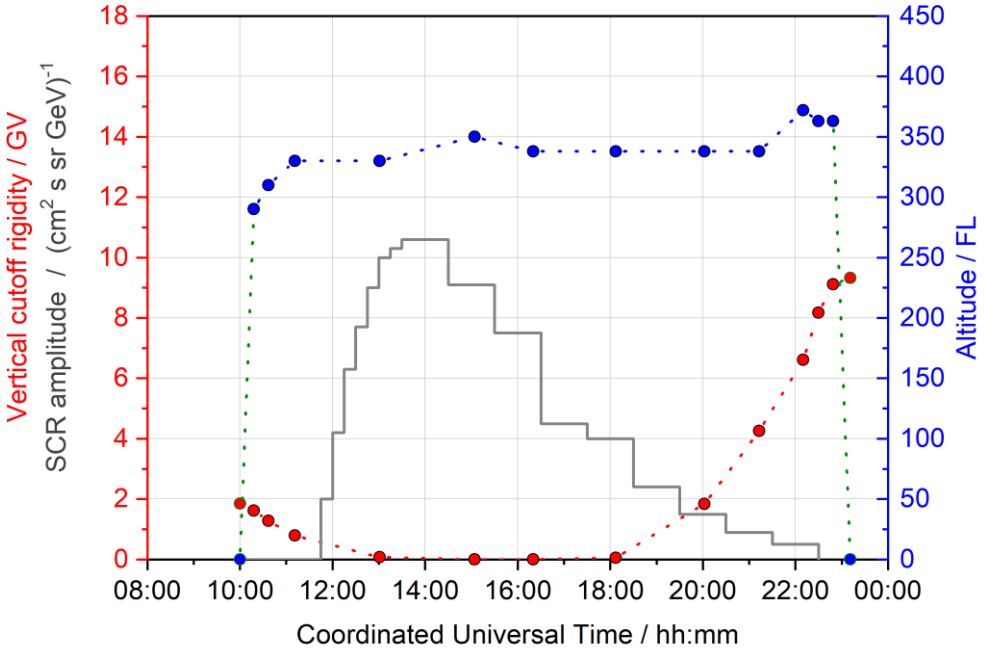

Figure 55: Flight altitude, vertical cutoff rigidity and SCR amplitude for Flight No. 00202 (29/09/1989): Chicago – Beijing

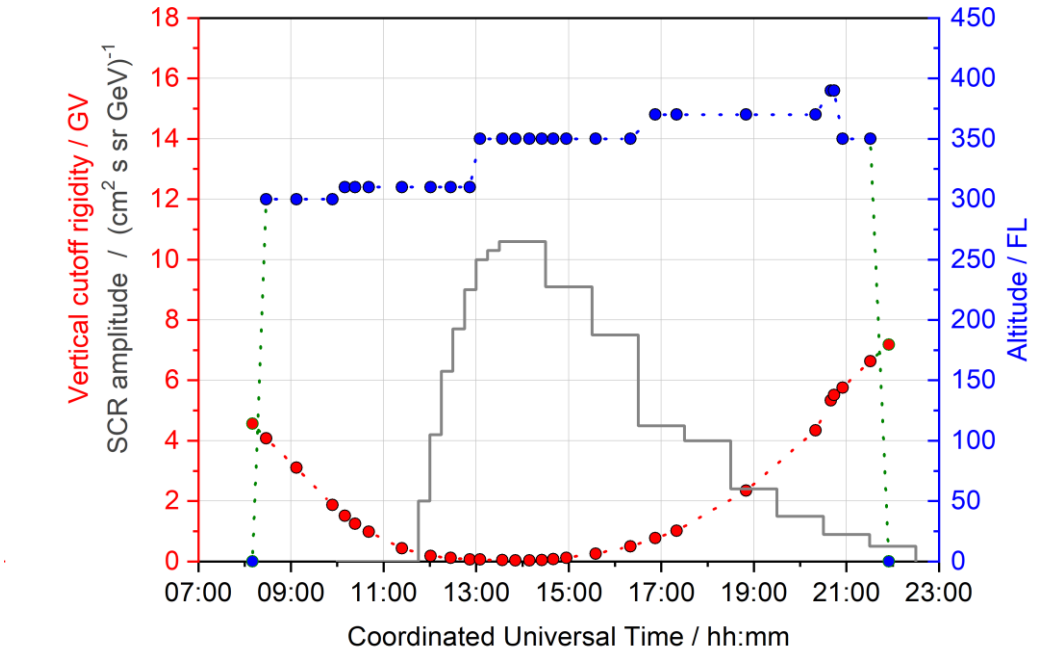

Figure 56: Flight altitude, vertical cutoff rigidity and SCR amplitude for Flight No. 00207 (29/09/1989): Sydney – Johannesburg

Appendix 3: Flight Data for GLE69

Flight No. 00863: San Francisco (KSFO) – Paris (LFPG)

```
00863;KSFO;LFPG;20/01/2005;04:15;20/01/2005;13:30;
00863;AER;000;00:00;373712N;1222230W;
00863;TOC;300;00:22;392236N;1195554W;
00863;INT;330;00:24;393154N;1193924W;
00863;INT;370;01:09;440518N;1121236W;
00863;INT;370;01:28;454830N;1083730W;
00863;INT;370;02:34;522024N;0964242W;
00863;INT;370;03:14;562424N;0900000W;
00863;INT;370;04:03;603942N;0800000W;
00863;INT;390;05:15;650000N;0600000W;
00863;INT;390;06:10;660000N;0400000W;
00863;INT;390;07:07;630000N;0200000W;
00863;INT;390;08:13;555212N;0042648W;
00863;INT;250;08:52;502106N;0003830E;
00863;TOD;250;08:56;494724N;0011348E;
00863;AER;000;09:15;490036N;0023254E;
```

Flight No. 00202: Chicago (KORD) – Beijing (ZBAA)

```
00202;KORD;ZBAA;20/01/2005;05:30;20/01/2005;18:41;
00202;AER;000;00:00;415800N;0875400W;
00202;TOC;290;00:18;431800N;0865100W;
00202;INT;310;00:37;452400N;0845400W;
00202;INT;330;01:11;494100N;0822400W;
00202;INT;330;03:01;642400N;0800000W;
00202;INT;350;05:04;801100N;0594800W;
00202;INT;338;06:20;873100N;0300000E;
00202;INT;338;08:07;750100N;1001200E;
00202;INT;338;10:02;592600N;1043200E;
00202;INT;338;11:13;502000N;1062800E;
00202;INT;372;12:10;442700N;1131400E;
00202;INT;363;12:30;415000N;1130900E;
00202;TOD;363;12:49;402300N;1152900E;
00202;AER;000;13:11;400500N;1163500E;
```

Flight No. 00207: Sydney (YSSY) – Johannesburg (FAJS)

```
00207;YSSY;FAJS;20/01/2005;02:00;20/01/2005;15:45;
00207;AER;000;00:00;335600S;1511000E;
00207;TOC;300;00:18;350600S;1491200E;
00207;INT;300;00:57;374200S;1444800E;
00207;INT;300;01:44;420000S;1400000E;
00207;INT;310;02:00;434200S;1381800E;
00207;INT;310;02:13;450000S;1370000E;
00207;INT;310;02:31;470000S;1350000E;
00207;INT;310;03:14;520000S;1300000E;
00207;INT;310;03:51;560000S;1250000E;
00207;INT;310;04:17;580000S;1200000E;
00207;INT;310;04:42;600000S;1150000E;
00207;INT;350;04:55;605400S;1115400E;
00207;INT;350;05:24;630000S;1050000E;
00207;INT;350;05:41;640000S;1000000E;
00207;INT;350;05:59;650000S;0950000E;
00207;INT;350;06:15;660000S;0900000E;
00207;INT;350;06:30;660000S;0850000E;
00207;INT;350;06:47;650000S;0800000E;
00207;INT;350;07:25;630000S;0700000E;
00207;INT;350;08:10;600000S;0600000E;
00207;INT;370;08:42;571800S;0544200E;
00207;INT;370;09:10;550000S;0500000E;
00207;INT;370;10:40;450000S;0430000E;
00207;INT;370;12:10;350000S;0350000E;
00207;INT;390;12:30;314800S;0331800E;
00207;INT;390;12:34;311200S;0330000E;
00207;INT;350;12:45;302400S;0321800E;
00207;TOD;350;13:21;274800S;0294800E;
00207;AER;000;13:45;260800S;0281400E;
```

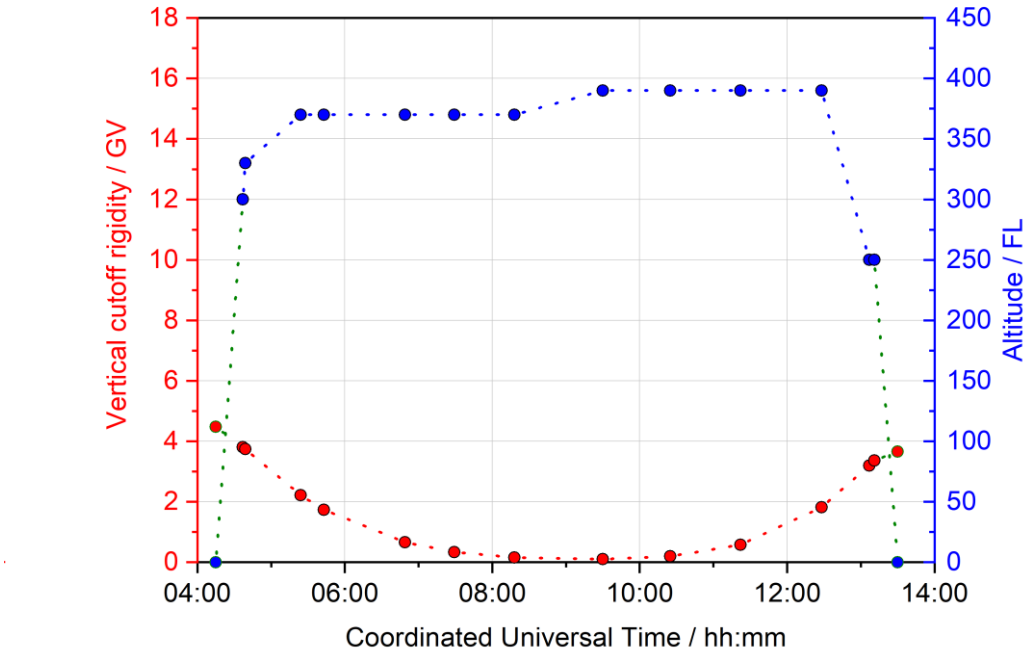

Figure 57: Flight altitude and vertical cutoff rigidity for Flight No. 00863 (20/01/2005): San Francisco – Paris

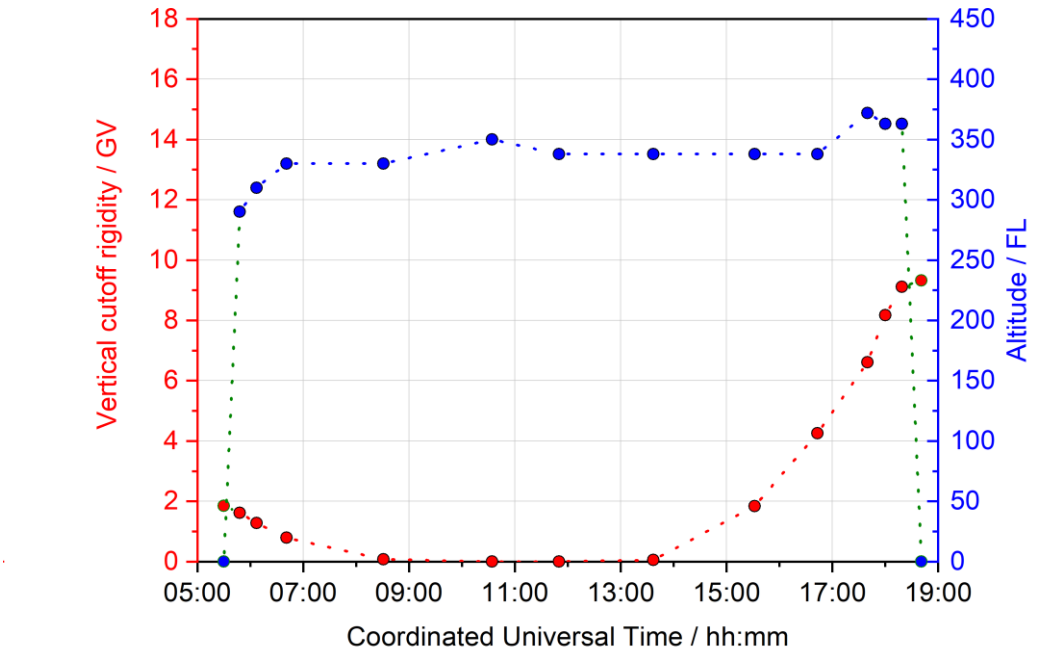

Figure 58: Flight altitude and vertical cutoff rigidity for Flight No. 00202 (20/01/2005): Chicago – Beijing

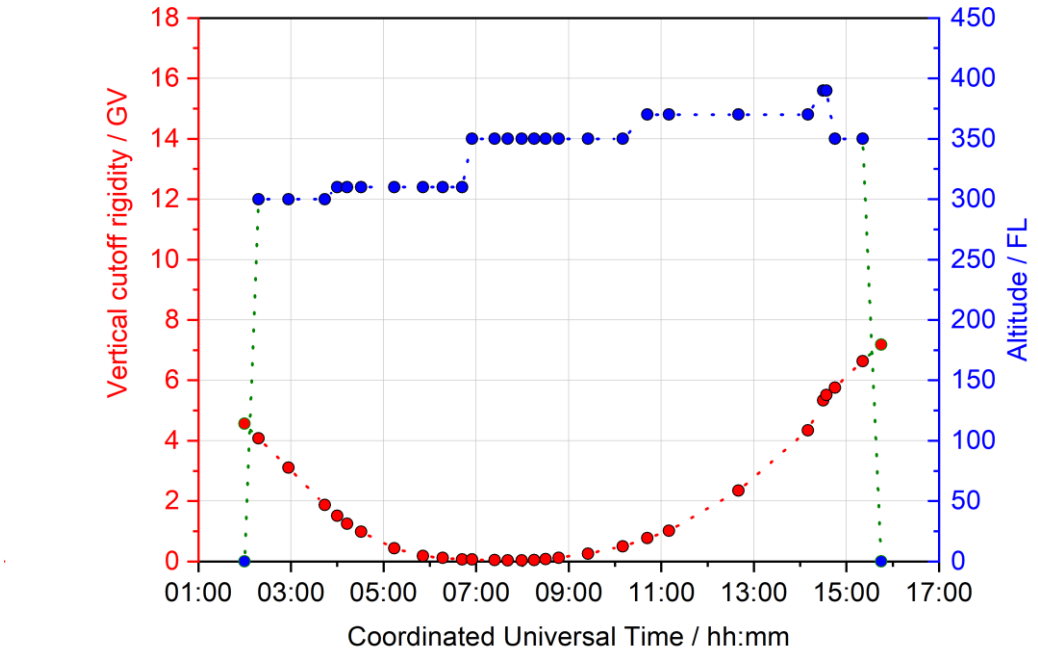

Figure 59: Flight altitude and vertical cutoff rigidity for Flight No. 00207 (20/01/2005): Sydney – Johannesburg

Appendix 4: Literature Data for GLE69

The following publications were provided to the contributors of the comparison:

- Belov, A. V., Eroshenko, E. A., Mavromichalaki, H., Plainaki, C., and Yanke, V. G., *Ground level enhancement of the solar cosmic rays on January 20, 2005*. In International Cosmic Ray Conference, volume 1 of International Cosmic Ray Conference, page 189, (2005).
- Bombardieri, D. J., Duldig, M. L., Humble, J. E., and Michael, K. J., *An Improved Model for Relativistic Solar Proton Acceleration Applied to the 2005 January 20 and Earlier Events.* Astrophy J, 682:1315–1327, (2008).
- Bütikofer, R., Flückiger, E. O., Desorgher, L., and Moser, M. R., *Analysis of the GLE on January 20, 2005: an update.* In 20th European Cosmic Ray Symposium, Lisbon (Portugal), (2006).
- Bütikofer, R., Flückiger, E. O., Desorgher, L., and Moser, M. R., *The extreme solar cosmic ray particle event on 20 January 2005 and its influence on the radiation dose rate at aircraft altitude.* Sci. Total Environ., 391(2), (2007).
- Dvornikov, V. M., Kravtsova, M. V., Lukovnikova, A. A., and Sdobnov, V. E., *Variations in the cosmic-ray rigidity spectrum during events of January 2005.* Bulletin of the Russian Academy of Science, Phys., 71:942–944 (2007).
- Makhmutov, V. S., Bazilevskaya, G. A., Vashenyuk, E. V., Balabin, Y. V., and Gvozdevsky, B. B., *Solar proton spectra in the 20 January 2005 GLE: Comparison of simulations with balloon and neutron monitor observations.* In Physics of Auroral Phenomena, Proc. XXXI Annual Seminar, Apatity, pp 122–125 (2008).
- Matthiä, D., *The Radiation Environment in the Lower Atmosphere A Numerical Approach*. PhD Thesis, Mathematisch-Naturwissenschaftliche Fakultät der Christian-Albrechts-Universität zu Kiel (2009).
- Matthiä, D., Heber, B., Reitz, G., Meier, M., Shiver, L., Berger, T., and Herbst, K., *Temporal and spatial evolution of the solar energetic particle event on 20 January 2005 and resulting radiation doses in aviation*. Journal of Geophysical Research (Space Physics), 114:8104 (2009).
- Plainaki, C., Belov, A., Eroshenko, E., Mavromichalaki, H., and Yanke, V., *Modeling ground level enhancements: Event of 20 January 2005.* Journal of Geophysical Research (Space Physics), 112:4102 (2007).
- Vashenyuk, E. V., Balabin, Y. V., Bazilevskaya, G. A., Makmutov, V. S., Stozhkov, Y. I., and Svirzhevsky, N. S., *Solar Particle Event 20 January, 2005 on stratosphere and ground level observations.* In International Cosmic Ray Conference, volume 1 of International Cosmic Ray Conference, p. 213 (2005).
- Vashenyuk, E. V., Balabin, Y. V., Gvozdevsky, B. B., Karpov, S. N., Yanke, V. G., Eroshenko, E. A., Belov, A. V., and Gushchina, R. T., *Relativistic solar cosmic rays in January 20, 2005 event on the ground based observations*. In International Cosmic Ray Conference, volume 1 of International Cosmic Ray Conference, p. 209 (2005).
- Vashenyuk, E. V., Mikroshnichenko, L. I., Balabin, Y. V., Perez-Peraza, J., and Gallegos-Cruz, A., *Two-component features of the two largest GLEs: February 23, 1956 and January 20, 2005.* In International Cosmic Ray Conference, volume 1 of International Cosmic Ray Conference, pp. 249–252 (2007).